



Master Thesis

im Rahmen des
Universitätslehrganges „Geographical Information Science & Systems“
(UNIGIS MSc) am Interfakultären Fachbereich für Geoinformatik (Z_GIS)
der Paris Lodron-Universität Salzburg

zum Thema

„Automated Burned Area Monitoring Using Sentinel-2 MSI“

Based on FIRMS alarms, burned area monitoring using
Copernicus Sentinel-2 MSI data and comparison to affected
Human Settlement Structures

vorgelegt von

Dipl. Geographin Alexandra Hander

104842, UNIGIS MSc Jahrgang 2017

Betreuer:

Prof. Dr. Stefan Lang

Dr. Lorenz Wendt

Zur Erlangung des Grades

„Master of Science (Geographical Information Science & Systems) – MSc(GIS)“

Reutern, 31. Januar 2020

Affidavit

I hereby assure that the present Master Thesis will be completed without external help and without other than the sources cited, and that the work has not yet been submitted to any other examination office in the same or similar form.

All statements of the Work that has been taken over literally or analogously is marked accordingly with the authorship.

Alexandra Hander

Acknowledgment

I would like to take this opportunity to thank everyone who helped me during my studies and this master thesis.

Above all, I would like to thank my two supervisors Prof. Dr. Stefan Lang and Dr. Lorenz Wendt. You have given me the opportunity to write my master's thesis on such an exciting and certainly future-oriented topic. Especially Dr. Lorenz Wendt supported and motivated me with a lot of patience and always with helpful feedback and suggestions.

Many thanks also to the whole UNIGIS team for the competent support of my part-time studies.

Finally, I would like to thank my family and friends for the patience, helpfulness and support they have shown me during the three years of my studies.

Abstract

Forest fires have large-scale environmental and socio-economic impacts, including loss of biodiversity, erosion, damage to infrastructure and, in the worst case, loss of life (Schroeder et al. ,2016; Lentile et al., 2006). Usually, wildfire is a naturally occurring phenomenon that occurs in areas with combustible vegetation, which can be found in wooded areas in the wild or near towns and settlements. (Poursanidis und Chrysoulakis 2017). In recent years, the world public has been alarmed by several natural fire disasters, armed conflicts and regional crises with enormous consequences (Lang et al. 2016). Especially the destruction of human settlements in conflict situations, where whole villages are razed to the ground by fire, can be expected to lead to population shifts and consequently to temporary or permanent refugee camps (Lang et al. 2016). Nevertheless it is considered one of the most severe natural risks globally (Poursanidis und Chrysoulakis 2017). No matter on what scale fires occurs, they have the ability to affect various ecological processes as they are responsible for the partial or total removal of the vegetation layer (Petropoulos et al. 2014). They can therefore be classified as one of the most widespread ecological disturbances in a natural ecosystem. Forest fires can also affect the dynamics of land cover both spatially and temporally and affect not only soil structure but also the composition and competition of specie (Li und Roy 2017).

The new data policy of the European Commission in cooperation with the ESA (European Space Agency 2019) makes it possible to obtain high-resolution, multitemporal and multispectral data free of charge using the Sentinel-2 satellites. The satellites provide useful information for a wide range of land applications, for example time series that can already be assessed for monitoring and mapping of burned areas (Verhegghen et al. 2016). The capabilities of these satellites and the knowledge gained from remote sensing will make it possible to detect large and inaccessible but also small and local potentially dangerous environmental phenomena across a wide electromagnetic spectrum. An example of this is the detection and delineation of wildfires and the post-fire effects, such as the study of Weirather et al. (2018) proves.

In this Master Thesis, burned areas shall be detected using Google Earth Engine™ (GEE) with the help of an automatable model sequence from sentinel-2 level 1C data. The model was developed based on several events in two different study areas. The

study areas were chosen not only because of their geographical location, but also because of the period in which a fire occurred. In the first area it is a locally and temporally only once short occurring fire, in the second area it is a large-area fire, lasting over a longer period of time with periods in between in which no fire was recorded. Therefore, pre- and post-images are used as Image Collection or as single images from 2018 for the occurred fire events. The appropriate time period is derived from existing active fire data from the Moderate Resolution Imaging Spectroradiometer (MODIS), which were acquired from the Fire Information for Resource Management System (FIRMS) (FIRMS FAQ | Earthdata) . Fire detection with MODIS is performed using a contextual algorithm that exploits the strong emission of mid-infrared radiation from fires (FIRMS FAQ | Earthdata). The Sentinel-2 satellites do not have these thermal bands and therefore do not detect fires by their thermal radiation, but can “see” burned areas by changes in the near and shortwave infrared

The model is mostly automated, from loading suitable data to determining the burned area by applying the differenced Normalized Burn Ratio (dNBR) to comparing with human settlement structures. However, individual changes have to be made manually. The results after passing through the process chain are characteristic areas that can be marked as burnt. In the study areas several gradations of the severity of a fire event can be determined and classified. Together with the data on settlement structure, the results obtained provide information on affected settlement areas or forest and agricultural areas.

The first study area (Rafina - Greece) serves as a validation area for the work process, as the results of the Copernicus Emergency Management Service are available for this purpose. For the second test area (Paradise – California) the validated workflow had to be adapted, but the core could be used in a similar form. A validation by an on-site inspection could not be performed due to the different location of the study areas.

Significant limitations in the derivation and classification of burnt surfaces result from the use of the Top of Atmosphere (TOA) reflectance data. Atmospherically corrected surface reflectance data would certainly be an advantage, but are currently not available in a global coverage in the GEE. As soon as the data are available in a global coverage, a modification of the workflow is useful and will lead to more accurate results.

According to initial findings, the workflow can be applied in different areas under the condition that settings have to be adjusted manually according to the circumstances. However, depending on the temporal accumulation of occurring events, significant changes in the workflow are necessary, so that I come to the conclusion that it is more likely to be two different process chains with the same main algorithm, depending on whether it is a single event or a temporally close accumulation of events.

Table of Contents

Affidavit.....	1
Acknowledgment	2
Abstract	3
Table of Contents	6
List of Figures	8
1. Introduction	13
1.1 Problem definition and relevance of the topic.....	13
1.2 Objective, research guiding questions and hypothesis.....	16
1.3 Aim of the thesis.....	17
2. Data and Software	18
2.1 Data.....	18
2.1.1 Sentinel-2 MSI	18
2.1.2 Level 1C Product	21
2.1.3 FIRMS	28
2.1.4 Global Human Settlement Layers (GHSL).....	29
2.1.5 Reference Products from the EMS	31
2.1.6 Reference Products from the Disastercharter.....	33
2.2 Software	34
2.2.1 Google Earth Engine	34
2.2.2 Erdas Imagine	36
3. Methodology	37
4. Workflow	41
4.1 First part of the workflow - FIRMS Alarm.....	43
4.2 Second Part of the workflow – Burned Area Monitoring.....	50
4.2.1 First Study Area – Rafina, Greece	50

4.2.2	Burned Area mapping using Sentinel-2 TOA reflectance data with the Cloud mask.....	51
4.2.3	Burned Area mapping using Sentinel-2 TOA reflectance data without the Cloud mask.....	61
4.2.4	Accuracy Assessment with a supervised Classification.....	68
4.2.5	Accuracy Assessment with the EMS Delineation Map.....	82
4.2.6	Destroyed Settlement Monitoring.....	87
4.2.7	Results.....	92
4.3	Evaluation and Adaptation of the workflow.....	95
4.3.1	Second Study Area - Paradise, California	95
4.3.2	FIRMS Alarms in AOI	97
4.3.3	Burned Area mapping using Sentinel-2 TOA reflectance data with the Cloud mask.....	98
4.3.4	Options for modifying the workflow	103
4.3.5	Burned Area Mapping using Sentinel-2 TOA reflectance data without the Cloud mask.....	108
4.3.6	Modifying the second workflow	112
4.3.7	Optical Comparison with the Fire situation map	116
4.3.8	Destroyed Settlement Monitoring.....	119
4.3.9	Results.....	122
5.	Conclusion	124
	Bibliography.....	127

List of Figures

Figure 1: SENTINEL-2 10 m spatial resolution bands (European Space Agency 2019)	19
Figure 2: SENTINEL-2 20 m spatial resolution bands (European Space Agency 2019)	19
Figure 3: SENTINEL-2 60 m spatial resolution bands (European Space Agency 2019)	20
Figure 4: Spectral bands for the SENTINEL-2A and 2B sensors (European Space Agency 2019)	20
Figure 5: Study Area Rafina with the two superimposed tiles	22
Figure 6: tiles for the Study Area Paradise	23
Figure 7: Resampling Grid (European Space Agency 2019)	24
Figure 8: Displayed FIRMS Alarms above a region (left side); structure of the data (right side)	29
Figure 9: Global Human Settlement Layer, reduced for a region (left side); structure of the data in the GEE (right side)	30
Figure 10: Delineation Map: Wildfire Rafina – Greece. Produced on 26/07/2018 (EMSR300 2018)	31
Figure 11: Grading Map: Wildfire Rafina – Greece. Produced 22/08/2018 (EMSR300 2018)	32
Figure 12: Settlement Structure from EMS and presented in the GEE	32
Figure 13: Situation Map: Forest Fires USA California. Produced 21/11/2018 by SERTIT	33
Figure 14: The Earth Engine interactive development environment (own example)	35
Figure 15: Erdas Imagine Spatial Modeler to calculate the dNBR (left side) and resulting Fire mask in red (right side), (own example)	36
Figure 16: Spectral Response Curves for Burned Areas and Healthy Vegetation (unburned Areas)	38
Figure 17: Burn Severity Classes	39
Figure 18: Above: first study area and corresponding FIRMS alarm (left); new study area (purple), limited to the extension of FIRMS Alarm (right). Below: second Study Area and all available corresponding FIRMS alarm (left); new study area (black) after selecting a specific alarm (right)	40

Figure 19: Overview over the workflow (own Presentation)..... 42

Figure 20: Earth Engine Code Loading and calculating FIRMS Alarms 43

Figure 21: FIRMS Alarms in AOI 44

Figure 22: masked extension of alarms 45

Figure 23: selected Alarm with the dates in GeometryEast 47

Figure 24: False Color Image Collection for the interpretation of burnt areas..... 47

Figure 25: False Color Composite on three different days with different cloud cover before and after the fire event..... 47

Figure 26: False Color Composites in the GeometryCenter for the first period 48

Figure 27: False Color Composites in the Geometry Center for the second period.. 49

Figure 28: False Color Composites in the Geometry Center for the third period 49

Figure 29: Study Area Rafina (left side); False Color Composite (B12, B8A, B5) Rafina, reduced to the new AOI 50

Figure 30: Sentinel-2 TOA data in the investigation period..... 51

Figure 31: Equation for NDWI..... 52

Figure 32: Equation for NDWI with selected bands 52

Figure 33: Equation for the MNDWI..... 53

Figure 34: Equation for calculation the MNDWI with the upscaled Band 3 53

Figure 35: MNDWI (Water in blue, Land in light brown) on the left side; Land- and Water Mask on the right side 54

Figure 36: Images with the new Band “NBR” and the added “date” property 55

Figure 37: highest summed dNBR..... 56

Figure 38: dNBR (left side) and False Color image (right side), both in 20 m resolution 57

Figure 39: classified dNBR and faulty areas..... 58

Figure 40: optical image in False Color, overlaid with the Fire mask, false detected parts, FIRMS Alarm (yellow) and the Fire mask (orange) as Overlay and Area of the fire mask (pink) which is covered by the FIRMS alarm..... 59

Figure 41: Statistics for burned area and the Comparison between Alarm and Fire mask..... 60

Figure 42: adjusted workflow (significant changes are shown in red)..... 61

Figure 43: pre- and postNBR..... 63

Figure 44: Pre- and PostFire Data in False Color (left side); Pre- and PostNBR in greyscale (right side) 64

Figure 45: Calculating the dNBR and the result..... 64

Figure 46: dNBR in grayscale and classified dNBR..... 65

Figure 47: generated Fire mask from the second Option and Statistic 65

Figure 48: generated Fire mask with the new Threshold from the second Option.... 66

Figure 49: Comparison between the Fire Masks and the FIRMS Alarm 67

Figure 50: collected Training Data 69

Figure 51: Basic Land Use Classification and Statistic of the classified burned area 71

Figure 52: Confusion Matrix representing resubstitution accuracy 72

Figure 53: Earth Engine Code to get a true validation accuracy 73

Figure 54: error matrix and the Validation overall accuracy 73

Figure 55: supervised classification of the differenced NBR..... 74

Figure 56: Land Use Classification with dNBR and Statistic of the classified burned area 74

Figure 57: Confusion Matrix representing resubstitution accuracy for Method 1 75

Figure 58: Earth Engine Code to get a true validation accuracy 75

Figure 59: error matrix and the Validation overall accuracy for Method 1 76

Figure 60: land cover dataset and Training overall accuracy from the single dNBR and statistic for burned area 77

Figure 61: Confusion Matrix representing resubstitution accuracy for Method 2 77

Figure 62: error matrix for the Validation overall accuracy for Method 2 78

Figure 63: Comparison between RF Accuracy and Validation overall Accuracy 79

Figure 64: Comparison between Consumers and Producers Accuracy 80

Figure 65: Comparison of all burned areas..... 81

Figure 66: Delineation Map from the EMS, mapped burnt areas are shown in orange 82

Figure 67: Observed Event from the EMS (Lila) on the left side; Statistic for the Area (right side)..... 82

Figure 68: Statistic for the burned Area in Comparison of the two Masks and statistic for the overlapping area..... 83

Figure 69: Left: Observed Area (purple); Center: Observed Area (purple), overlaid by Fire mask (orange); Right: Fire mask, overlaid by Observed Area 84

Figure 70: Left: Observed Area EMS (purple), overlaid by Fire mask (orange); Right: statistic for the overlapping area between Observed Area and the Fire mask from the second workflow (threshold 99)..... 85

Figure 71: left side: Fire Event from EMS, overlaid by Fire mask using Threshold 200; right side: statistic for the overlapping area 85

Figure 72: Comparison of the fire masks to the burned area from EMS 86

Figure 73: Comparison in ha between the burned area and the area concerned to the three different Fire masks generated from the two approaches..... 86

Figure 74: Fire Mask 1 (orange) and the affected Settlement structures (blue) (left); Fire Mask 2 and the affected Settlement structures (blue) (center); Fire Mask 3 and the affected Settlement structures (blue) (right side) 87

Figure 75: Statistics for the burned Settlement..... 88

Figure 76: Affected settlement structures 89

Figure 77: Import of the Global Human Settlement Layer..... 90

Figure 78: Loading Settlement data and comparison with the first Fire mask..... 90

Figure 79: Fire Mask (orange) and Open Source Settlement Layer (red) as Overlay on the left side; affected Settlement structures (blue) on the right side 90

Figure 80: Statistic for the burned BuiltUpArea..... 91

Figure 81: Clouds (left), not detected by the masking algorithm (center) and falsely classified (right). 92

Figure 82: Comparison between the burned areas..... 94

Figure 83: second study Area (left side) and the new study area in False Color 96

Figure 84: Workflow for the second study area 96

Figure 85: FIRMS Alarms in AOI for 2018 97

Figure 86: new Study Area and registered Fires 97

Figure 87: Image Collection with the missing Tiles..... 98

Figure 88: List of all calculated NBR (left side)..... 99

Figure 89: Land Mask in red (left side) and median NBR in greyscale (right side) ... 99

Figure 90: highest summed dNBR with the date and the result..... 101

Figure 91: Result of the burnt area after modification of the permitted Cloudy Pixel Percentage 101

Figure 92: generated Fire mask and burned area in ha..... 102

Figure 93: modified workflow, Changes are shown in red 103

Figure 94: Maximum NBR image, minim 104

Figure 95: Complete Cloud Coverage after a fire event 104

Figure 96: modified workflow for second study Area 105

Figure 97: Earth Engine Code getting dNBR from a single pre- and postFire Mosaic
..... 106

Figure 98: dNBR in greyscale (left) and classified dNBR (right) 106

Figure 99: Fire Mask on the left side (in orange) and the statistic 107

Figure 100: preNBR (left side) and postNBR (right side)..... 110

Figure 101: NBR mosaic Image Collection 111

Figure 102: Changed workflow for the second study area 112

Figure 103: preFire Image Collection in False Color (upper left); postFire Image
Collection in False Color (upper right); preNBR mosaic (lower left) and postNBR
mosaic (lower right) 113

Figure 104: Earth Engine Code calculating dNBR and result on the right side..... 113

Figure 105: Fire Mask in orange (left side), T21 Mask in yellow (center), overlaid from
the Fire Mask and the Comparison between the two masks in green (right side)... 114

Figure 106: Statistic of the Fire Mask and the Comparison to the T21 Mask..... 114

Figure 107: classified burned area as final result 115

Figure 108: Fire situation map, Paradise (Butte County); affected built-up area in red
(Disastercharter 591 2018)..... 116

Figure 109: Forest Fires in November 2018 – Situation Map; burned area in pink
(Disastercharter 591 2018)..... 117

Figure 110: optical Comparison between the three different Masks. Left: first Fire Mask
from the first Workflow, center: second Fire mask from the first Workflow, right: Fire
Mask from the second Workflow..... 117

Figure 111: Comparison of the different burned areas in ha..... 118

Figure 112: Damaged or Destroyed Structures in Butte County..... 119

Figure 113: Fire mask (light orange); overlaid from GHSL 120

Figure 114: affected Human Settlement Structures..... 120

1. Introduction

1.1 Problem definition and relevance of the topic

Even though a wildfire is a natural phenomenon that occurs in areas with combustible vegetation, in forested areas in the wilderness or in nearby towns and settlements, it is considered one of the most severe and widespread natural risks in the world (Poursanidis und Chrysoulakis 2017). Petropoulos et al. (2014) defines a forest fire as a “*rapidly spreading fire that often occurs in forest areas*”. Forest fires, but also fires in unwooded, open areas, have the ability to influence various ecological processes, as they are responsible for the partial or complete degradation of the vegetation layer (Petropoulos et al. 2014). Significant environmental, economic and social impacts, including damage to wildlife habitats, soil erosion, watershed degradation and loss of human life, constitute a permanent threat from this natural risk (Poursanidis und Chrysoulakis 2017). Wildfires can therefore be classified as one of the most widespread ecological disturbances in a natural ecosystem. The dynamics of land cover both spatially and temporally can be influenced by wildfires and influence not only the soil structure, but also the composition and competition between species (Li und Roy 2017).

With variations during the fire seasons, South Europe, North America, Central Asia and Australia are the main areas on the planet that are annually affected (Poursanidis und Chrysoulakis 2017) and in this regions wildfires cost billions in worldwide losses each year. According to the Munich Re, exposure has been rising steadily, especially in the Mediterranean, over the last few years (Munich Re 2018). The year 2018 for example was characterized by a harsh fire season in various parts of the world, especially California and Greece were hit by severe fires.

Since wildfires are a global phenomenon and systematic burned area mapping is of increasing importance for science and applications, Satellite data of any spatial resolution play a decisive role (Huang et al. 2016). They mention that Satellite data have been used long to systematically monitor fire globally at coarse spatial resolution, using algorithms that detect the location of active fires at the time of satellite overpass and using burned area mapping algorithms that map the spatial extent of the areas affected by fires. But nowadays there is an urgent need for moderate and high spatial resolution burned area products at regional to global scale because Climate change will bring many changes to the world and it is expected that the frequency and severity

of natural hazards and related disasters will increase globally (Weirather et al. 2018). Wildfires affect thousands of people every year because they cause enormous land losses and destroy settlements. Especially in recent years the world public has been alarmed by several disasters, armed conflicts and regional crises with enormous consequences (Gutjahr und Nolz 2016). The destruction of human settlements in conflict situations, where whole villages are razed to the ground by fire, can be expected to lead to population shifts and consequently to temporary or permanent refugee camps (Lang et al. 2016). The early planning of humanitarian operations can be decisively supported by the development of remote sensing based operational information services and tailor-made products (Lang et al. 2016). In the end fires causes billions of Dollar worth of damage. It is therefore very important to develop measures that help deal with the consequences of fires (Weirather et al. 2018). Satellite data play a major role in supporting knowledge about fire severity by delivering rapid information to map areas damaged by fire in an accurately and prompt way. Filipponi (2018) emphasizes that accurate and rapid mapping of fire damaged areas is fundamental to support fire management, account for environmental loss, define planning strategies, monitor the restoration of vegetation and especially the loss of human settlement. Remote sensing tools have proven useful to exactly estimate fire-affected areas and burn severity, to aid for example in forest fire prevention, assessment or monitoring on global, regional and local scales (Chuvienco 2009). In order to quantify the effects of fires, the extent of the burnt area must be recorded and delimited. Additionally, the severity of the burn and the unburned areas within the affected area are identified (Poursanidis und Chrysoulakis 2017). The most currently existing global products are based on coarse spatial-resolution sensors like MODIS (250 m – 500 m) (Roteta et al. 2019). The detection of small fires (< 100 ha) becomes very challenging using those pixel sizes. Although small fires are usually less catastrophic than large fires, they still play a significant part in land use transformation (Roteta et al. 2019). Extrapolating relations between active fires and small burn patches estimated that 26 % of the global burned areas was the result of small fires (Roteta et al. 2019). Optical data from the Sentinel missions, MODIS, the Landsat missions, SPOT, Aster, IKONOS and the WorldView generations II, III and IV are available in a wide range for the mapping of such destroyed, burnt settlement areas (Poursanidis und Chrysoulakis 2017). In addition, SAR radar data from Sentinel-1,

ALOS PALSAR, Radarsat-2, ERS-2, Envisat ASAR, COSMO-SkyMed and TerraSAR-X are used for forest fire mapping (Poursanidis und Chrysoulakis 2017). However, at least with the freely available data (Landsat, MODIS, ASTER) it was only possible to systematically monitor fires globally with coarse spatial resolution (Huang et al. 2016) and Algorithms were used which detect the location of active fires at the time of the overflight and map the spatial extent of the areas affected by fires (Huang et al. 2016). The increasing availability of medium spatial resolution sensors such as Landsat-OLI (30 m) or Sentinel-2 Multi Spectral Instrument (10 m) had overcome those limitations to detect smaller fires (Roteta et al. 2019). Roteta et al. (2019) mentioned, that the poor temporal resolution of the Landsat Satellites (8 days if both Landsat-7 and Landsat-8 is used) is one of the main limitations of using Landsat-OLI for burned area mapping. With the launch of the two Sentinel-2 Satellites and a 5-day revisiting frequency (Huang et al. 2016), this problem will be mitigated, even more if the Landsat-8 and Sentinel-2 data are integrated. Poursanidis und Chrysoulakis (2017) demonstrate also, that the combination of ESA's Sentinel missions (Sentinel 1 radar with 10 m spatial resolution, Sentinel 2 - optical with 10 m spatial resolution and Sentinel 3 - optical with 1 km spatial resolution and two optimized bands for fire detection) are optimal tools for fire detection, especially in difficult conditions like clouds or smoke. Even after the fire, the systems can assist in the mapping of burnt areas (Poursanidis und Chrysoulakis 2017). Numerous studies have already dealt with the extraction of burnt areas from satellite data using indices (for example the study from Weirather et al. (2018), Wooster et al. (2012), Huang et al. (2016) or Filipponi (2018). The goal of this paper is not to demonstrate this, but rather to investigate whether the combination of existing FIRMS alarms and Sentinel-2 MSI data, which are timed to coincide, can be used to automatically monitor burnt areas worldwide.

The following questions and thoughts can serve as an example:

- Does every FIRMS alarm really indicate an existing fire?
- Are the associated Sentinel-2 satellite images available at any time of the alarm?
- Are the burnt areas visible in the corresponding images?
- Can affected settlement structures be derived?

In order to answer this kind of questions, the focus of this paper is on the comparison between existing FIRMS alarms and the detection of the same areas as burned areas from Sentinel-2 MSI data.

If the burnt areas are successfully deduced, the final question is whether human settlement structures are affected.

1.2 Objective, research guiding questions and hypothesis

Based on the above-mentioned problem definition, the following research-guiding questions arise, with which this thesis will deal:

- How often and when are FIRMS alarms registered and how are they displayed?
- Is it possible to find suitable Sentinel-2 MSI data based on the registered alarms?
 - If so, under what conditions is this data available?
 - If not, what settings must be made to ensure that sufficient data is available?
- Can burn areas be identified and extracted from the Sentinel-2 data?
- Is a derivation to affected human settlement structures possible?
 - What data is required here?
- Can a workflow be created to find an automated methodology to the previous questions?
 - If so, can this methodology be applied worldwide for each study area?
 - If not, what adjustments are necessary or how high is the degree of automation?

The concrete research question should therefore be:

Is it possible, based on existing FIRMS alarms, to automatically or semi-automatically extract fire areas from Sentinel-2 MSI data and to derive affected human settlement structures?

1.3 Aim of the thesis

Answering this specific question is the aim of this paper. An algorithm is to be developed in which, on the basis of existing FIRMS alarms, the Sentinel-2 MSI data can be found at the right time. If FIRMS correspond to identifiable burnt areas, affected settlement structures should be derived.

2. Data and Software

2.1 Data

2.1.1 *Sentinel-2 MSI*

Sentinel-2 (S2) is an Earth observation mission developed by ESA (European Space Agency) as part of the Copernicus Program to acquire terrestrial observations in support of environmental services and natural disaster management (Roteta et al. 2019). The mission comprises a constellation of two polar-orbiting identical satellites, S2-A (launched in June 2015) and S2-B (launched in March 2017), which are placed in the same sun-synchronous orbit, phased at 180° to each other (European Space Agency 2019). It aims at monitoring variability in land surface conditions, and its wide swath width (290 km) and high revisit time (10 days at the equator with one satellite, and 5 days with 2 satellites under cloud-free conditions which results in 2-3 days at mid-latitudes) (European Space Agency 2019) will support monitoring of Earth's surface changes (Roteta et al. 2019). The coverage limits are from between latitudes 56° south and 84° north (<https://sentinel.esa.int/web/sentinel/missions/sentinel-2>, last accessed on June 2019). The main sensor is the Multi Spectral Instrument (MSI), a pushbroom scanner that provides a wide spectral coverage over the visible, near infrared (NIR) and short-wave infrared (SWIR) domains (amounting to 13 spectral bands), with medium spatial resolution (from 10 m to 60 m depending on the wavelength) (Roteta et al. 2019). Sentinel-2 is the result of close collaboration between ESA, the European Commission, industry, service providers and data users. The mission has been designed and built by a consortium of around 60 companies led by Airbus Defense and Space, and supported by the CNES French space agency to optimize image quality and by the DLR (German Aerospace Centre) to improve data recovery using optical communications (European Space Agency 2015). The 10 m and 20 m spatial resolution bands of SENTINEL-2 and the high revisit time of the mission will support the rapid acquisition and delivery of images to support disaster relief efforts. This includes mapping of urban areas, including at-threat buildings and complex structures, that have been previously identified as being at risk from natural hazards such as earthquakes and flooding. It will also contribute towards the identification of potential relief staging areas and status of supply routes and enable their use in pre- and post-event mission planning and control over the mission lifetime.

Only Satellite Data from the Sentinel 2 missions are used in this work. In Google Earth Engine™, it is possible to get open access on the Data. In this cloud-based platform the data can be analyzed and utilized. The Sentinel 2A and 2B satellites provide the opportunity for moderate spatial resolution burned area mapping. Combined, the systems will provide multi-spectral global coverage up to every 5 days (Huang et al. 2016). The MSI (Multi Spectral Instrument) has 13 spectral bands ranging from 0.433 μm to 2.19 μm;

- four 10 m visible and near-infrared (NIR) bands
- six 20 m red edge, near-infrared (NIR) and short-wave infrared (SWIR) bands
- three 60 m bands for atmospheric correction and for characterizing aerosols, water vapor and cirrus clouds

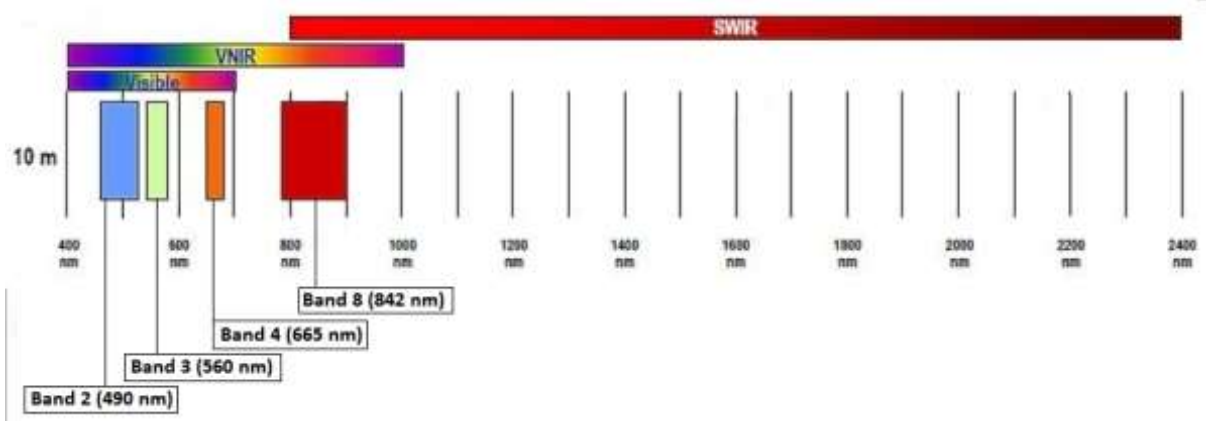


Figure 1: SENTINEL-2 10 m spatial resolution bands (European Space Agency 2019)

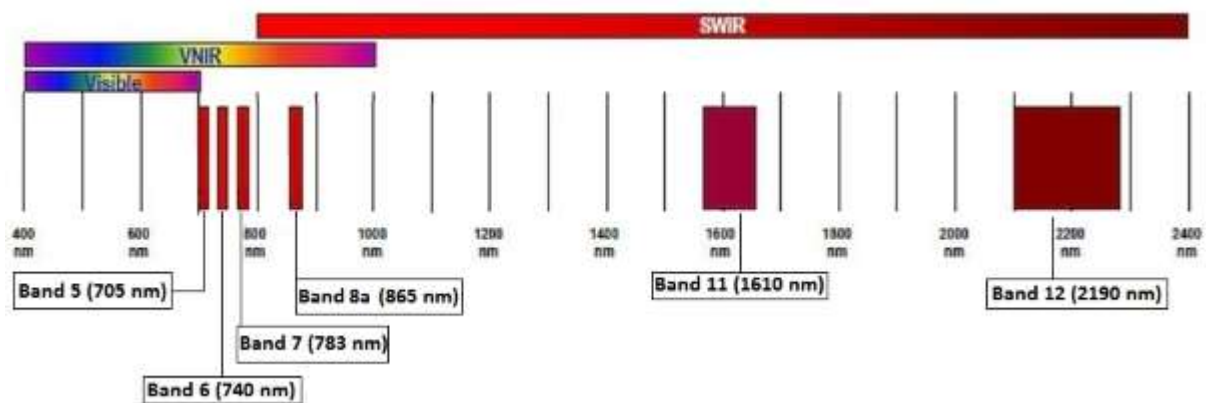


Figure 2: SENTINEL-2 20 m spatial resolution bands (European Space Agency 2019)

BURNED AREA MONITORING USING COPERNICUS SENTINEL-2

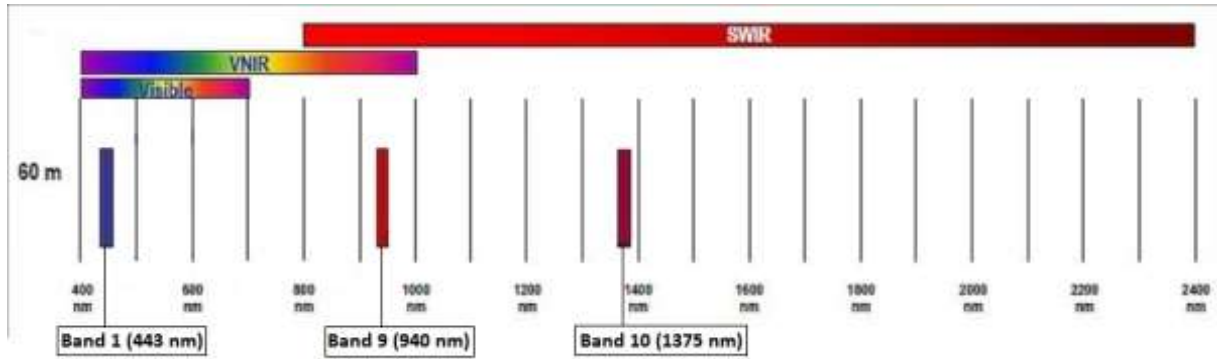


Figure 3: SENTINEL-2 60 m spatial resolution bands (European Space Agency 2019)

Band Number	S2A		S2B		Spatial resolution (m)
	Central wavelength (nm)	Bandwidth (nm)	Central wavelength (nm)	Bandwidth (nm)	
1	442.7	21	442.2	21	60
2	492.4	66	492.1	66	10
3	559.8	36	559.0	36	10
4	664.6	31	664.9	31	10
5	704.1	15	703.8	16	20
6	740.5	15	739.1	15	20
7	782.8	20	779.7	20	20
8	832.8	106	832.9	106	10
8a	864.7	21	864.0	22	20
9	945.1	20	943.2	21	60
10	1373.5	31	1376.9	30	60
11	1613.7	91	1610.4	94	20
12	2202.4	175	2185.7	185	20

Figure 4: Spectral bands for the SENTINEL-2A and 2B sensors (European Space Agency 2019)

2.1.2 Level 1C Product

The input data for the Workflow are the Level 1C Product. This product includes Top-Of-Atmosphere (TOA) reflectance with sub-pixel multispectral registration in UTM projection and WGS84 geodetic system in tiles of 100 x 100 km.

The following section briefly discusses the processing of the data towards a Level-1C product. Since most of the work is created in the GEE (loading the data, creating the algorithm, etc.), you can already fall back on the completely processed Level-1C products.

All information about creating the Level-1C product is taken from the official ESA website (European Space Agency 2019) or from the Sentinel-2 User Handbook (European Space Agency 2015).

Two successive operations are undertaken in order to obtain a Level-1C product from Level-1B products:

- Resampling of the Level-1B image to achieve an orthoimage in TOA reflectance
- Calculations of cloud and land/water masks for a tile in the Level-1C geometry.
- *Resampling*

Resampling comprises five main steps:

1. Selection of tiles intersecting the image footprint
2. Projection (geographic coding)
3. Computation of resampling grids linking the image in native geometry to the target geometry (orthoimage)
4. Resampling of each spectral band in the geometry of the orthoimage using the resampling grids and an interpolation filter
5. Computation of TOA reflectance image in the target geometry

- *Tiling Module*

The goal of this module is to select the list of predefined tiles which will be produced. The Earth's surface is split into several adjacent tiles in a given representation (UTM/WGS84). Some tiles may overlap between them. Each tile is defined by:

- an identifier
- a projection code (the default projection is the geographic coding, all EPSG projection shall be supported)
- an anchorage point (ground coordinates of the upper-left pixel of the tile)
- the pixel size in line and column
- the tile size in number of lines and of columns
- the tile bounding box coordinates in geographic representation

The Sentinel-2 Level 1C products will be split into tiles. The user manual for Copernicus Sentinel 2 explains how the tiles are constructed. The first 2 numbers of a tile name (such as **10TEK**) correspond to the UTM zone. The world is divided in 60 UTM zones of 6 degrees width in longitude, with numbers increasing towards the East. Zone 1 for example is over the Pacific Ocean. Each zone is divided in latitude, by chunks of 6 degrees. This is represented by a letter, which increases from South to North. And finally, each chunk is divided in 110 km tiles, with a 10 km overlap, from West to East, second Letter, and South to North, third Letter. For instance, one of the tiles for the study Area Rafina – Greece has the id **35SKC**. 35 is the UTM zone, S is the latitudinal chunk. K denotes the West-East tile position within the chunk and C the South-North position.

The first study area is covered by two tiles almost superimposed. The second study area is covered by four tiles, which do not overlap but appear next to each other due to the size of the study area.



Figure 5: Study Area Rafina with the two superimposed tiles

The second Study area Paradise (California) with the associated tiles are shown in Figure 6.



Figure 6: tiles for the Study Area Paradise

Depending on the size of the study area, it is either covered by several tiles or several tiles next to each other cover the area. In the course of the development of the workflow it will become clear whether the size of the study area makes a difference in the image selection.

- *Resampling function*

The resampling function is intended to obtain radiometric information in the target geometry.

- Geometric transformation.
- Radiometric interpolation.

- *Geometric Transformation*

The geometric transformation allows linking of the points of the target image with the points of the initial image. For SENTINEL-2, a resampling grid is used and computed for each spectral band and each detector. For each tile, there are 13 by 12 resampling grids.

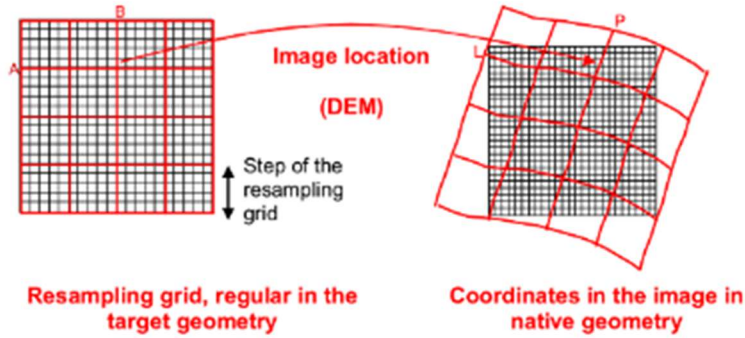


Figure 7: Resampling Grid (European Space Agency 2019)

The values of the resampling grid are computed for the footprint of the detector plus a small margin by extrapolation of the viewing directions. For each point of the orthoimage, the coordinates of the corresponding pixel in the native image are calculated by bi-linear interpolation of the four adjacent nodes.

- *Radiometric Interpolation*

Interpolation estimates the radiance values of the target point, knowing the radiance of neighbouring pixels. A linear algorithm is used for this operation with B-spline functions.

- *TOA Reflectance Computation*

The numeric digital counts (CN) of each pixel image (i,j) and each spectral band (k) are converted in TOA reflectance (ρ). This conversion takes into account the equivalent extra-terrestrial solar spectrum (E_s), the incoming solar direction defined by its zenith angle (θ_s) for each pixel of the image and the absolute calibration (A_k) of the instrument MSI.

The conversion equation is:

$$\rho_k(i,j) = \frac{\pi \times CN_{k,NTDI}(i,j)}{A_{k,NTDI} \times E_s \times d(t) \times \cos(\theta_s(i,j))}$$

Equation 1: TOA conversion (European Space Agency 2019)

where:

$CN_{k,NTDI}$ is the equalized numeric digital count of the pixel (i,j) with NTDI, the number of SENTINEL-2 TDI lines

E_s is the equivalent extra-terrestrial solar spectrum and depends on the spectral response of the SENTINEL-2 bands

The component $d(t)$ is the correction for the sun-Earth distance variation. It utilizes the inverse square law of irradiance, under which, the intensity (or irradiance) of light radiating from a point source is inversely proportional to the square of the distance from the source.

$$d(t) = \frac{1}{(1 - 0.01673 \times \cos(0.0172 \times (t - 2)))^2}$$

Equation 2: Earth Sun distance (European Space Agency 2019)

where:

t is the Julian Day corresponding to the acquisition date.

0.01673 is the Earth orbit eccentricity.

0.0172 is the Earth angular velocity (radians/day).

For Level-1C products, the noise model is also adapted to the new range of TOA reflectance radiometric values. The parameters (A_k, E_s) of the Level-1B noise model are corrected using Equation 1 by replacing CN_k with the Level-1B parameters A_k1B and E_s1B .

- *Computation of the Masks*

The last operation to obtain the final Level-1C product is computation of the cloud masks and the land/water mask for a tile in the Level-1C geometry. The cloud mask specifies cloud type: cirrus or opaque cloud. Level-1B technical masks (defective, no data pixels, etc) are then reprojected to the Level-1C geometry.

The Level-1C products embed:

- Vector mask (GML format)
- cloud mask including an indicator specifying cloud type:
 - dense cloud
 - cirrus cloud
- statistical information: percentage of cloudy pixels and of cirrus pixels in the cloud mask.

- *Cloud Mask (Dense/Cirrus)*

The cloud mask enables cloudy and cloud-free pixels to be identified. The mask includes both dense clouds and cirrus clouds with an indicator specifying the cloud type.

Processing is performed with data sampled at 60 m spatial resolution for all spectral bands.

- *Identification of Dense Clouds*

The dense clouds are characterised by a high reflectance in the blue spectral region (B2). The method used to identify dense cloud pixels is based on B2 reflectance threshold. To avoid false detection, mainly due to snow/cloud confusion, SWIR reflectance in B11 and B12 are also used. Snow and clouds both have a high reflectance in the blue. Cloud reflectance is high in the SWIR, whereas snow presents a low reflectance.

Additional criteria based on B10 reflectance are added to avoid high altitude ice cloud and snow confusion (both having a low reflectance in the SWIR bands B11 and B12). At B10, there is a high atmospheric absorption band and only high-altitude clouds are detected. However, this last criterion is only applied after a first detection of cloud pixel in the blue band where cirrus is transparent.

- *Cirrus Cloud*

Cirrus clouds are thin, transparent or semi-transparent clouds, forming at high altitudes, approximately 6-7 km above the Earth's surface. The method of identifying cirrus cloud pixels from dense cloud pixel is based on two spectral criteria:

- B10 corresponds to a high atmospheric absorption band so only high-altitude clouds can be detected
- cirrus cloud, being semi-transparent, cannot be detected in the B2 blue band

A pixel with low reflectance in the B2 band and high reflectance in the B10 band has a good probability of being cirrus cloud but this is not a certainty. Some dense clouds have a low reflectance in the blue and can be identified as cirrus cloud.

To limit false detections (due to high reflectance in the blue or due to the fact that clouds are not spectrally registered), a filter using morphology-based operations is applied on both dense and cirrus masks performing:

- erosion, to remove isolated pixels
- dilatation, to fill the gap and extend clouds.

If after morphology operations, a pixel is both dense and cirrus, the dense cloud mask prevails.

The cloud mask can be set to three values:

- 0 is a cloud-free pixel
- 1 is a dense cloud pixel
- 2 is a cirrus cloud pixel

If measurements are not available in one or several bands needed to calculate the cloud mask, the mask value is set to NODATA.

After all filtering steps, the cloud mask is available at a spatial resolution of 60 m. It is then resampled at spatial resolutions of 10 m and 20 m for each corresponding spectral band. The resampling is not a geometric transformation but a radiometric interpolation.

All these processing steps ensure that a pixel identified as cloud-free is actually cloud-free.

2.1.3 FIRMS

Active Fire data over the areas from the Moderate Resolution Imaging Spectroradiometer (MODIS) were acquired from the Fire Information for Resource Management System (FIRMS) (FIRMS FAQ | Earthdata). It was developed to provide near real-time active fire locations to natural resource managers that faced challenges obtaining timely satellite-derived fire information. FIRMS was developed by the University of Maryland, with funds from NASA's Applied Sciences Program and the United Nations Food and Agriculture Organization (Earthdata.nasa.gov 2019). The MODIS data are available from 2000 to date, comprising of 1 km detections from the combined 4 overpasses of the sensors on the Terra and Aqua satellites. The MODIS instrument on board the two satellites acquire data continuously providing global coverage every 1-2 days. For this reason there are at least 4 daily MODIS observations for almost every area on the equator, with the number of observations increasing (due to overlapping orbits) closer to the poles (FIRMS FAQ | Earthdata).

The satellites take a snapshot of events as it passes over the earth. Each hotspot/active fire detection represents the centroid of a 1km pixel that is flagged by the algorithm as containing one or more fires within the pixel (Giglio 2016). For MODIS the pixel is approximately 1km. The location is the center point of the pixel although the fire is often less than the size of the pixel (FIRMS FAQ | Earthdata).

The fires that are actively burning at the time of the satellite overpass are detected using thresholds in the middle and thermal infra-red channels (Verhegghen et al. 2016). Fire detection is performed using a contextual algorithm that exploits the strong emission of mid-infrared radiation from fires (FIRMS FAQ | Earthdata). The MODIS algorithm examines each pixel of the MODIS swath, and ultimately assigns to each one of the following classes: missing data, cloud, water, non-fire, fire, or unknown (Giglio et al. 2003).

The Earth Engine version of the Fire Information for Resource Management System (FIRMS) dataset contains the LANCE (NASA's Land, Atmosphere Near real-time Capability for EOS) fire detection product in rasterized form. The near real-time active fire locations are processed by LANCE using the standard MODIS MOD14/MYD14 Fire and Thermal Anomalies product (Giglio 2016).

The data are rasterized as follows:

For each FIRMS active fire point, a 1km bounding box (Figure 8) is defined. Pixels in the MODIS sinusoidal projection that intersect the FIRMS bounding box are identified. If multiple FIRMS boxes intersect the same pixel, the one with higher confidence is retained. In case of a tie, the brighter one is retained (Google Earth Engine 2019).



Figure 8: Displayed FIRMS Alarms above a region (left side); structure of the data (right side)

2.1.4 Global Human Settlement Layers (GHSL)

The Global Human Settlement Layers (GHSL) (DG/JRC/E1 2016) is a framework to produce global spatial information on population and on the physical size of settlements on the planet (ec.europa.eu/jrc/en/global-human-settlement-layer). The GHSL processes large volumes of heterogeneous data including global and continental satellite image archives, fine-scale satellite imagery, census data and volunteered geographic information (Joint Research Centre 2016). The information generated aims to be an objective and systematically account of the presence of population and built-up infrastructure on the Earth's surface. All layers produced at the Joint Research Centre (Joint Research Centre 2016) are used as evidence-based analytical knowledge to support the implementation of the EU regional urban policy. GHSL is the most spatially global detailed data available today dedicated to human settlements and shows the greatest temporal depth (Martino et al. 2015). The information is extracted from Landsat image records organized in four collections corresponding to the epochs 1975, 1990, 2000, and 2014 (Martino et al. 2015). The Layer has a Resolution of 38 m (Earth Engine Data Catalog).

BURNED AREA MONITORING USING COPERNICUS SENTINEL-2



```
builtUp
* Image JRC/GHSL/P2016/BUILT_LDSMT_GLOBE_V1 (1 band)
  type: Image
  id: JRC/GHSL/P2016/BUILT_LDSMT_GLOBE_V1
  version: 1571719398982399
  *bands: List (1 element)
    * 0: "built", unsigned int8, EPSG:3857, 1639x1193 px
      id: built
      crs: EPSG:3857
      *crs_transform: List (6 elements)
      *data_type: unsigned int8
      *dimensions: [1639,1193]
      *origin: [169399,315399]
      *properties: Object (24 properties)
```

Figure 9: Global Human Settlement Layer, reduced for a region (left side); structure of the data in the GEE (right side)

2.1.5 Reference Products from the EMS

Operational services based on the methodological references for burned area mapping have been developed in the past years to provide near-real time information on wildfires. Through an activation request, the Copernicus Emergency Management Service (EMS) delivers high spatial resolution wildfire maps generated from satellite data to determine the perimeter of the fires and distribution of fire severity levels. The Service uses satellite imagery and other geospatial data to provide free of charge mapping service in cases of natural disasters, human-made emergency situations and humanitarian crisis throughout the world (EMSR300 2018). It is provided during all phases of the emergency management cycle. The maps are produced in two temporal modes:

Rapid Mapping → Standardized mapping products are provided. For example, to ascertain the situation before the event (reference product), to roughly identify and assess the most affected locations (first estimate product), assess the geographical extent of the event (delineation product) or to evaluate the intensity and scope of the damage resulting from the event (grading product).

Risk & Recovery Mapping → activities dealing with prevention, preparedness, disaster risk reduction and recovery phases. There are three broad product categories: Reference Maps, Pre-disaster Situation Maps and Post-disaster Situation Maps.



Figure 10: Delineation Map: Wildfire Rafina – Greece. Produced on 26/07/2018 (EMSR300 2018)



Figure 11: Grading Map: Wildfire Rafina – Greece. Produced 22/08/2018 (EMSR300 2018)

In the course of the question whether human settlements are affected by the detected burnt area, such data must be available in form of raster or vector data. The EMS provides vector data generated from high resolution Pleiades data on human settlement structures for download. These data can be used later in the project as an additional reference.

```

*FeatureCollection users/Coral234/EMSR300_02RAFINA_DEL_v...
  type: FeatureCollection
  id: users/Coral234/EMSR300_02RAFINA_DEL_v2_built_up_a
  version: 1561894150609160
  ▶ columns: Object (10 properties)
  ▶ features: List (80 elements)
  ▶ properties: Object (1 property)
    
```



Figure 12: Settlement Structure from EMS and presented in the GEE

2.1.6 Reference Products from the Disastercharter

The Charter is a worldwide collaboration, through which satellite data are made available for the benefit of disaster management. By combining Earth observation assets from different space agencies, the Charter allows resources and expertise to be coordinated for rapid response to major disaster situations (International Charter Space and Disaster Management 2019). In addition to the space agencies that form the Charter, national and regional disaster monitoring organisations (for example the German Aerospace Centre (DLR)) also support the Charter's efforts as co-operating bodies. Members and co-operating bodies join an international initiative to provide support to those in need following major disasters, and benefit from the wide distribution of data that the Charter offers. The satellite data obtained by the Charter offers invaluable aid to the end-users - typically disaster relief organisations. Following a successful activation of the Charter, they may receive satellite data of affected areas within a matter of hours or days; depending on the type of the disaster and available satellite resources.

The data is delivered on an ongoing basis throughout the duration of the Charter activation and provides valuable information about a disaster that is not possible to obtain on the ground (International Charter Space and Disaster Management 2019).

The following graphic shows the situation map of the registered fires in California in November 2018. Burnt areas are shown in orange, potentially burning areas (at the time of activation) in yellow. Affected built Up areas are shown in red.



Figure 13: Situation Map: Forest Fires USA California. Produced 21/11/2018 by SERTIT

2.2 Software

2.2.1 *Google Earth Engine*

Google Earth Engine™ (GEE) is a cloud-based platform for planetary-scale geospatial analysis that brings Google's massive computational capabilities to bear on a variety of high-impact societal issues including deforestation, drought, disaster, disease, food security, water management, climate monitoring and environmental protection (Gorelick et al. 2017). The Engine consists of a multi-petabyte analysis-ready data catalog. It is accessed and controlled through an Internet-accessible application programming interface (API) and an associated web-based interactive development environment (IDE) that enables rapid typing and visualization of the results (Gorelick et al. 2017). The data catalog houses a large repository of publicly available geospatial datasets, including observations from a variety of satellite imaging systems in optical and non-optical wavelength, environmental variables, weather and climate forecasts and hindcasts, land cover, topographic and socio-economic datasets (Google Earth Engine 2019).

A significant advantage is the fact that all the data are preprocessed to a ready-to-use but information-preserving form that allows efficient access and removes many barriers associated with data management (Gorelick et al. 2017). The easily accessible and user-friendly front-end provides a convenient environment for interactive data and algorithm development (Figure 14). Mutanga und Kumar (2019) emphasises that Users are also able to add and curate their own data and collections, while using Google's cloud resources to undertake all the processing. The end result is that this now allows scientists, independent researchers, hobbyists and nations to mine this massive warehouse of data for change detection, map trends, and quantify resources on the Earth's surface like never before.

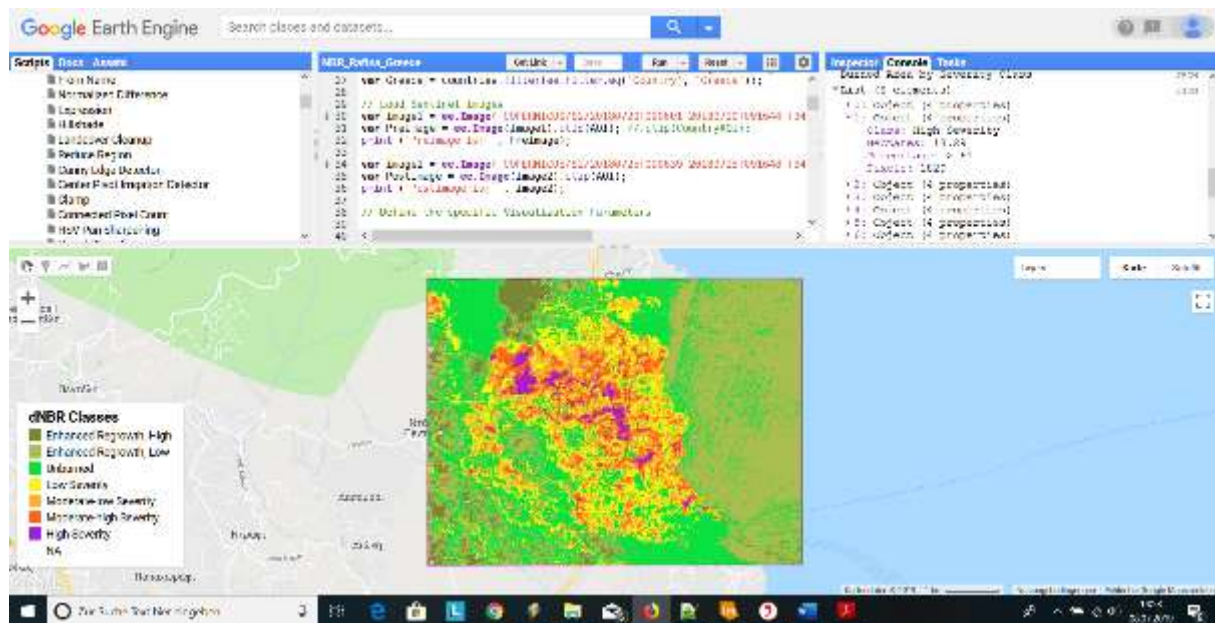


Figure 14: The Earth Engine interactive development environment (own example)

The Earth Engine public data catalog (Earth Engine Data Catalog) is a multi-petabyte curated collection of widely used geospatial datasets. The bulk of the catalog is made up of Earth-observing remote sensing imagery, including the entire Landsat archives as well as complete archives of data from Sentinel-1 and Sentinel-2 (Gorelick et al. 2017). Related images, such as all of the images produced by a single sensor, are grouped together and presented as a “collection”. Collections provide fast filtering and sorting capabilities that make it easy for users to search through millions of individual images to select data that meets specific spatial, temporal or other criteria (Gorelick et al. 2017). To enable fast visualization during algorithm development, a pyramid of reduced-resolution tiles is created for each image and stored in the tile database. Each level of the pyramid is created by down sampling the previous level by a factor of two until the entire image fits into a single tile. When a portion of data from an image is requested for computation at a reduced resolution, only the relevant tiles from the most appropriate pyramid level need to be retrieved from the tile database (Gorelick et al. 2017).

Processing within the GEE therefore has numerous advantages. Loading the data and creation of the algorithm for the detection of burnt areas as well as the comparison to affected settlement structures will therefore be set up and processed in the present work exclusively with GEE.

3. Methodology

The aim of this work is to find out whether Sentinel-2 MSI data can be used to detect burned areas in the same area, taking into account an existing and known FIRMS alarm. The core of the algorithm is thus based on the FIRMS alarms, which are loaded into the GEE and displayed. It is examined whether the Sentinel-2 data on the alarms detected by FIRMS can be used to detect fire areas or whether there are alarms that cannot be detected by the optical data used. Furthermore, it is inspected whether there is a restriction of the data regarding cloud cover due to a temporal accumulation of alarms. The question must be clarified whether there is a difference if there is only one alarm or if several alarms, triggered by fires in quick succession, do not allow an interpretation in the optical data.

In the first step the FIRMS alarm for a selected study area are loaded into the GEE and displayed. The algorithm will be adapted to the extent that for each alarm a recording date will be extracted into a list and provided. This date is then used to find suitable Sentinel-2 MSI data. In the next Step the Normalized Burn Ratio NBR and the differenced Normalized Burn Ratio (dNBR) derived therefrom is used for extraction of burned areas.

Filipponi (2018) mentioned that Fire severity often is estimated by visual inspection or measured in situ by means of field observation of several ecological parameters. He points out that the most widely used approach for assessing post-fire effects in the field are the Composite Burn Index (CBI) and its modified versions Geometrically structure CBI and weighted CBI (Filipponi 2018). But the Threshold-based classification of Normalized Burn Ratio difference (dNBR) has turned into a methodological reference to obtain burn severity maps.

The input data for the burned area algorithm is the Sentinel-2 level-1C product. Normalized Burn Ratio is frequently used to estimate burn severity. Imagery collected before a fire will have very high near infrared band values and very low mid infrared band values for healthy vegetation and an Imagery collected over a forest after a fire will have very low near infrared band values and very high mid infrared band values. The conclusion is therefore, a high NBR value generally indicates healthy or unburned vegetation while a low value indicates bare ground and recently burned areas (Fig. 16).

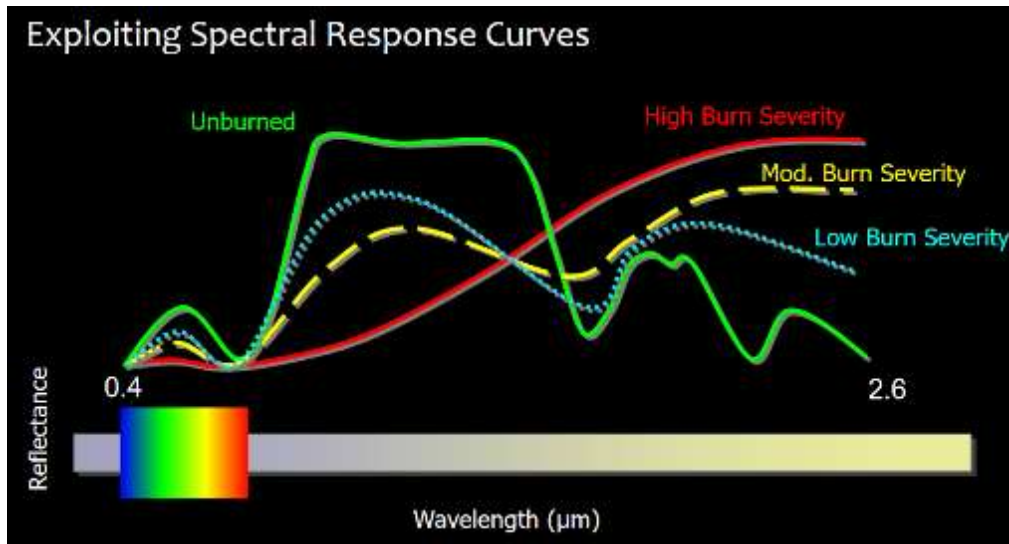


Figure 16: Spectral Response Curves for Burned Areas and Healthy Vegetation (unburned Areas)

(https://disasters.nasa.gov/sites/default/files/miscfiles/08_ARSET_Postfire_Mapping.pdf)

The NBR was developed for Landsat TM / ETM+ making use of the near-infrared (NIR) and short-wave infrared (SWIR) bands for its calculation. The NBR was computed according to the following formula:

$$NBR = \frac{NIR - SWIR}{NIR + SWIR}$$

Equation 3: Calculating the NBR

Since the Sentinel satellites cover the wavelength range with more bands than the Landsat satellites, those bands were chosen which are closest to the Landsat bands. Weirather et al. (2018) point out that band 12 for SWIR and band 8 or 8A for NIR are suitable. Subsequently bands 12 and 8A both have a resolution of 20 m, band 8A was chosen over band 8, which has a 10 m resolution (Weirather et al. 2018).

The dNBR is calculated according to the following formula

$$dNBR \text{ or } \Delta NBR = \text{PreNBR} - \text{PostNBR}$$

Equation 4: Calculating the dNBR

and can be used for burn severity assessment, as areas with higher dNBR values indicate more severe damage whereas areas with negative dNBR values might show increased vegetation productivity.

Weirather et al. (2018) mentioned, that the NBR and dNBR values derived from satellite remote sensing vary due to different image characteristics and image acquisition conditions. To distinguish between burned and unburned areas, field visits would help in choosing suitable thresholds. However, the aim is to develop an automated workflow applicable to the whole world that does not require any field assessment. It was therefore decided to classify thresholds for burned and unburned areas from a purely empirical method based on optical interpretation. A first approach to find such thresholds is the classification according to burn severity ranges proposed by the United States Geological Survey taken from the publication of Teodoro and Amaral (Teodoro und Amaral 2019).

Severity level	dNBR Range (scaled by 1000)	dNBR Range (unscaled)
Enhanced Regrowth, high (PostFire)	-500 to -251	-0.500 to -0.251
Enhanced Regrowth, low (PostFire)	-250 to -101	-0.250 to -0.101
Unburned	-100 to +99	-0.100 to +0.990
Low Severity	+100 to +269	+0.100 to +0.269
Moderate-low Severity	+270 to +439	+0.270 to +0.439
Moderate-high Severity	+440 to +659	+0.440 to +0.659
High Severity	> +660	> +0.660

Figure 17: Burn Severity Classes

These values are now used to create a thematic burn severity layer depicting severity as unburned to low, low, moderate, high and increased greenness (increased postfire vegetation response).

To create and test the algorithm, two fire events in two different regions were chosen as test areas. The study areas were selected from a registered event of the Copernicus Emergency Management Service (EMS) and of the International Charter Space and Major Disasters (Disastercharter), which allowed me to use the finally maps as a reference for the accuracy assessment. The 2018 fire season was chosen. In order to ensure the greatest possible diversity, one event with a short and locally occurring fire

(Rafina – GREECE; (EMSR300 2018)) and one with a large-area fire that lasts over a long period of time and always starts again (Paradise – CALIFORNIA; (Disastercharter 591 2018)).

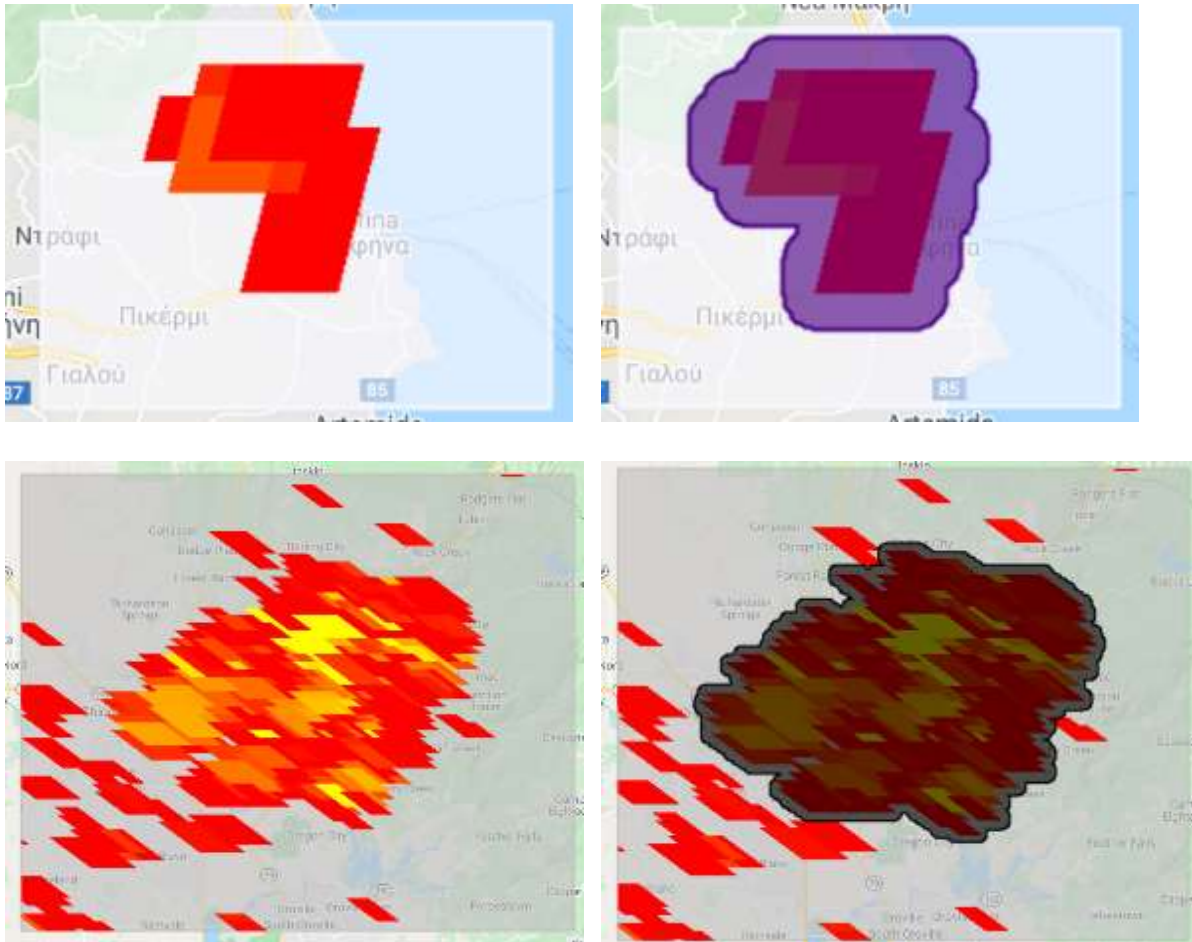


Figure 18: Above: first study area and corresponding FIRMS alarm (left); new study area (purple), limited to the extension of FIRMS Alarm (right). Below: second Study Area and all available corresponding FIRMS alarm (left); new study area (black) after selecting a specific alarm (right)

4. Workflow

In the first approach, Sentinel-2 TOA (Top of Atmosphere) data together with the cloud mask provided by ESA were loaded to get cloudless images in a collection. In Google Earth Engine™, it is possible to choose between Sentinel-2 TOA reflectance data and already processed Sentinel-2 surface reflectance data. Unfortunately, a worldwide coverage of the surface reflectance data is not yet provided in the GEE. From the preFire and postFire period, I selected all images with less than 5% cloudy pixels, using the metadata provided by ESA. The images were selected only for the buffered extent from the FIRMS alarm. A water/land mask was created from the found data using the MNDWI to exclude shadow and water areas. Since the NBR and dNBR are calculated at 20 m, this is retained for the water index. The 20-m MNDWI is calculated as:

$$\text{MNDWI}_{20\text{m}} = \frac{\rho_3^{20\text{m}} - \rho_{11}}{\rho_3^{20\text{m}} + \rho_{11}}$$

where ρ_{11} is the TOA reflectance of Band 11 (SWIR) and $\rho_3^{20\text{m}}$ is the TOA reflectance of band 3 (green) with the new spatial resolution of 20 m (Du et al. 2016).

Within the Image Collection the NBR was calculated for each available image. With regard to the calculation of the delta (dNBR) the system index was converted and added as a "date" to each image in the collection as a separate property, so that each image could later be offset against its previous image. From the NBR Image Collection a dNBR Image Collection was generated and finally the burned areas. The dNBR Image Collection is a collection of rasterdata, each containing the value from the calculation of the dNBR as a pixel value. The goal was not only to display the burnt area, but also to be able to indicate when this burnt area can be recognized in the satellite images. Therefore, all dNBR values per image within the buffered FIRMS Alarm extent were summed up and the image with the highest summed value was chosen. The result was classified by severity and the burned area was derived using an empirical threshold value to compare the resulted burned area to the FIRMS alarm. For each of the two study areas, different thresholds were tested and the one that showed the best results was chosen. The goal of the comparison to the FIRMS alarm was a mathematical evaluation of both areas to be able to deduce whether the

detection of fire areas using Sentinel 2 data is possible in the area of the available FIRMS data.

Furthermore, the result was evaluated using a supervised classification and compared with the data and maps of the respective organizations

The model serves to represent the main steps of the entire algorithm. Individual changes resulting from the conditions of the respective Study Area are not included.

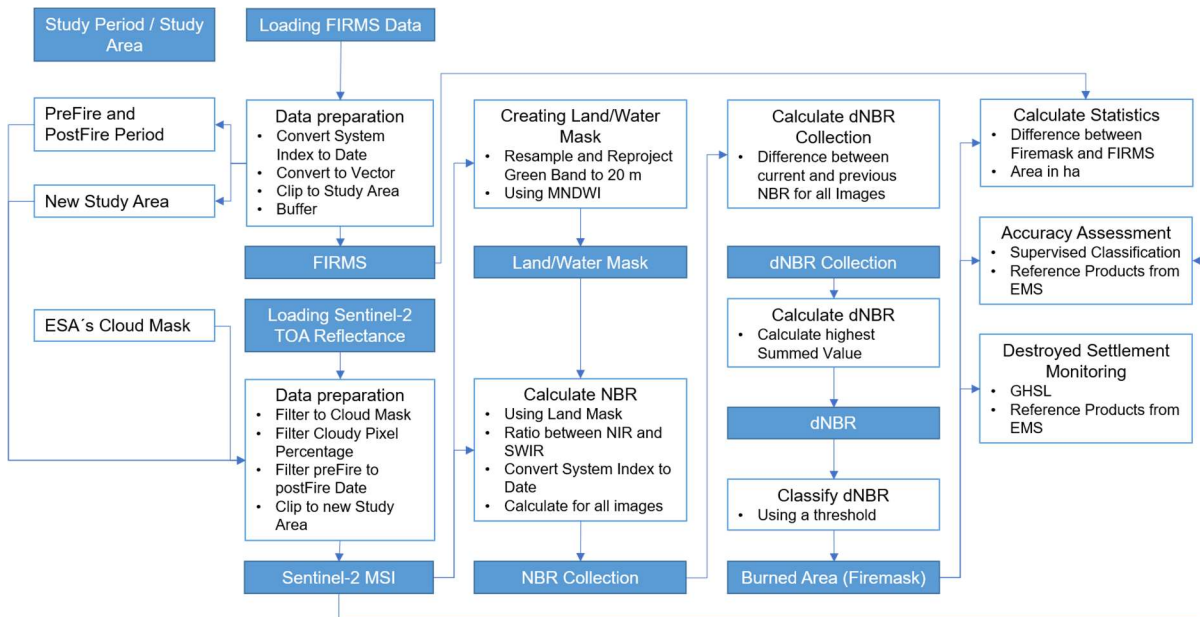


Figure 19: Overview over the workflow (own Presentation)

4.1 First part of the workflow - FIRMS Alarm

The aim of the first part of the workflow is to extract the date and extension from the existing alarms. With this information, the appropriate Sentinel-2 Data can be found later. In this way you can check whether and with what restrictions suitable Sentinel-2 data are available for the same period and the same extension and whether this data can be used to detect burned areas. The first step is to load the FIRMS alarms and extract the date and extent of them. In the code listed below, all FIRMS alarm from 2018 are designated and the band T21, which detects the temperature over an area, is selected. At that point the dates of the alarms are listed in a list.

```
//-----LOADING FIRMS ALARMS and clip to AOI-----//
var FIRMS_filtered = ee.ImageCollection('FIRMS')
// filter all alarms for 2018
  .filterDate('2018-01-01', '2018-12-31')
// filter the alarms for a specified AOI
  .filterBounds(AOI)
// select Band T21
  .select('T21')
// Function to convert day to date
  .map(function(image) {
    var date = ee.Date(image.get('system:time_start')).format("YYYY-DDD");
    date = ee.Date(date);
    return image.set('date', date);
  })
  .map(function(image) {
    var ID = ee.String(image.get('system:index'));
    return image.set('ID', ID);
  })
  .map(function(image) {
    var date = ee.Date(image.get('system:time_start'));
    return image.set('date_time', date);
  });
// Create a list of start days
var dayOfYearList = ee.List.sequence(1, 365, 5);
print('dayOfYearList: ', dayOfYearList);
// Function to convert day to date
var dateFromDayOfYear = function(day) {
  var dateString = ee.String('2018').cat(ee.String(ee.Number(day).toInt()));
  return ee.Date.parse('YYYYD', dateString);
};
// Create a list of start dates
var startDateList = dayOfYearList.map(dateFromDayOfYear);
print('startDateList: ', startDateList);
// Function to return an image consisting of count of valid pixels in the date range
var checkDateRange = function(start) {
  var end = ee.Date(start).advance(5, 'day');
  var dateRangeFiltered = FIRMS_filtered.filter(ee.Filter.date(start, end));
  var pixelCount = dateRangeFiltered.reduce(ee.Reducer.count());
  // return the image with a new property for start date
  return pixelCount.set({start_date: start});
};
```

Figure 20: Earth Engine Code Loading and calculating FIRMS Alarms

Due to the repetition rate of the two Sentinel-2 satellites of 5 days, only every fifth alarm is added to the list for a better overview. This can be adjusted individually.

In the following, the calculations are calculated only for the study area.

```
// Limit the pixels for a AOI
// Count total pixels within AOI
var totalPixelCountAOI = function(image) {
  var countDict = ee.Image(image).reduceRegion({
    reducer: ee.Reducer.count(),
    geometry: AOI,
    scale: 500})
  var totalCount = countDict.get('T21_count')
  // Create a featurecollection with null geometry
  // FeatureCollection helps because you can filter by properties
  return ee.Feature(null, {'date': ee.Image(image).get('start date'), 'totalCount': totalCount})
}
// Map the functions over all dates
var yearImages = startDateList.map(checkDateRange);
var yearCounts = ee.FeatureCollection(yearImages.map(totalPixelCountAOI))
print (yearCounts)
// Apply filter on results
var rangesWithNoFiresAOI = yearCounts.filter(ee.Filter.eq('totalCount', 0))
// Ranges with fire
var rangesWithFiresAOI = yearCounts.filter(ee.Filter.gt('totalCount', 0))
print('List of Fires in AOI', rangesWithFiresAOI.aggregate.array('date'))
```

```
{
  type: ImageCollection
  id: FIRMS
  version: 157946b97b766b96
  bands: 1
  *features: List (262 elements)
  *properties: Object (246 propert
  *FeatureCollection (75 elements)
  *List of Fires in AOI
  *List (5 elements)
  *0: Date (2018-04-01 00:00:00)
  *1: Date (2018-05-26 00:00:00)
  *2: Date (2018-05-31 00:00:00)
  *3: Date (2018-07-20 00:00:00)
  *4: Date (2018-08-29 00:00:00)
  table is
  *FeatureCollection (5 elements, 3
```

The result is that Five alarms were registered for the specified AOI in 2018. The corresponding data are shown in the list.



Figure 21: FIRMS Alarms in AOI

In Figure 21 the alarms registered for the given AOI are displayed. According to the list, five alarms have been registered, but only three are displayed. There are areas in which several alarms are registered during the year, but only the one with higher confidence is retained. Several alarms are then displayed as one alarm. Therefore, it is now necessary to check each individual alarm, when it took place and which alarms were registered several times.

The alarms are masked, vectorized and buffered for this purpose. The buffer or the expansion should ensure that the area can be completely covered by corresponding Sentinel-2 data. It should also be avoided that the edges aren't included in the calculation.

```

//Creation AOI mask for vectorization
var T21 = FIRMS_filtered.mosaic().clip(AOI).select('T21');
var zones = T21.gt(0);
zones = zones.updateMask(zones.neq(0));
Map.addLayer(zones, firesVis, 'zones', false);
//Creation of vector
var vectors = zones.addBands(T21).reduceToVectors({
  geometry: AOI,
  crs: T21.projection(),
  scale: 500,
  geometryType: 'polygon',
  eightConnected: false,
  labelProperty: 'zone',
  reducer: ee.Reducer.mean()});
//Function for creating buffer
var buffer = function(feature) {
  return feature.buffer(2000)};
//Creation buffer
var BoundsInAOI = vectors.map(buffer);
Map.addLayer (BoundsInAOI, {palette: ['F000FF']}, 'Bounds in AOI', false);

//-----Split the whole alarm in the single part -----

var bounds_AOI_West = BoundsInAOI.filterMetadata("system:index", "equals", "+5270+8474").first();
var GeometryWest = ee.Feature(bounds_AOI_West).geometry();
Map.addLayer(GeometryWest, {palette: ['F000FF']}, 'West');

var bounds_AOI_Center = BoundsInAOI.filterMetadata("system:index", "equals", "+5308+8474").first()
var GeometryCenter = ee.Feature(bounds_AOI_Center).geometry();
Map.addLayer(GeometryCenter, {palette: ['F000FF']}, 'Center');

var bounds_AOI_East = BoundsInAOI.filterMetadata("system:index", "equals", "+5344+8474").first()
var GeometryEast = ee.Feature(bounds_AOI_East).geometry();
Map.addLayer(GeometryEast, {palette: ['F000FF']}, 'East');

```

Then the total vector is split into the individual areas. Only from this point is it possible to assign the corresponding data to each displayed alarm. For the sake of clarity, the areas are now referred to as “Geometry West, Center and East”.



Figure 22: masked extension of alarms


```
// Example for one Single AOI
var newAOI = GeometryCenter
// Count total pixels within AOI GeometryWest
var totalPixelCountNewAOI = function(image) {
  var countDict = ee.Image(image).reduceRegion({
    reducer: ee.Reducer.count(),
    geometry: newAOI,
    scale: 500});
  var totalCount = countDict.get('TPI_count');
  // Create a FeatureCollection with null geometry
  // FeatureCollection helps because you can filter by properties
  return ee.Feature(null, {date: ee.Image(image).get('start_date'), 'totalCount': totalCount});
};
// Map the functions over all dates
var yearImages = startDatesList.map(checkDateRange);
var yearCounts = ee.FeatureCollection(yearImages.map(totalPixelCountNewAOI));
// print(yearCounts)
// Apply filter on results
var rangesWithNoFiresNewAOI = yearCounts.filter(ee.Filter.eq('totalCount', 0));
// Ranges with fire
var rangesWithFiresNewAOI = yearCounts.filter(ee.Filter.gt('totalCount', 0));
print('List Fire in newAOI:', rangesWithFiresNewAOI.aggregate_array('date'));

// Create 'dateOfInterest' for analysing the time Series before and after the fire
var dateOfInterest = ee.Date('2018-07-20');
var newDate = dateOfInterest;
var preFire = newDate.advance(-30, 'day');
var postFire = newDate.advance(30, 'day');
print('dateOfInterest is:', newDate); print('PreFireDate is:', preFire); print('PostFireDate is:', postFire);
```

```
GeometryCenter
* Polygon, 170 vertices

GeometryEast
* Polygon, 158 vertices
  type: Polygon
  * coordinates: List (1 element)

List Fire in newAOI:
= List (3 elements)
* 0: Date (2018-04-07 00:00:00)
* 1: Date (2018-05-21 00:00:00)
* 2: Date (2018-08-28 00:00:00)

dateOfInterest is:
* Date (2018-07-20 00:00:00)

PreFireDate is:
* Date (2018-06-20 00:00:00)

PostFireDate is:
* Date (2018-08-28 00:00:00)
```

The geometries and associated alarms are now listed. In the GeometryWest an alarm was registered on 2018-05-26, while in the GeometryCenter (see code below) three alarms were registered at different times, but which are displayed as a superimposed alarm. In GeometryEast only one alarm was recorded. To keep the workflow dynamic, only the appropriate AOI (the selected alarm) must be entered in the code to check the individual alarms.

The following checks whether actual burnt areas can be detected in Sentinel-2 data for each alarm date. As described in point 2.1.3, for each FIRMS active fire point, a 1km bounding box is defined. Pixels in the MODIS sinusoidal projection that intersect the FIRMS bounding box are identified. It is now necessary to compare whether each of these identified points can be found in the resolution of the Sentinel-2 data, or whether the mean geometric resolution of the data means that very small fires with a small extent cannot be detected.

- *Date of Interest 2018-07-20 in GeometryEast*

For the first example, it can now be seen that an alarm was detected in GeometryEast on 20 July 2018. In order to find the appropriate satellite images, a period before and after the alarm is defined as preFire and postFire. Due to the repetition rate of the Sentinel-2 satellites (5 days per satellite), 30 days before and 30 days after the alarm were selected to ensure cloud-free images for the detection of the burned areas. A longer period should not be chosen, as then different vegetation cycles already come into effect and can falsify the results. Furthermore, a longer period of time makes it more likely that past fires are included in the data.



```
List Fire in GeometryEast:
[{"type": "Date", "value": "2018-07-20 00:00:00"}]
  0: Date (2018-07-20 00:00:00)

PreFireDate is:
  Date (2018-06-20 00:00:00)

dateOfInterest is:
  Date (2018-07-20 00:00:00)

PostFireDate is:
  Date (2018-08-19 00:00:00)
```

Figure 23: selected Alarm with the dates in GeometryEast

For the period found, the corresponding Sentinel-2 data is loaded as an Image Collection. A more detailed analysis of the data regarding cloud coverage will follow later. This section only checks whether sentinel-2 data are available for the selected time period and geographic extent and whether burned areas can be displayed from this data by optical interpretation.



The band selection on the left side clearly shows the burned areas in the selected area. This section is therefore suitable for setting up an algorithm for the detection of burned areas.

Figure 24: False Color Image Collection for the interpretation of burnt areas

In Comparison the Sentinel-2 data before and after the event, presented as false colour composite in bands 12, 8A and 5.



Figure 25: False Color Composite on three different days with different cloud cover before and after the fire event

The website <https://apps.sentinel-hub.com/sentinel-playground/> offers the possibility to display all available Sentinel-2 data for any area. Here the optical comparison to the

found Image Collection from the GEE shall take place. The comparison of the data allows at first sight the detection of burned areas after the event (FIRMS-ALARM).

When the GeometryCenter is selected, three alarms are listed, which are then interpreted optically using Sentinel-2 data.

- *Date of Interest 2018-04-01 in the GeometryCenter*

List Fire in newAOI:

▼ List (3 elements)

- ▶ 0: Date (2018-04-01 00:00:00)
- ▶ 1: Date (2018-05-31 00:00:00)
- ▶ 2: Date (2018-08-29 00:00:00)

dateOfInterest is:

▶ Date (2018-04-01 00:00:00)

PreFireDate is:

▶ Date (2018-03-02 00:00:00)

PostFireDate is:

▶ Date (2018-05-01 00:00:00)






Figure 26: False Color Composites in the GeometryCenter for the first period

The data available after the event is used for visual interpretation. Now it can be seen that at the time of the FIRMS alarm there is no cloud cover, but no fire area can be localized. The following images are almost completely covered with clouds, so that no localization of the fire or burned area is possible. A cloudless image is only available about one month after the event, but burned areas cannot be detected optically. In this case, it may not be possible to detect burned surfaces with the help of the sentinel data and the associated mean spatial resolution of 20 m or the registered fire has not caused a burn area that could be detected in Sentinel-2 data.

- *Date of Interest 2018-05-31*

List Fire in newAOI:

▼ List (3 elements)

- ▶ 0: Date (2018-04-01 00:00:00)
- ▶ 1: Date (2018-05-31 00:00:00)
- ▶ 2: Date (2018-08-29 00:00:00)

dateOfInterest is:

▶ Date (2018-05-31 00:00:00)

PreFireDate is:

▶ Date (2018-05-01 00:00:00)

PostFireDate is:

▶ Date (2018-06-30 00:00:00)

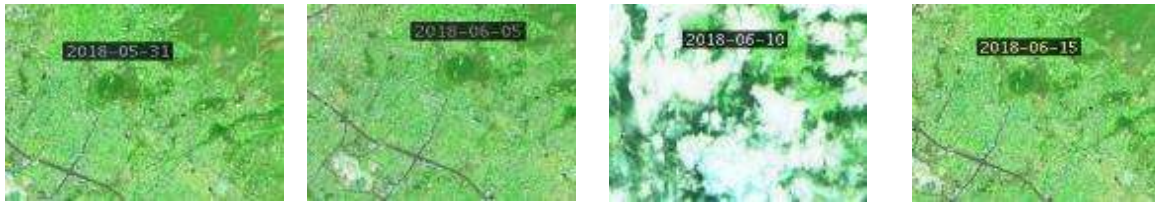


Figure 27: False Color Composites in the Geometry Center for the second period

The next period shows a similar picture. FIRMS probably perceive a higher temperature value which is perceived from a fire, but optical interpretation and detection of a burned area is not possible via the sentinel data.

- *Date of Interest 2018-08-29*

List Fire in newAOI:

▼ List (3 elements)

- ▶ 0: Date (2018-04-01 00:00:00)
- ▶ 1: Date (2018-05-31 00:00:00)
- ▶ 2: Date (2018-08-29 00:00:00)

dateOfInterest is:

▶ Date (2018-08-29 00:00:00)

PreFireDate is:

▶ Date (2018-07-30 00:00:00)

PostFireDate is:

▶ Date (2018-09-28 00:00:00)



Figure 28: False Color Composites in the Geometry Center for the third period

The third example is no different from the first two. With the help of the sentinel data, it is not possible to detect burned areas in the present area (GeometryCenter). However, it can be concluded, that there have been individual sources of fire in this area, which are recorded by MODIS but these cannot be localized due to the resolution of the sentinel data.

Overall it can be said that four out of five registered fires were either not detectable due to the geometric resolution of the Sentinel-2 data, or the fires apparently occurred very locally and did not create a burn area.

The complete code can be viewed in the Google Earth Engine with the following link:

<https://code.earthengine.google.com/310d86c8a2d73868f813baf66805e507>

4.2 Second Part of the workflow – Burned Area Monitoring

4.2.1 First Study Area – Rafina, Greece

The first study areas were selected from a registered event of the Copernicus Emergency Management Service (EMS) which allowed me to use the finally maps as a reference for the accuracy assessment. The 2018 fire season was chosen. The first event (Rafina - GREECE; (EMSR300 2018)), took place in the eastern part of Attica around the port of the city of Rafina on 23.-26. July 2018. It was a single, locally confined fire where 1,275.9 hectares were destroyed (EMSR300 2018). The fire destroyed over 700 houses and claimed 102 lives (2018 Attica wildfires).

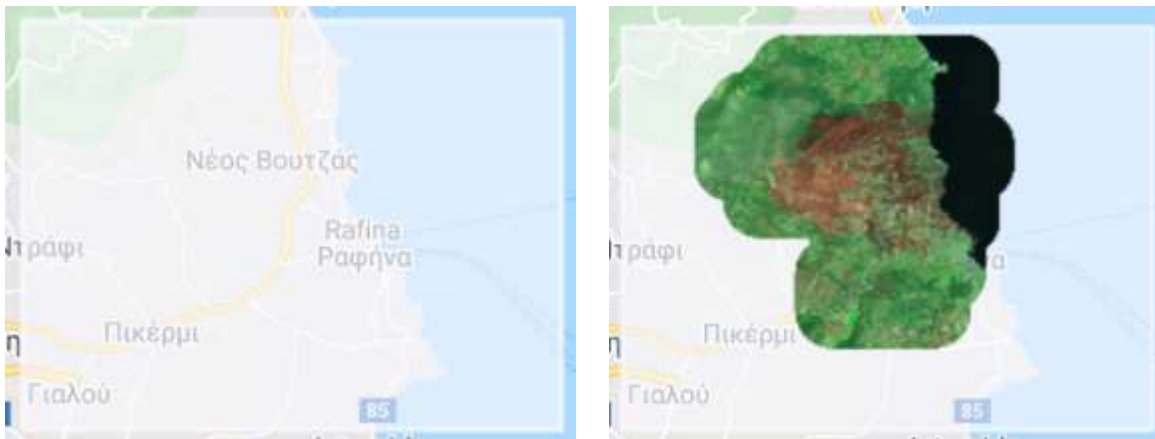


Figure 29: Study Area Rafina (left side); False Color Composite (B12, B8A, B5) Rafina, reduced to the new AOI

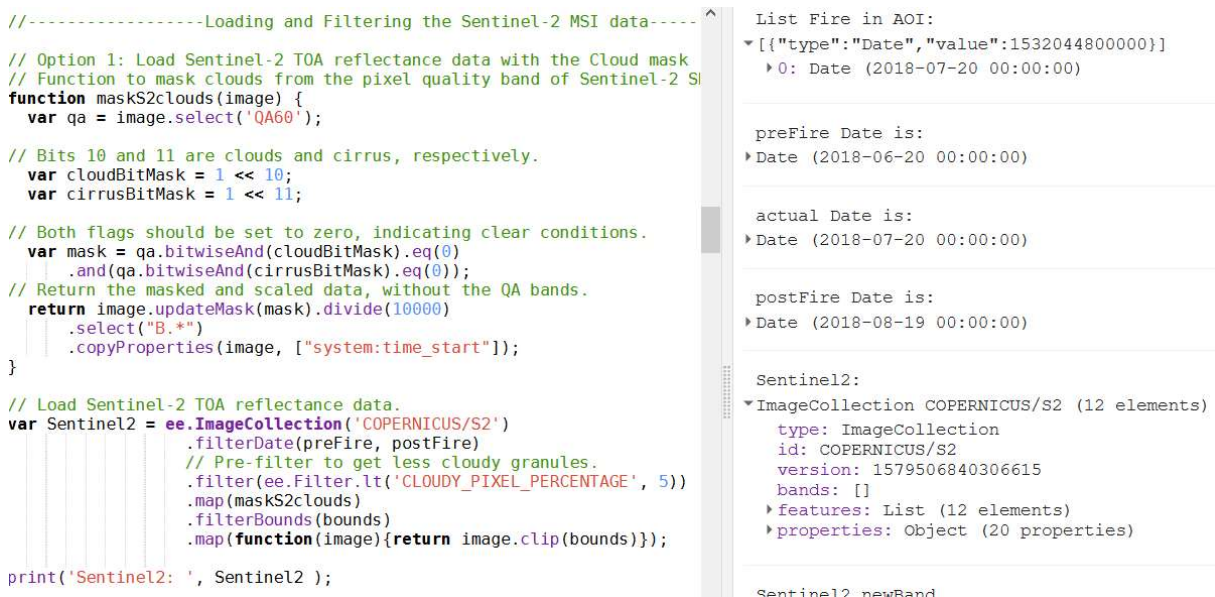
For the first example two different possibilities are presented to calculate and show burned areas in the study area.

4.2.2 Burned Area mapping using Sentinel-2 TOA reflectance data with the Cloud mask

In the first approach Sentinel-2 TOA (Top of Atmosphere) data together with the cloud mask provided by ESA will be used to create cloud-free images in a collection. In addition, only images in the collection with less than 5% cloudy pixels, using the metadata provided by ESA, are used. Many experiments with a higher Cloudy Pixel Percentage have shown that correct results are shown in the collection, but the individual images then have gaps due to the cloud mask (see the results in the conclusion). If the Cloudy Pixel Percentage is prefiltered, considerably fewer images will enter the collection, but there will be fewer holes in the data.

- *Filtering and Loading the Satellite Data*

In the first part, the cloud mask provided by ESA is loaded and applied to the Sentinel-2 data. The Image Collection now consists of twelve records, six records before the FIRMS alarm and six records after.



```
//-----Loading and Filtering the Sentinel-2 MSI data-----
// Option 1: Load Sentinel-2 TOA reflectance data with the Cloud mask
// Function to mask clouds from the pixel quality band of Sentinel-2 S
function maskS2clouds(image) {
  var qa = image.select('QA60');

  // Bits 10 and 11 are clouds and cirrus, respectively.
  var cloudBitMask = 1 << 10;
  var cirrusBitMask = 1 << 11;

  // Both flags should be set to zero, indicating clear conditions.
  var mask = qa.bitwiseAnd(cloudBitMask).eq(0)
    .and(qa.bitwiseAnd(cirrusBitMask).eq(0));
  // Return the masked and scaled data, without the QA bands.
  return image.updateMask(mask).divide(10000)
    .select("B.*")
    .copyProperties(image, ["system:time_start"]);
}

// Load Sentinel-2 TOA reflectance data.
var Sentinel2 = ee.ImageCollection('COPERNICUS/S2')
  .filterDate(preFire, postFire)
  // Pre-filter to get less cloudy granules.
  .filter(ee.Filter.lt('CLOUDY_PIXEL_PERCENTAGE', 5))
  .map(maskS2clouds)
  .filterBounds(bounds)
  .map(function(image){return image.clip(bounds)});

print('Sentinel2: ', Sentinel2 );
```

```
List Fire in AOI:
▼ [{"type": "Date", "value": 1532044800000}]
  ▶ 0: Date (2018-07-20 00:00:00)

preFire Date is:
▶ Date (2018-06-20 00:00:00)

actual Date is:
▶ Date (2018-07-20 00:00:00)

postFire Date is:
▶ Date (2018-08-19 00:00:00)

Sentinel2:
▼ ImageCollection COPERNICUS/S2 (12 elements)
  type: ImageCollection
  id: COPERNICUS/S2
  version: 1579506840306615
  bands: []
  ▶ features: List (12 elements)
  ▶ properties: Object (20 properties)

Sentinel2.newBand
```

Figure 30: Sentinel-2 TOA data in the investigation period

On the left side you can see the code for loading the data; on the right side the pre- and postfire period and the resulted Image Collection.

- *Creating a Water mask*

In order to limit burned areas to land areas and to avoid shadow effects, a Land/Water mask is created, which is generated from the NDWI (Water Index). The NDWI is designed to:

- maximize the reflectance of the waterbody in the green band
- minimize the reflectance of water body in the NIR band

(Du et al. 2016).

The NDWI is calculated as:

$$NDWI = \frac{\rho_{Green} - \rho_{NIR}}{\rho_{Green} + \rho_{NIR}}$$

Figure 31: Equation for NDWI

where ρ_{Green} is the TOA reflectance value of the green band and ρ_{NIR} is the TOA reflectance value of the NIR band. Comparing to the raw Digital Numbers (DN), TOA reflectance is more suitable in calculating NDWI (Du et al. 2016). The freely-available Sentinel-2 Level-1C dataset is already a standard product of TOA reflectance (European Space Agency 2019). McFEETERS (1996) points out that no additional pre-processing is required, and the NDWI for Sentinel-2 can be directly calculated as:

$$NDWI_{10m} = \frac{\rho_3 - \rho_8}{\rho_3 + \rho_8}$$

Figure 32: Equation for NDWI with selected bands

where ρ_3 is the TOA reflectance of the Band 3 (the green band) and ρ_8 is the TOA reflectance of the Band 8 (the NIR band). Band 3 and Band 8 of Sentinel-2 have the spatial resolution of 10 m, and thus, the calculated NDWI also has the spatial resolution of 10 m.

McFEETERS (1996) emphasize that a main limitation of the NDWI is that it cannot suppress the signal noise coming from the land cover features of built-up areas efficiently. Du et al. (2016) noticed that the water body has a stronger absorbability in

the SWIR band than that in the NIR band, and the built-up class has greater radiation in the SWIR band than that in the NIR band. Based on this finding, the MNDWI was proposed, which is defined as:

$$\text{MNDWI} = \frac{\rho_{\text{Green}} - \rho_{\text{SWIR}}}{\rho_{\text{Green}} + \rho_{\text{SWIR}}}$$

Figure 33: Equation for the MNDWI

where ρ_{SWIR} is the TOA reflectance of the SWIR band. In general, compared to NDWI, water bodies have greater positive values in MNDWI, because water bodies generally absorb more SWIR light than NIR light. Soil, vegetation and built-up classes have smaller negative values, because they reflect more SWIR light than green light (Du et al. 2016).

For Sentinel-2, the green band has the spatial resolution of 10 m, while the SWIR band (Band 11) has the spatial resolution of 20 m. Thus, the MNDWI needs to be calculated at a spatial resolution of either 10 m or 20 m (McFEETERS 1996). Since the NBR and dNBR are also calculated at 20 m, this is retained for the water index. The 20-m MNDWI is calculated as:

$$\text{MNDWI}_{20\text{m}} = \frac{\rho_3^{20\text{m}} - \rho_{11}}{\rho_3^{20\text{m}} + \rho_{11}}$$

Figure 34: Equation for calculation the MNDWI with the upscaled Band 3

where ρ_{11} is the TOA reflectance of Band 11 (SWIR) of Sentinel-2 and $\rho_{320\text{m}}$ is the TOA reflectance of Band 3 (green) of Sentinel-2 with a spatial resolution of 20 m (Du et al. 2016).

After upscaling Band 3 to 20 m resolution, the MNDWI is calculated as follows:

```
//-----Create a second Water mask-----//
// Create a Water mask from the MNDWI
// First resample and reproject the Green Band to 20 m
function addnewBand(image) {
  var band3 = Sentinel2.first()
  .select('B3');
  var band11 = Sentinel2.first()
  .select('B11');
  //print('CRS:', band11.projection().crs());
  var band3new = band3
  .reduceResolution
  ({reducer: ee.Reducer.mean(),
  maxPixels: 1024}).resample('bilinear')
  // Request the data at the scale and projection of the band 11.
  .reproject
  ({crs: band11.projection().crs(),
  scale: 20}).rename('Green20m');
  return image.addBands(band3new);}
var Sentinel2_newBand = Sentinel2.map(addnewBand);
// Create a function to calculate MNDWI per image
function addMNDWI(image) {
  // Compute the MNDWI
  var vis = image.select('Green20m');
  var swir = image.select('B11');
  var mndwi = vis.subtract(swir).divide(vis.add(swir)).rename('MNDWI');
  return image.addBands(mndwi);}
var Sentinel2_MNDWI = Sentinel2_newBand.map(addMNDWI);
// Select MNDWI from ImageCollection
var mndwi = Sentinel2_MNDWI.select('MNDWI');
// Calculate Median of all images
var medianMNDWI = mndwi.median();
Map.addLayer(medianMNDWI.clip(bounds), {min:-1, max:1, palette:['brown','white','blue']}, 'MNI')
// Change this threshold to allow more or less water in mask
var mndwiThreshold = 0.35;
var water2 = medianMNDWI.gt(mndwiThreshold);
var land2 = water2.eq(0);
Map.addLayer(water2.clip(bounds), {min:0, max:1, palette:['black','blue']}, 'water', false);
Map.addLayer(land2.clip(bounds), {min:0, max:1, palette:['black','brown']}, 'land', false);
var watermask2 = water2.updateMask(water2);
Map.addLayer(watermask2, {min:0, max:1, palette:['black','blue']}, 'watermask', false);
```

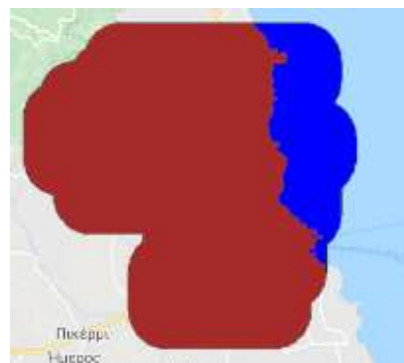


Figure 35: MNDWI (Water in blue, Land in light brown) on the left side; Land- and Water Mask on the right side

The newly created image collection still contains twelve images, but each of these has been extended by the band 'green20m' and the 'MNDWI'. The threshold value for generating a land mask was chosen purely empirically and will certainly have to be adapted for other test areas.

- Calculating the NBR

In the next step, the NBR is calculated for each image in the collection. This is calculated from the difference between the bands NIR and SWIR. With regard to the calculation of the delta (dNBR), i.e. the difference between a before and after image, the system index is converted and added as “date” to the collection as a separate property for each image, so that each image can later be offset against its previous image.

```
// Create a function to calculate NBR per image
function addNBR(image) {
  // Compute the NBR
  var nir = image.select('B04');
  var swir = image.select('B12');
  var nbr = nir.subtract(swir).divide(nir.add(swir)).rename('NBR');
  return image.addBands(nbr);
}

var Sentinel2_collection = Sentinel2.map(addNBR);
.map(function(image) {
  var date = ee.Date(image.get('system:time_start')).format('YYYY-MM-DD');
  return image.set('date', ee.Date(date));
});
.map(function(image) {
  var ID = ee.String(image.get('system:index'));
  return image.set('id', ID);
});
.map(function(image) {
  var date = ee.Date(image.get('system:time_start'));
  return image.set('date_time', date);
});
// clip image to the landmask
.map(function(image){
  return image.updateMask(landmask2);
});

var NBR = Sentinel2_collection.select('NBR').sort('system:time_start');

//make a list of all NBR
var NBRlist = ee.List(NBR.aggregate_array('system:time_start'));
print ('NBRlist ', NBRlist);
//-----//
```

```
*ImageCollection COPERNICUS/S2 (12 elements)
type: ImageCollection
id: COPERNICUS/S2
metadata: 1579588040306615
bands: []
*features: List (12 elements)
*0: Image (14 bands)
  type: Image
  *bands: List (14 elements)
  *0: "B1", float [0, 6.553500175476074], EPSG
  *1: "B2", float [0, 6.553500175476074], EPSG
  *2: "B3", float [0, 6.553500175476074], EPSG
  *3: "B4", float [0, 6.553500175476074], EPSG
  *4: "B5", float [0, 6.553500175476074], EPSG
  *5: "B6", float [0, 6.553500175476074], EPSG
  *6: "B7", float [0, 6.553500175476074], EPSG
  *7: "B8", float [0, 6.553500175476074], EPSG
  *8: "B8A", float [0, 6.553500175476074], EPSG
  *9: "B9", float [0, 6.553500175476074], EPSG
  *10: "B10", float [0, 6.553500175476074], EPSG
  *11: "B11", float [0, 6.553500175476074], EPSG
  *12: "B12", float [0, 6.553500175476074], EPSG
  *13: "NBR", float, EPSG:32634, 5490x5490 px
*properties: Object (3 properties)
  ID: 20180630T090551_20180630T091915_T340GH
  date: Date (2018-06-30 09:05:50)
  date_time: Date (2018-06-30 09:19:15)
  system:index: 20180630T090551_20180630T091915
  system:time_start: 1530350550
```

Figure 36: Images with the new Band “NBR” and the added “date” property

- Calculating the delta NBR

As mentioned above, NBR is frequently used to estimate burn severity. Imagery collected before a fire will have very high near infrared band values and very low mid infrared band values and an Imagery collected over a forest after a fire will have very low near infrared band values and very high mid infrared band values. The dNBR can so be used for burn severity assessment, as areas with higher dNBR values indicate more severe damage whereas areas with negative dNBR values might show increased vegetation productivity.

The result is an Image Collection with a newly added band called 'NBRdiff'. The values of this band result from the difference between the NBR of a before and after image.

```
// Create a function to calculate dNBR per image
var NBRdiff = ee.ImageCollection.fromImages(NBRlist.map(function(date){
  // get the image corresponding to the date
  var currentImage = NBR.filter(ee.Filter.eq('system:time_start', date))
  // get the 'previous' image in the collection
  var indexCurrent = NBRlist.indexOf(date);
  var indexPrevious = ee.Algorithms.If(indexCurrent.eq(0), indexCurrent,
  var datePrevious = NBRlist.get(indexPrevious);
  var previousImage = NBR.filter(ee.Filter.eq('system:time_start', date)
  // Subtract the current image from the previous
  var diffImage = previousImage.subtract(currentImage).select(['NBR']).[0];
  // return the image
  return currentImage.addBands(diffImage)
  .set('system:index_previous', previousImage.get('system:indo
}));
// print and add to the map
print('Difference image collection', NBRdiff);
```

```
*2: Image (2 bands)
type: Image
bands: List (2 elements)
#0: "NBR", float, EPSG:32634, 5490x5490 px
#1: "NBRdiff", float, EPSG:32634, 5490x5490 px
properties: Object (6 properties)
ID: 20180705T091019_20180705T091702_T140GH
date: Date (2018-07-05 09:03:00)
date_time: Date (2018-07-05 09:17:02)
system:index: 2
system:index_previous: 20180630T090551_20180630
system:time_start: 153078222920
```

As you can see, a new band was added to each image, which contains the values from the difference of two images. The date of the before and after image is shown to see which two images were offset at which time.

Burned areas can only be displayed if the Difference is higher than the previous image. Therefore, in the next step, all pixel values of the 'NBRdiff' per image within the buffered FIRMS Alarm extent are summed and the image with the highest summed values is selected. In the best and most probable case, this image is after the fire event.

```
// -----Get the dNBR image with the highest summed value-----//
// compute summed value for every image
var NBRdiffsum = NBRdiff.map(function(img) {
  var sum = img.reduceRegion({ reducer: ee.Reducer.sum(), geometry: bounds, scale: 20 })
  return img.set(sum.get('NBRdiff'))
})
// list with the summed values
print('NBRdiffsum is: ', NBRdiffsum.aggregate_array('sum'))
// image with the summed value
var NBRdiffmaxSummedValue = ee.Image(NBRdiffsum.sort('sum', false).first())
// date of the image with the maximum value
print('Date is: ', NBRdiffmaxSummedValue.date())
print('NBRdiffmaxSummedValue is: ', NBRdiffmaxSummedValue)
```

```
NBRdiffsum is:
*List (12 elements)
Date is:
*Date (2018-08-04 09:10:49)
NBRdiffmaxSummedValue is:
*Image (2 bands)
type: Image
bands: List (2 elements)
#0: "NBR", float, EPSG:32634, 5490x5490 px
#1: "NBRdiff", float, EPSG:32634, 5490x5490 px
properties: Object (7 properties)
ID: 20180804T090849_20180804T091349_T140GH
date: Date (2018-08-04 09:08:00)
date_time: Date (2018-08-04 09:13:49)
sum: 14065.25620089865
system:index: 6
system:index_previous: 20180715T090549_20180715
system:time_start: 153170844920
```

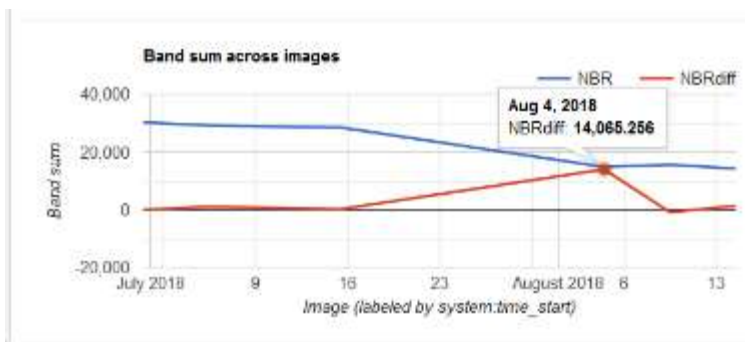


Figure 37: highest summed dNBR

The Image from 2018-08-04 has the highest summed dNBR value. This means that on this date the burned area can also be interpreted and detected optically. A fire event inevitably leads to a higher Cloud Cover in the image. In case of a strong fire event, the image may even be almost completely covered by a cloud cover. The previously set cloud mask and the filtering based on Cloud Cover leads to a high number of images being excluded from the collection, especially after the fire event. In principle, a fire event can be detected relatively quickly in satellite images. However, the filtering mentioned above leads to the fact that an Image Collection is only available with a time interval in which all the conditions mentioned apply and the area of fire is recognizable.

The result is then multiplied by 1000 to bring it into line with the USGS standard and to better find the thresholds for classification.

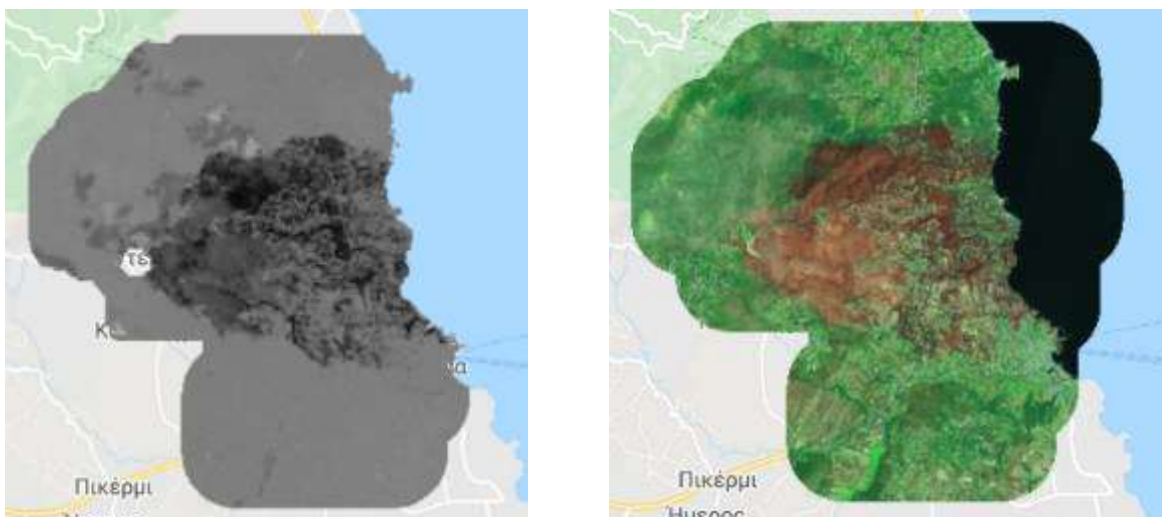


Figure 38: dNBR (left side) and False Color image (right side), both in 20 m resolution

In the left picture the burned area can be seen very well due to its very dark demarcation to the surroundings. However, the disadvantage of the cloud mask becomes apparent. In very simple terms the cloud mask is generated in an Image Collection according to the following scheme: As described in point 2.1.2 special bands of the satellite are used to detect clouds (no matter if Dense Clouds or Cirrus Clouds). Since an Image Collection is always calculated and created from the mean values of all existing images, clouds are usually replaced by information from previous or subsequent images. If there are not enough cloud-free images in a collection, the information cannot be “replaced” and a “gap” remains in the record. This is shown very well in this example.

The darker areas in the north-west of the area show another problem. The cloud mask used probably did not recognize all parts of the Cirrus cloud cover and therefore there are faulty areas in the image. These are certainly not burnt areas, as they are not visible in the optical data set. It is therefore a high ice cloud cover, which is not contained in the cloud mask and is therefore recorded due to the reflectivity in the dNBR and was therefore incorrectly classified. These areas can be identified particularly well in the classification. Here, these areas are classified as 'low severity' and, in contrast to the optical data set, are immediately conspicuous.

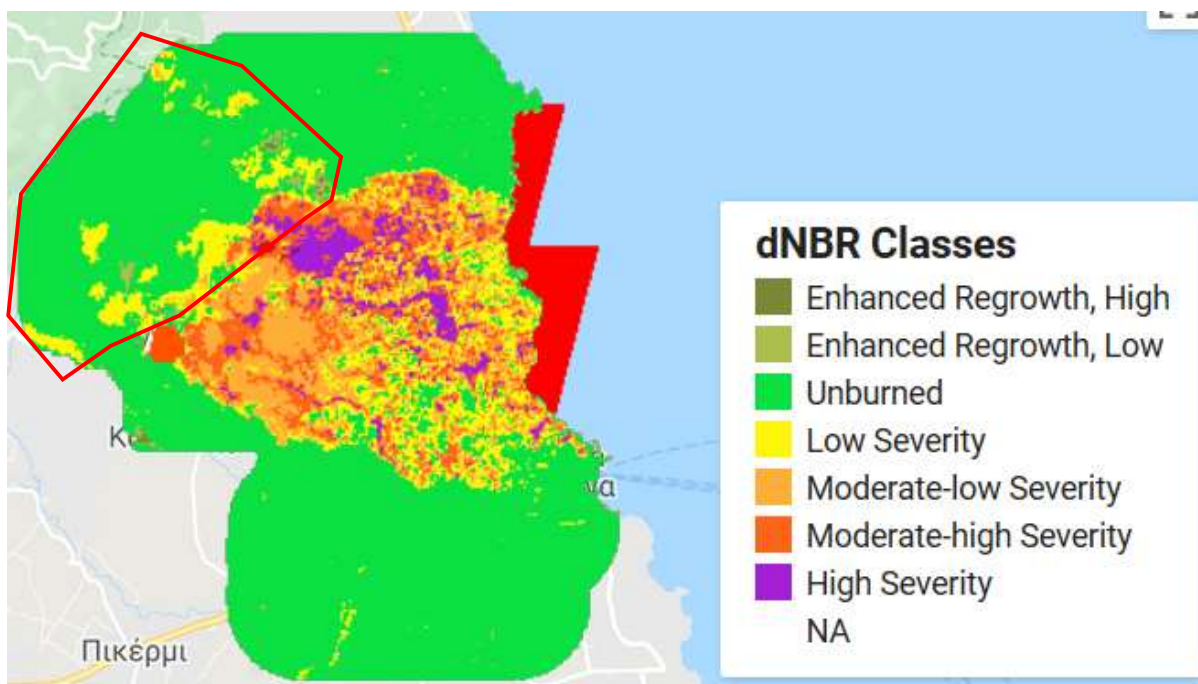


Figure 39: classified dNBR and faulty areas

- *Creating the Fire Mask and Comparison of burned areas to FIRMS alarm*

With the result as dNBR it is now possible to create a thematic layer using a threshold value, which is used as a comparison to the FIRMS alarm. The threshold value was derived from a purely empirical method. The data of the FIRMS alarm are also masked. Only in this way is it possible to compare the area of the alarm with the area of the classified fire area. The goal is thus a computational comparison of both areas to be able to deduce whether the detection of burned areas with the help of Sentinel-2 data is possible and reasonable compared to the FIRMS data.

```
//-----Create a binary mask for burned areas using a threshold-----//
// Create a binary mask for burned areas with a Threshold

var FiremaskThreshold = 99;
var Firemask = dNBR_scaled.gt(FiremaskThreshold).reduce('sum').toInt();
Map.addLayer(Firemask.updateMask(Firemask), {palette: ['FF7F50']}, 'Firemask');

// get the statistic (pixel count and area in ha) for the Firemask
var statFiremask = Firemask.reduceRegion({
  reducer: ee.Reducer.sum(),
  geometry: bounds,
  scale: 20,
  maxPixels: 1e9});
print ('Sum Pix for Firemask is: ', statFiremask);
var pixelArea = Firemask.multiply(ee.Image.pixelArea());
var totalArea = pixelArea.reduceRegion('sum', bounds, 20);
var pix = ee.Number(statFiremask.get('sum'));
var hect = pix.multiply(400).divide(10000);
print ('total Area in ha for Firemask', hect);

// Create a binary mask for the FIRMS alarm.
var FIRMS_mask = FIRMS_StudyArea.max();
var FIRMS_mask_bounds = ee.Image(FIRMS_mask).clip(bounds);
var T21mask = FIRMS_mask_bounds.eq(1);
Map.addLayer(T21mask, {palette: ['FFFF00']}, 'T21mask');

//Comparison between masked FIRMS data and the brand mask generated from the workflow
var CompT21Firemask = T21mask.eq(1).or(Firemask.eq(1)).reduce('sum').toInt();
Map.addLayer(CompT21Firemask.updateMask(CompT21Firemask), {palette: ['FF00FF']}, 'Comparison');

var statsCompT21Firemask = CompT21Firemask.reduceRegion({
  reducer: ee.Reducer.sum(),
  geometry: bounds,
  scale: 20,
  maxPixels: 1e9});
print ('Sum Pix from Comparison between T21 and Firemask: ', statsCompT21Firemask);
var pixelAreasCompT21Firemask = CompT21Firemask.multiply(ee.Image.pixelArea());
var totalAreasCompT21Firemask = pixelAreasCompT21Firemask.reduceRegion('sum', bounds, 20);
var pixComp = ee.Number(statsCompT21Firemask.get('sum'));
var hectComp = pixComp.multiply(400).divide(10000);
print('total Area in ha for Comparison between T21 and Firemask:', hectComp);
```

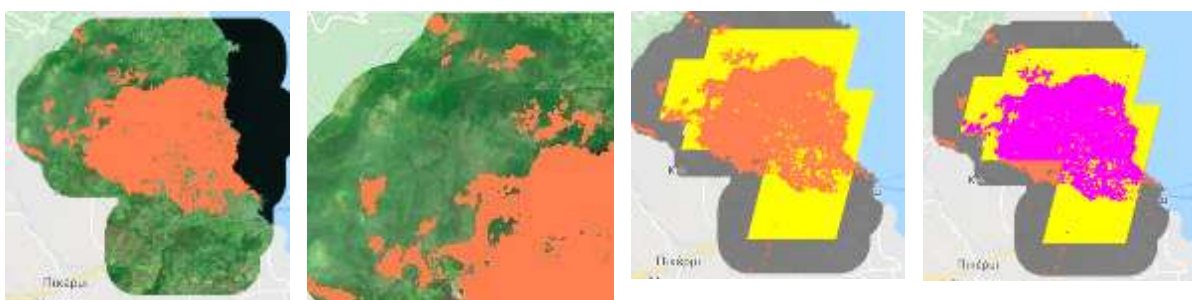


Figure 40: optical image in False Color, overlaid with the Fire mask, false detected parts, FIRMS Alarm (yellow) and the Fire mask (orange) as Overlay and Area of the fire mask (pink) which is covered by the FIRMS alarm

As mentioned above and also can be seen in Figure 40, the area which results from the calculation of the dNBR as burned area has faulty areas. Especially the north-western part of the study area is affected. A comparison with the alarm shows this quite quickly. From the optical data it can be seen that despite a cloud mask, a slight

cirrus cloudiness is present in this area, which leads to erroneous values in the dNBR. In this area, a large part of the area is vegetation. If they were affected by the fire, this would be visible in the optical image. Therefore, it can be assumed that the dNBR has incorrect values in this area.

```

Sum Pix for Firemask is:
▼Object (1 property)
  sum: 37834.90196078431

total Area in ha for Firemask
1513.3960784313724

Sum Pix from Comparison between T21 and Firemask:
▼Object (1 property)
  sum: 33752

total Area in ha for Comparison between T21 and Firemask:
1350.08

```

Figure 41: Statistics for burned area and the Comparison between Alarm and Fire mask

The statistics of the burned area show that according to the calculation almost 1.514 ha of area were burnt. It is not clear whether the burned area is vegetation or urban. A comparison with the FIRMS data shows an area of 1.350 ha. This means that 1350 ha can be detected overlapping with the FIRMS alarm. Thus, it shows up that from Sentinel-2 data with the first method an approximately similar area can be detected, as made available by FIRMS.

The complete code can be viewed in the Google Earth Engine with the following link:

<https://code.earthengine.google.com/293383468679d1a5a088e54eb06009f2>

4.2.3 Burned Area mapping using Sentinel-2 TOA reflectance data without the Cloud mask

As shown in the first method, the cloud mask provided leads to holes in the data. In addition, using the cloud mask leads to the fact that the resulting Image Collection does not include a lot of meta data, e.g. the Cloudy Pixel Percentage. Now we will try to find out whether different or more accurate results can be expected without using the cloud mask. The goal is to modify the existing workflow in such a way that only the NBR images before and after the event are selected which have the lowest Cloudy Pixel Percentage. Therefore, the workflow is modified as follows:

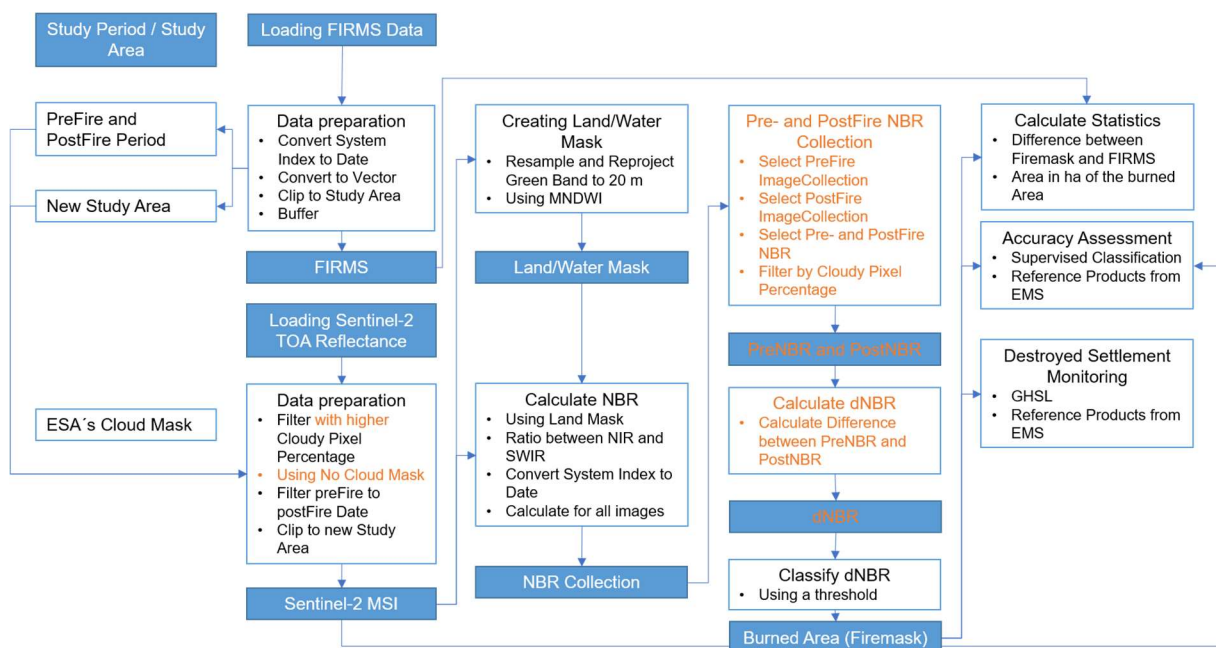


Figure 42: adjusted workflow (significant changes are shown in red)

- *Loading the data and Calculating the NBR for the land area for the entire collection*

First, the data is loaded without using the cloud mask and the NBR for the land area is calculated for the entire collection. Then only the data with the lowest Cloudy Pixel Percentage in the image will be used.

// Option 2: Load Sentinel-2 TOA reflectance data and without the Cloud Mask

```
var S2Data = ee.ImageCollection('COPERNICUS/S2')
  .filterDate(preFire, postFire)
  .filter(ee.Filter.lt('CLOUDY_PIXEL_PERCENTAGE', 20))
  .filterBounds(bounds)
  .map(function(image){return image.clip(bounds)});

// Create a function to calculate NBR per image
function addNBR(image) {
  // Compute the NBR
  var nir = image.select('B8A');
  var swir = image.select('B12');
  //var nbr = S2_MNDWI.normalizedDifference(['B8A', 'B12']).rename('NBR');
  var nbr = nir.subtract(swir).divide(nir.add(swir)).rename('NBR');
  return image.addBands(nbr)
}
// add the NBR
var S2_collection = S2Data.map(addNBR)
  .map(function(image) {
var date = ee.Date(image.get('system:time_start')).format("YYYY-MM-dd");
return image.set('date', ee.Date(date));
  })
  .map(function(image) {
var ID = ee.String(image.get('system:index'));
return image.set('ID', ID);
  })
  .map(function(image) {
var date = ee.Date(image.get('system:time_start'));
return image.set('date_time', date);
  })
// clip image to the landmask
  .map(function(image){
return image.updateMask(landmask)//.addBands(watermask.clip(bounds));
  });

print('S2_collection is: ', S2_collection)

// select the nbr from the whole imagecollection
// calculate the dNBR = preNBR - postNBR

var nbr = S2_collection.select('NBR').sort('system:time_start');

print ('nbr', nbr)
Map.addLayer(nbr.select('NBR'), {min: -1, max: 1, palette: grey}, 'NBR', false);

var newlist = ee.List(nbr.aggregate_array('system:time_start'))//.slice(1); // remove
print ('newlist ', newlist)
```

- *Selecting the preFire and postFire NBR*

After the successful calculation of the NBR for each image in the collection, the data is separated as PreFire Collection and PostFire Collection. Then the NBR is selected and finally filtered for the lowest Cloudy Pixel Percentage in the image. The result is a single PreFire and PostFire record (Fig. 43). Finally, the dNBR can be calculated from this.

```
//-----Select preFire and postFire ImageCollection for the Data-----//
// select the preNBR and the postNBR because of the CLOUDY_PIXEL_PERCENTAGE
// get the preFire ImageCollection with the NBR
var S2_collection_preFire = ee.ImageCollection(S2_collection)
  .filterDate(preFire, newDate);
// get the postFire ImageCollection with the NBR
var S2_collection_postFire = ee.ImageCollection(S2_collection)
  .filterDate(newDate, postFire);
// get the PreFire Image with the NBR, only the image with the fewest Cloudy Pixel Percentage
var S2_preFire = ee.ImageCollection(S2_collection_preFire)
  .sort('CLOUDY_PIXEL_PERCENTAGE')
  .first();
// get the postFire Image with the NBR, only the image with the fewest Cloudy Pixel Percentage
var S2_postFire = ee.ImageCollection(S2_collection_postFire)
  .sort('CLOUDY_PIXEL_PERCENTAGE')
  .first();
var preNBR = S2_preFire.select('NBR');
var postNBR = S2_postFire.select('NBR');
```

preNBR is:

```
▼ Image COPERNICUS/S2/20180705T091019_20180705T091702_T34SGH (1 band)
  type: Image
  id: COPERNICUS/S2/20180705T091019_20180705T091702_T34SGH
  version: 1530903317239804
  ▶ bands: List (1 element)
  ▶ properties: Object (64 properties)
```

postNBR is:

```
▼ Image COPERNICUS/S2/20180814T090549_20180814T091348_T35SKC (1 band)
  type: Image
  id: COPERNICUS/S2/20180814T090549_20180814T091348_T35SKC
  version: 1534372313562650
  ▶ bands: List (1 element)
  ▶ properties: Object (64 properties)
```

Figure 43: pre- and postNBR

As a result, the before image with the lowest cloud coverage is from the SGH tile, while the after image is from the SKC tile. However, since the two tiles overlap the study area, these differences can be neglected for the area.



Figure 44: Pre- and PostFire Data in False Color (left side); Pre- and PostNBR in greyscale (right side)

In Figure 44 the before and after image is shown as a false color image. The burned area can be seen very well in the after image. This is also reflected in the NBR images. The very bright areas, which are a sign of high reflectance in the MIR and low reflectance in the NIR, also allow the conclusion to be drawn about burned areas.

- *Calculating the dNBR*

For the calculation of the dNBR two data sets received after the selection are subtracted from each other according to Equation 4.

```
// difference between pre- and postfire NBR
var dNBR_unscaled = preNBR.subtract(postNBR);

// Scale product to USGS standards
var dNBR_oneImage = dNBR_unscaled.multiply(1000);

print("Difference Normalized Burn Ratio: ", dNBR_oneImage);
```

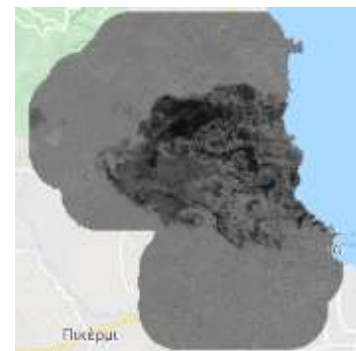


Figure 45: Calculating the dNBR and the result

The modification of the workflow shows good results. At first glance, the very dark areas show the burnt areas and are congruent with the optically interpretable areas from the satellite images. The following classification of the dNBR into different degrees of severity of the burned areas is shown in Fig. 46. Here it can be seen that despite the exclusion of shadow areas with the help of the MNDWI the very dark areas of the dNBR are erroneously indicated as 'low Severity'. Nevertheless, very good results can be achieved with the workflow.

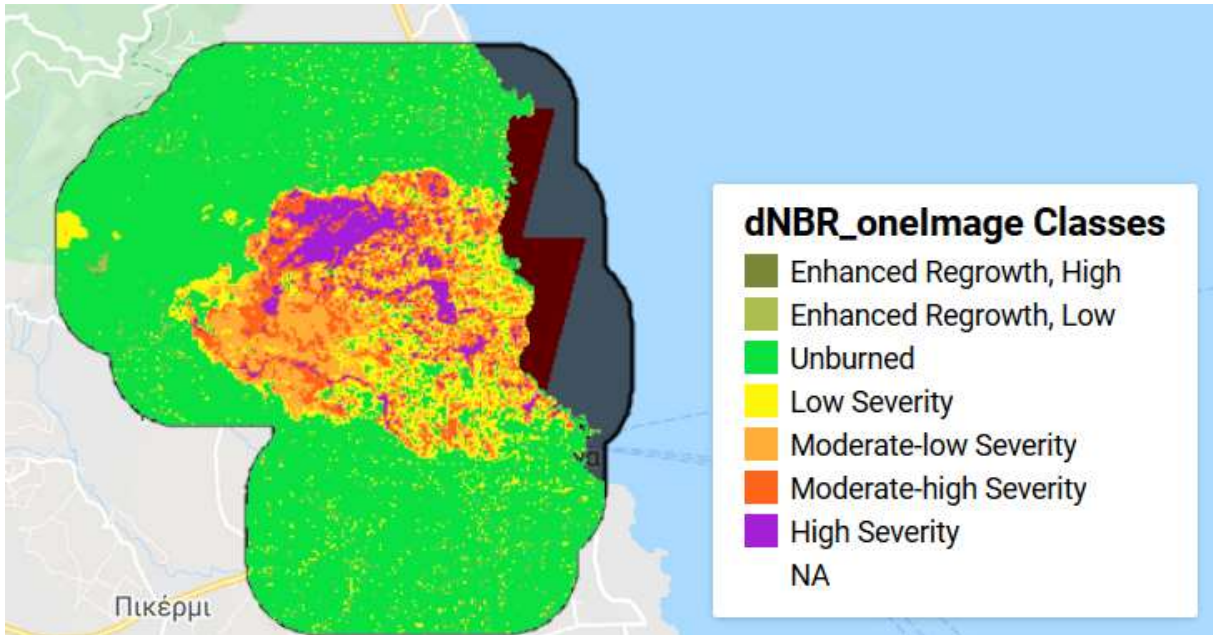


Figure 46: dNBR in grayscale and classified dNBR

The following statistics on the area size of the resulting fire mask confirm this.

- *Creating the Fire Mask*

In the next step a fire mask is created from the dNBR using a threshold value. From this in turn, the number of pixels and area size in ha can be derived.

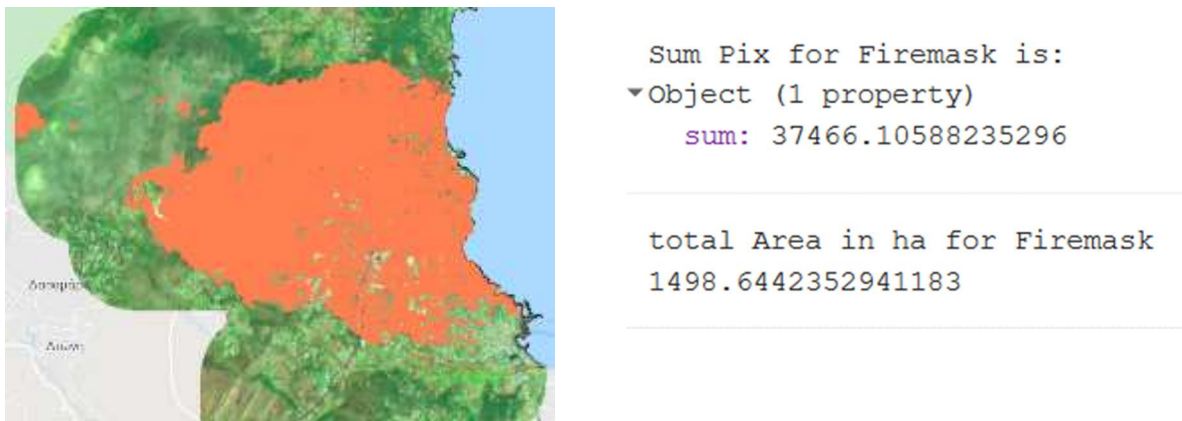
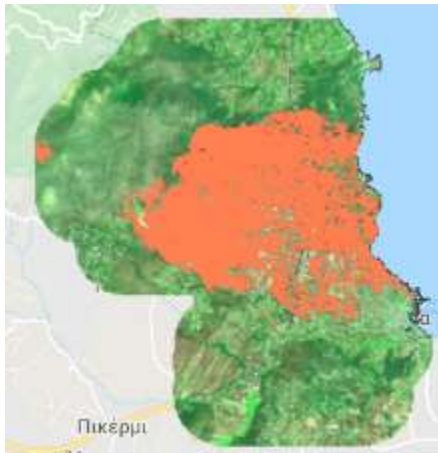


Figure 47: generated Fire mask from the second Option and Statistic

The newly created mask is shown in Figure 46. Already at first sight you can see the faulty areas, which extend over the whole picture. Although the optically identifiable burned area is well covered by the mask and also the area size resembles strongly the first Mask, there are individual pixels over the entire image which are incorrectly classified as burnt. Therefore, an adjustment of the threshold is necessary to reduce the erroneous areas. After numerous tests, the limit value 200 or 0.2 is set as the best result (see Fig. 48).



```
Sum Pix for Firemask is:  
▼ Object (1 property)  
  sum: 29847.043137254903
```

```
total Area in ha for Firemask  
1193.881725490196
```

Figure 48: generated Fire mask with the new Threshold from the second Option

After adjusting the threshold value for the second method, the result is a fire area mask which shows a large coverage to the visually interpreted fire area. The area is now reduced to almost 1200 ha. Missing pixels, with the exception of an area in the western part of the study area, are not visible.

The complete code can be viewed in the Google Earth Engine with the following link:

<https://code.earthengine.google.com/ff3aaa5dc39be47bebda55f7ec89ecb3>

- Comparison between the two Fire Masks

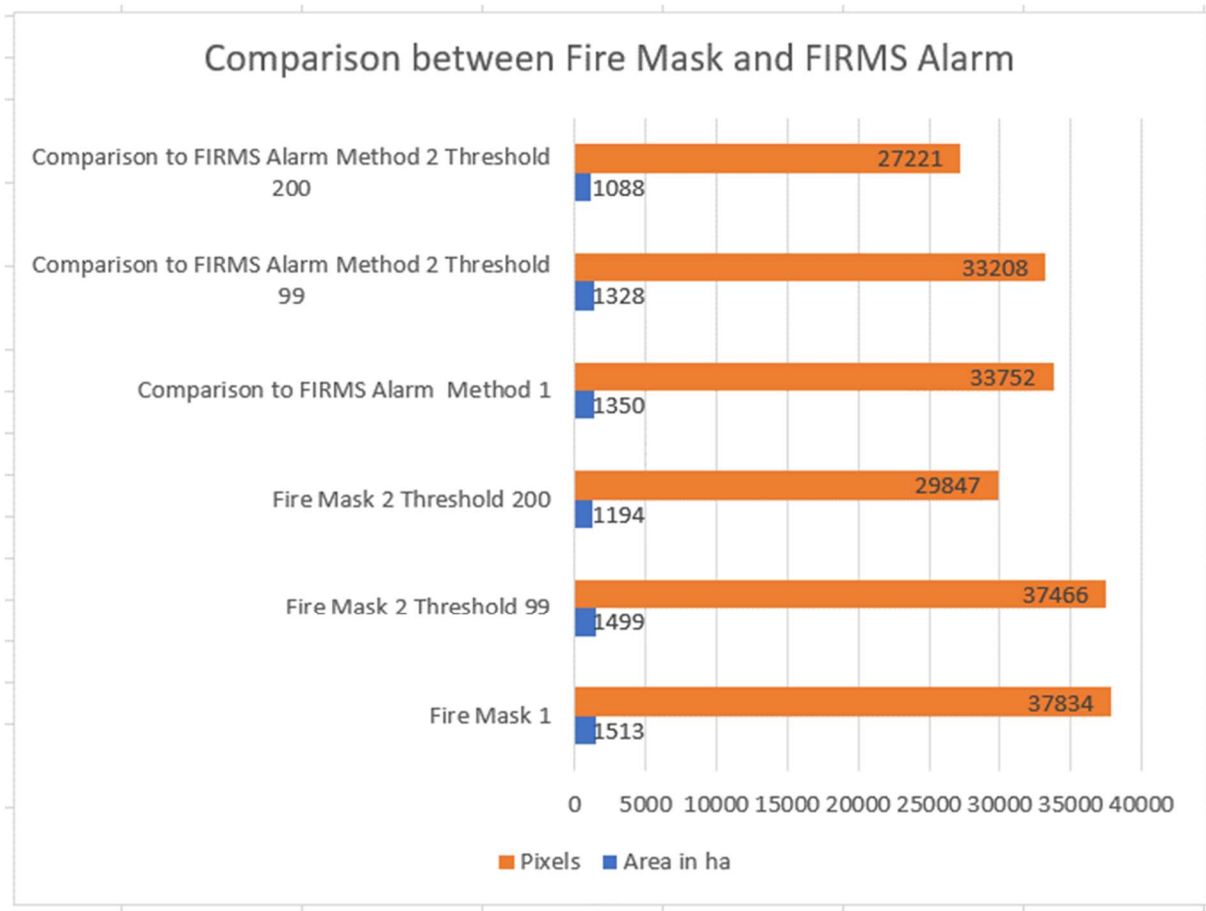


Figure 49: Comparison between the Fire Masks and the FIRMS Alarm

When comparing the individual fire masks to each other, it can be seen that the largest burnt area is detected when using the cloud mask in the first method. When using an Image Collection and the provided Cloud mask it results in 1.513 ha burnt area. Without the use of a Cloud mask and a filtering according to the lowest Pixel Percentage, almost 1.500 ha are detected as burnt area with a threshold of 99. This is very similar to the result of the first method, but there are many incorrectly detected pixels in the image. After adjusting the threshold, the faulty areas could be eliminated, the area size is reduced to almost 1.200 ha.

The comparison of the fire masks with the area size of the alarm shows a similar picture. With the first method, 1.350 ha can be detected consistently. With the second method 1.328 ha are found overlapping with a lower threshold value and 1.088 ha with a higher value.

A first conclusion can be drawn by comparing the two results to the optically identifiable burnt area. The greatest agreement with the existing FIRMS Alarm is achieved by the first method. In addition, the result provides the greatest coverage of the optically identified burnt area. If the same threshold value is used in the second workflow, there is a similarly high degree of agreement with the alarm, but many incorrectly classified pixels occur throughout the entire data set. Increasing the threshold value solves the problem of misclassified pixels, but as a result has the lowest coverage to the FIRMS alarm.

In the following, both methods will be tested with the help of a supervised classification.

4.2.4 Accuracy Assessment with a supervised Classification

Multispectral classification is the process of sorting pixels into a finite number of individual classes, or categories of data, based on their data file values. If a pixel satisfies a certain set of criteria, the pixel is assigned to the class that corresponds to that criteria. This process is also referred to as image segmentation. Depending on the type of information you want to extract from the original data, classes may be associated with known features on the ground or may simply represent areas that look different to the computer.

In a supervised classification, reference classes are used. This ensures which class the classification result is. The following steps are usually performed:

- Determination of land use or land cover classes (spectral classes such as coniferous forest, deciduous forest, water, agriculture, etc.)
- Survey of suitable training areas (reference areas for each class)
- Implementation of the actual classification with the help of a suitable classification algorithm
- Verification, evaluation and verification of results

The general workflow for classification in the Google Earth Engine (Google Earth Engine 2019) is:

- Selection of the appropriate image from an Image Collection.
- Collect training data.

Merges characteristics that have a common property, a common class label, and the same numeric values.

- Instantiate a classifier.
- Train the classifier using the training data.
- Classify an image or feature collection.
- Estimate classification error with independent validation data.

The training data is a Feature Collection with a property storing the class label and properties storing predictor variables. Training and/or validation data can come from a variety of sources. To collect training data interactively in Earth Engine, it is possible to use the geometry drawing tools. Using `ee.Classifier` to get a classifier from one of the constructors and `classifier.train()` to train the classifier. Classify an Image or Feature Collection you have to use the command `classify()` (Google Earth Engine 2019).

- *Supervised Classification of the Image*

The first step is to select the appropriate image and to collect the training data. The typical Land Use classes and the class "burnedArea" were chosen.

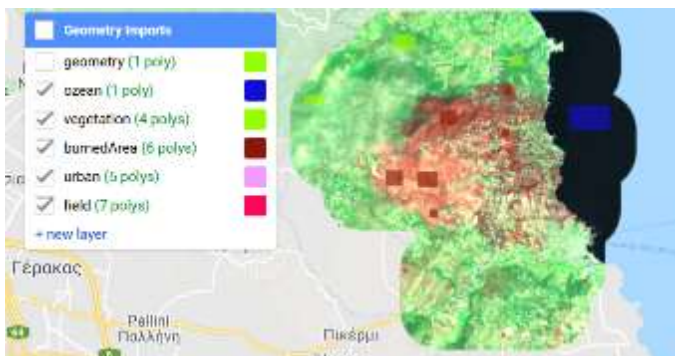


Figure 50: collected Training Data

After loading a cloud free Single Image and collecting the training data you have to make a Feature Collection for each class (5 total) and to merge them into one Feature Collection using the command `FeatureCollection.merge()`. This will convert them into one collection in which the property **landcover** has a value that is the class (0 - 4). The Feature Collection called **training** has the reflectance value from each band stored for every training point along with its class label.

In the next step I have to instantiate a classifier using the command `ee.Classifier.randomForest()` and train it on the Training data specifying the features to

use (training), the landcover categories as the class Property I want to categorize the imagery into, and the reflectance in Band 2 – Band 12 (without Band 1, 9 and 10 because of the 60 m spatial resolution) of the Sentinel-2 imagery as the input Properties.

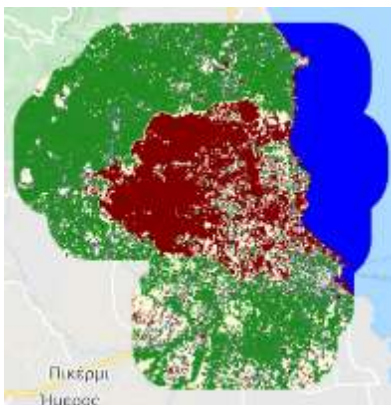
There are many automatic land classification algorithms, such as minimum distance classification (MDC), maximum likelihood classification (MLC), classification and regression trees (CART), random forest (RF), support vector machine (SVM), back propagation (BP) neural network, multiscale segmentation, and object-oriented classification methods (Hu und Hu 2019). Akar und Güngör (2012) compared the classification accuracy of RF, SVM, and MLC in the Trabzon region of Turkey based on multispectral imagery. Similarly, many relevant researchers have used the different classification algorithms described above to conduct research in different research areas. Hu und Hu (2019) accentuate that the given model parameters and environments in different study areas differ, so it is difficult to determine which classification algorithm is the most common and broadly applicable. Since the comparison of the methods should not be the subject of this work, I join the most widespread method and exclusively use the randomForest classifier for this work because the random forest classifier is an established classifier that can accommodate non-monotonic and nonlinear relationships between predictor variables (Kumar und Roy 2017), can handle correlated variables and does not make assumptions about the statistical distributions of the variables (Kumar und Roy 2017). Random forests are an ensemble form of decision tree classifications in which many trees are grown by recursively partitioning a random subset of the training data into more homogeneous subsets called nodes (Kumar und Roy 2017). The random forest classifier reduces the probability of over-matching predictor variables to the training data by independently matching a large number of decision trees, each tree growing using a random substitute of the training data and a limited number of randomly selected predictor variables (Kumar und Roy 2017).

At the end the Image will be classified with the *classify* command and displayed it.

```

var newfc = ozean.merge(vegetation).merge(burnedArea).merge(urban).merge(field);
print(newfc, 'newfc')
// Select the bands for training
var bands = ['B2', 'B3', 'B4', 'B5', 'B6', 'B7', 'B8', 'B8A', 'B11', 'B12'];
// Sample the input imagery to get a FeatureCollection of training data.
var training = S2_Oneimage.select(bands).sampleRegions({
  collection: newfc,
  properties: ['landcover'],
  scale: 20
});
// Make a Random Forest classifier and train it.
var classifier = ee.Classifier.randomForest().train({
//var classifier = ee.Classifier.cart().train({
  features: training,
  classProperty: 'landcover',
  inputProperties: bands
});
// Classify the input imagery.
var classified = S2_Oneimage.select(bands).classify(classifier);
// Define a palette for the Land Use classification.
var palette = [
  '0000FF', // water (0) // blue
  '228B22', // vegetation (1) // green
  '800000', // burnedArea (2) // brown
  '708090', // urban (3) // grey
  'FFF8DC' // field (4) // light brown
];
// Display the classification result and the input image.
Map.addLayer(classified, {min: 0, max: 4, palette: palette}, 'Land Use Classification');
// Get a confusion matrix representing resubstitution accuracy.
print('RF error matrix: ', classifier.confusionMatrix());
print('RF accuracy: ', classifier.confusionMatrix().accuracy());

```



```

Classified pixel count within region
▼Object (1 property)
  ▼classification: Object (5 properties)
    0: 29463.580392156913
    1: 73847.26274509795
    2: 33702.3568627451
    3: 22456.89411764707
    4: 20719.592156862764

```

```

Burned Area (ha) in region
1348.094274509804

```

Figure 51: Basic Land Use Classification and Statistic of the classified burned area

The result shows the classification with the five selected classes. In addition, it is indicated that 1349 ha of land have been classified as burnt. In the southern part of the scene and on the shore, however, the areas that have not been burnt can be seen very well. In the southern part of the scene it is mainly arable land with a similar spectral signature which is wrongly classified as burnt land. In the eastern part it is the transition area between land and water, which is wrongly classified over the whole scene. Unfortunately, adapting the test areas did not lead to better results.

To get an idea of how well or poorly the pixels have been classified, I assess the accuracy of the trained classifier using a confusion Matrix. In this particular example, I am just looking at the trainAccuracy, which basically describes how well the classifier was able to correctly label resubstituted training data, i.e. data the classifier had already seen (see code below).

- *Confusion Matrix representing accuracy*

	Actually Ocean	Actually Vegetation	Actually Burned Area	Actually Urban	Actually Field	Accuracy
Classified Ozean	1980	0	0	0	0	100 %
Classified Vegetation	0	1313	0	5	7	99,1 %
Classified Burned Area	0	0	1937	0	0	100 %
Classified Urban	0	5	1	46	0	88,5 %
Classified Field	0	5	2	1	144	94,7 %
Accuracy	100 %	99,2 %	99,8 %	88,5 %	95,4 %	99,5 %

Figure 52: Confusion Matrix representing resubstitution accuracy

The Matrix shows, that 100% of actual Ocean pixels are classified as Ocean, 99,2% of actual Vegetation pixels are classified as Vegetation, 99,8% of actual Burned Area pixels are classified as Burned Area, 88,5% of actual Urban pixels are classified as Urban and 95,4% of actual Field pixels are classified as Field. The matrix also shows that 100% of classified Burned Area pixels are burned Area on the Map. In total, 99,5% of all pixel match with the actual map.

To get a true validation accuracy, I need to show the *classifier* new ‘testing’ data. The code at the end holds out data for testing, applies the *classifier* to the testing data and assesses the *errorMatrix* for this withheld validation data.

- *Error Matrix for the classified image*

```

var trainingData_test = trainingS2_Oneimage.randomColumn('random');
var trainingS2_Oneimage = trainingData_test.filterMetadata('random', 'less_than', 0.8);
var validationS2_Oneimage = trainingData_test.filterMetadata('random', 'not_less_than', 0.8);
// Train a RF classifier with default parameters.
var trainedS2_Oneimage = ee.Classifier.randomForest().train(trainingS2_Oneimage, 'landcover', bands);
// Classify the image with the same bands used for training.
var classifiedS2_Oneimage = S2_Oneimage.select(bands).classify(trainedS2_Oneimage);

//Accuracy assessment

var validation = validationS2_Oneimage.classify(trainedS2_Oneimage);
var errorMatrixS2_Oneimage = validation.errorMatrix('landcover', 'classification');
var acc = ee.FeatureCollection([
  ee.Feature(null, { // feature as dictionary and without geometry
    "array": errorMatrixS2_Oneimage.array(),
    "Validation overall accuracy": errorMatrixS2_Oneimage.accuracy(),
    "Consumers Accuracy": errorMatrixS2_Oneimage.consumersAccuracy(),
    "Producers Accuracy": errorMatrixS2_Oneimage.producersAccuracy(),
    "Kappa coefficient": errorMatrixS2_Oneimage.kappa(),
  })
]);
Export.table.toDrive({
  collection: acc,
  description: "AccuracyS2_Oneimage",
  folder: "GEE",
  fileNamePrefix: "AccuracyS2_Oneimage",
  fileFormat: "CSV"});

```

Figure 53: Earth Engine Code to get a true validation accuracy

ErrorMatrix	364	0	0	0	0
	0	280	0	1	2
	0	0	410	0	1
	0	0	0	5	2
	0	2	1	1	30

		Consumers Accuracy	Producers Accuracy	Kappa coefficient	Validation overall Accuracy
Classification without dNBR	Ocean	100,00%	100,00%	98,70%	99,10%
	Vegetation	99,20%	98,90%		
	burned Area	99,70%	99,70%		
	Urban	71,40%	71,40%		
	Field	85,70%	88,20%		

Figure 54: error matrix and the Validation overall accuracy

The result of the supervised classification or the associated Confusion Matrix shows an overall accuracy of 99,1 %. This means that most pixels were classified correctly and especially burnt areas, on which the main focus lies, could be classified very well.

- Supervised classification of the image compared to the dNBR for Method 1

The results of the supervised classification can now be used to compare how well the dNBR was classified. For this purpose, the result of the differenced NBR (NBRdiff) is included in the supervised classification.

```
// Classify the NBRdiff with the supervised classification
// Add the NBRdiff as a band to the image
var NBRdiff2 = NBRdiffmaxValue.select('NBRdiff');
print ('NBRdiff2', NBRdiff2);
var image2 = S2_Oneimage.addBands(NBRdiff2);

//print(image2);

var fc = ozean.merge(vegetation).merge(burnedArea).merge(urban).merge(field);
var bands = ['NBRdiff'];
var training = image2.select(bands).sampleRegions({
  collection: fc,
  properties: ['landcover'],
  scale: 20,
  geometries:true
});

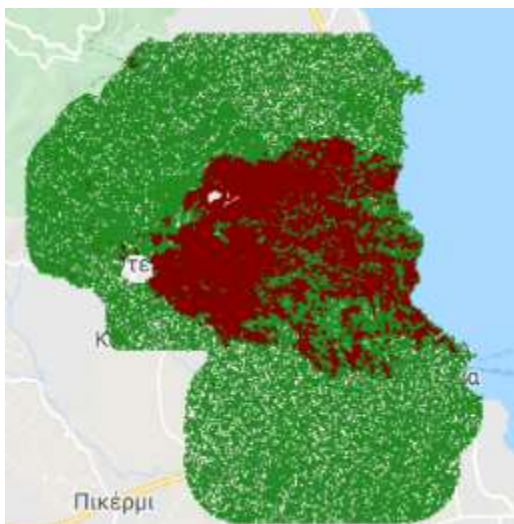
var classifier2 = ee.Classifier.randomForest().train({
  features: training,
  classProperty: 'landcover',
  inputProperties: bands
});

var classified2 = image2.select(bands).classify(classifier2);

Map.addLayer(classified2,
{min: 0 , max: 4, palette: ['0000FF', '228B22', '800000','708090','FFF8DC']},
'dNBR class');

var trainAccuracy2 = classifier2.confusionMatrix();
print('Resubstitution error matrix: ', trainAccuracy2);
print('Training overall accuracy: ', trainAccuracy2.accuracy());
```

Figure 55: supervised classification of the differenced NBR



```
Resubstitution error matrix:
▼List (5 elements)
  ▶ 0: [0,0,0,0,0]
  ▶ 1: [0,997,7,20,44]
  ▶ 2: [0,4,1551,0,0]
  ▶ 3: [0,15,0,23,1]
  ▶ 4: [0,40,0,4,68]
```

```
Training overall accuracy:
0.9513338139870223
```

Burned Area (ha) in region
1015.6

Figure 56: Land Use Classification with dNBR and Statistic of the classified burned area

By adding the dNBR as a reference to the supervised classification, the area classified as burnt has been reduced to 1016 ha.

	Actually Ocean	Actually Vegetation	Actually Burned Area	Actually Urban	Actually Field	Accuracy
Classified Ozean	0	0	0	0	0	0
Classified Vegetation	0	997	7	20	44	93,4 %
Classified Burned Area	0	4	1551	0	0	99,7 %
Classified Urban	0	15	0	23	1	59 %
Classified Field	0	40	0	4	68	60,7 %
Accuracy	0	94,4 %	99,9 %	48,9 %	60,2 %	95,1 %

Figure 57: Confusion Matrix representing resubstitution accuracy for Method 1

With the differenced NBR as a reference the accuracy of the supervised classification changes as follows: Ocean is not classified because the NBRdiff is only calculated for the landcover parts. 94,4 % of actual Vegetation pixels are classified as Vegetation, 99,9 % of actual Burned Area pixels are classified as Burned Area, 48,9 % of actual Urban pixels are classified as Urban and 60,2 % of actual Field pixels are classified as Field. The matrix also shows that 99,7 % of classified Burned Area pixels are burned Area on the Map. In total, 95,1 % of all pixel match with the actual map.

```

var trainingData_test = trainingImage2.randomColumn('random');
var trainingImage2 = trainingData_test.filterMetadata('random', 'less_than', 0.8);
var validationImage2 = trainingData_test.filterMetadata('random', 'not_less_than', 0.8);
// Train a RF classifier with default parameters.
var trainedImage2 = ee.Classifier.randomForest().train(trainingImage2, 'landcover', bands);
// Classify the image with the same bands used for training.
var classifiedImage2 = image2.select(bands).classify(trainedImage2);

//Accuracy assessment

var validation = validationImage2.classify(trainedImage2);
var errorMatrixImage2 = validation.errorMatrix('landcover', 'classification');
var acc = ee.FeatureCollection([
  ee.Feature(null, { // feature as dictionary and without geometry
    "array": errorMatrixImage2.array(),
    "Validation overall accuracy": errorMatrixImage2.accuracy(),
    "Consumers Accuracy": errorMatrixImage2.consumersAccuracy(),
    "Producers Accuracy": errorMatrixImage2.producersAccuracy(),
    "Kappa coefficient": errorMatrixImage2.kappa(),
  })
]);
Export.table.toDrive({
  collection: acc,
  description: "AccImage2Method1",
  folder: "GEE",
  fileNamePrefix: "AccImage2Method1",
  fileFormat: "CSV"});

```

Figure 58: Earth Engine Code to get a true validation accuracy

The true validation accuracy is listed below.

Matrix with dNBR	0	0	0	0	0
	0	226	3	6	20
	0	3	421	0	0
	0	7	0	2	0
	0	19	0	2	15

		Consumers Accuracy	Producers Accuracy	Kappa coefficient	Validation overall Accuracy
Classification Method 1 with dNBR	Ocean	0	0,00%	84,40%	91,70%
	Vegetation	88,60%	88,60%		
	burned Area	99,30%	99,30%		
	Urban	20,00%	22,20%		
	Field	42,90%	41,60%		

Figure 59: error matrix and the Validation overall accuracy for Method 1

Consumers Accuracy and Producers Accuracy now make it clear that with the help of the dNBR vegetation and burnt areas show a high overall accuracy. Other land cover classes such as Urban and Field are no longer properly classified. However, these classes are not incorrectly classified but are no longer considered by the dNBR. It can therefore be assumed that the dNBR was classified very well in this workflow.

The complete code can be viewed in the Google Earth Engine with the following link:

<https://code.earthengine.google.com/0b6fdd32d670ec0e00edb056440e61cd>

- *Supervised classification of the image compared to the dNBR for Method 2*

A supervised classification for the second method is now also performed for comparison purposes. Since the image was already classified with method 1, only the single-dNBR is added as a band and the classification is performed. At the end, I will also evaluate how well the dNBR was classified using the second method. In order to be able to make a statement about whether and which method is considered the better one, the same "Landcover" classes and training areas were used as for method 1.



Resubstitution error matrix:

```

List (5 elements)
  ▶ 0: [0,0,0,0,0]
  ▶ 1: [0,1003,1,14,50]
  ▶ 2: [0,0,1554,0,1]
  ▶ 3: [0,18,0,16,5]
  ▶ 4: [0,47,0,2,63]
    
```

Training overall accuracy:
0.9502523431867339

Burned Area (ha) in region2
1348.9440000000006

Figure 60: land cover dataset and Training overall accuracy from the single dNBR and statistic for burned area

The result shows that 1.349 ha were burnt using the dNBR from the second method. For comparison with the previous method, which indicated 1.016 ha as burnt, 333 ha more are now shown.

	Actually Ocean	Actually Vegetation	Actually Burned Area	Actually Urban	Actually Field	Accuracy
Classified Ocean	0	0	0	0	0	0
Classified Vegetation	0	1003	1	14	50	93,9 %
Classified Burned Area	0	0	1554	0	1	99,9 %
Classified Urban	0	18	0	16	5	41 %
Classified Field	0	47	0	2	63	56,25 %
Accuracy	0	93,9 %	99,9 %	50 %	52,9 %	95 %

Figure 61: Confusion Matrix representing resubstitution accuracy for Method 2

With the single dNBR as a reference the accuracy of the supervised classification changes as follows: Ocean is not classified because the single dNBR is only calculated

for the landcover parts. 93,9 % of actual Vegetation pixels are classified as Vegetation, 99,6 % of actual Burned Area pixels are classified as Burned Area, 50 % of actual Urban pixels are classified as Urban and 52,9 % of actual Field pixels are classified as Field. The matrix also shows that 99,9 % of classified Burned Area pixels are burned Area on the Map. In total, 95 % of all pixels match also with the actual map.

The true validation accuracy is shown below

Matrix with dNBR	0	0	0	0	0
	0	204	4	4	27
	0	0	397	0	0
	0	4	0	1	1
	0	29	0	1	9

		Consumers Accuracy	Producers Accuracy	Kappa coefficient	Validation overall Accuracy
Classification Method 2 with dNBR	Ocean	0	0,00%	80,70%	89,70%
	Vegetation	86,10%	85,40%		
	burned Area	99,00%	100,00%		
	Urban	16,70%	16,70%		
	Field	24,30%	23,10%		

Figure 62: error matrix for the Validation overall accuracy for Method 2

Consumers Accuracy and Producers Accuracy now make it clear that with the help of the single dNBR vegetation and burnt areas show also a high overall accuracy, but vegetation is no longer so well classified. It can therefore be assumed that the single dNBR was also classified very well in this workflow but is worse overall than with the first method.

The complete code can be viewed in the Google Earth Engine with the following link:

<https://code.earthengine.google.com/d6a158a8832d6d6a6e2d9f2a3c037b9a>

Comparison of the results:

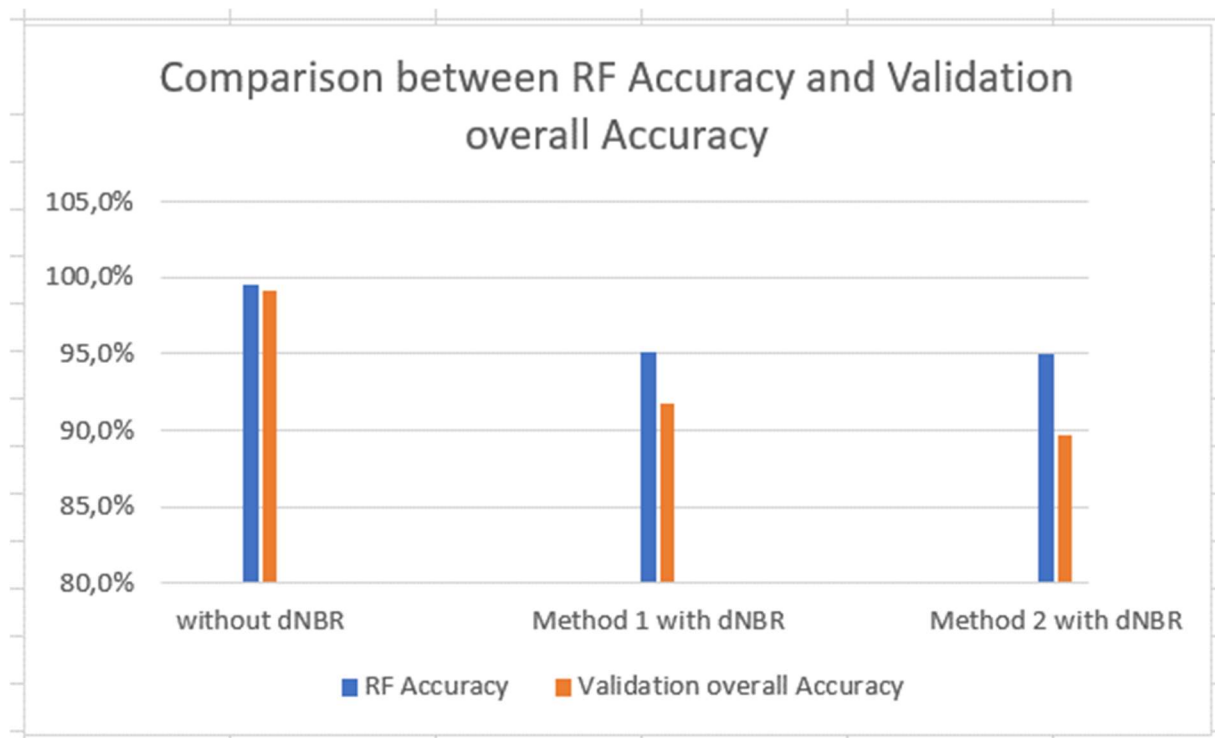


Figure 63: Comparison between RF Accuracy and Validation overall Accuracy

The overall accuracy of the three different land cover datasets was 0.99 for the land cover dataset without the dNBR, 0.91 for the classified dNBR land cover dataset generated from the First method and 0.89 for the classified dNBR land cover dataset from the second method which used the lowest cloudy pixel percentage. The kappa coefficient was between 0.99 and 0.80. Especially the validation overall Accuracy achieves higher values with the first method, because significantly fewer incorrectly classified pixels appear in the dNBR and thus show a higher agreement with the supervised classification.

COMPARISON BETWEEN CONSUMERS AND PRODUCERS ACCURACY

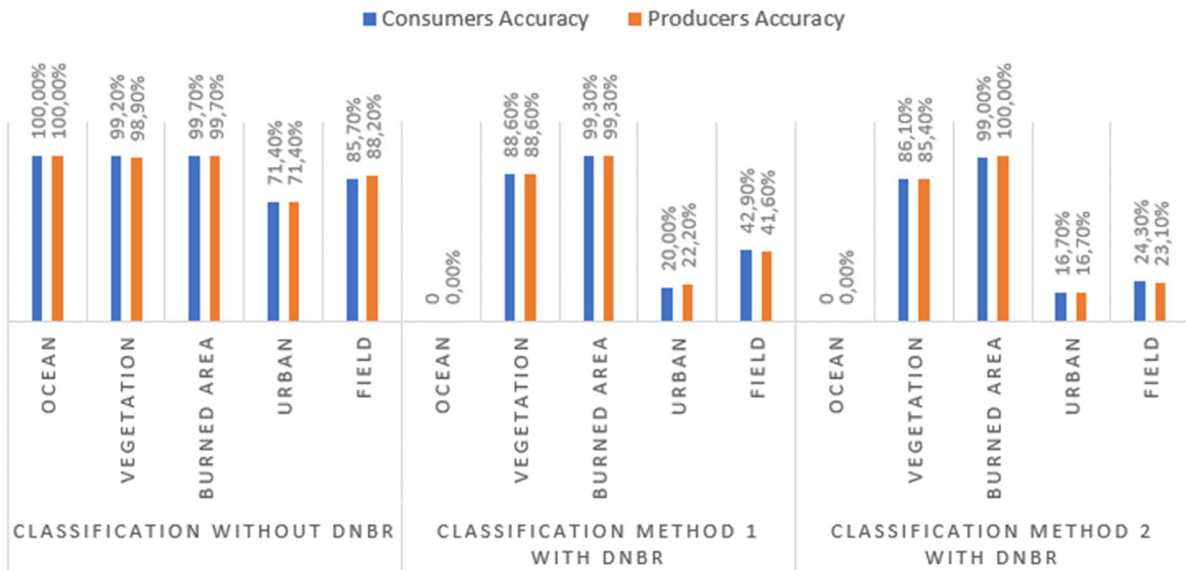


Figure 64: Comparison between Consumers and Producers Accuracy

Further analysis showed that Vegetation and burned area exhibited higher classification accuracy than Urban and Field, and the Consumers Accuracy and the Producers Accuracy values were above 0.85. The accuracy was low for Urban and Field, with a Consumers Accuracy between 0.17 and 0.20 and Producers Accuracy between 0.24 and 0.42, considered in each case for the classified dNBR classifications. The comparison for the Urban and Field classes shows that better accuracy is achieved with the first method than with the second.

The comparison of the methods confirms the first assumption that better results are achieved with the first method.

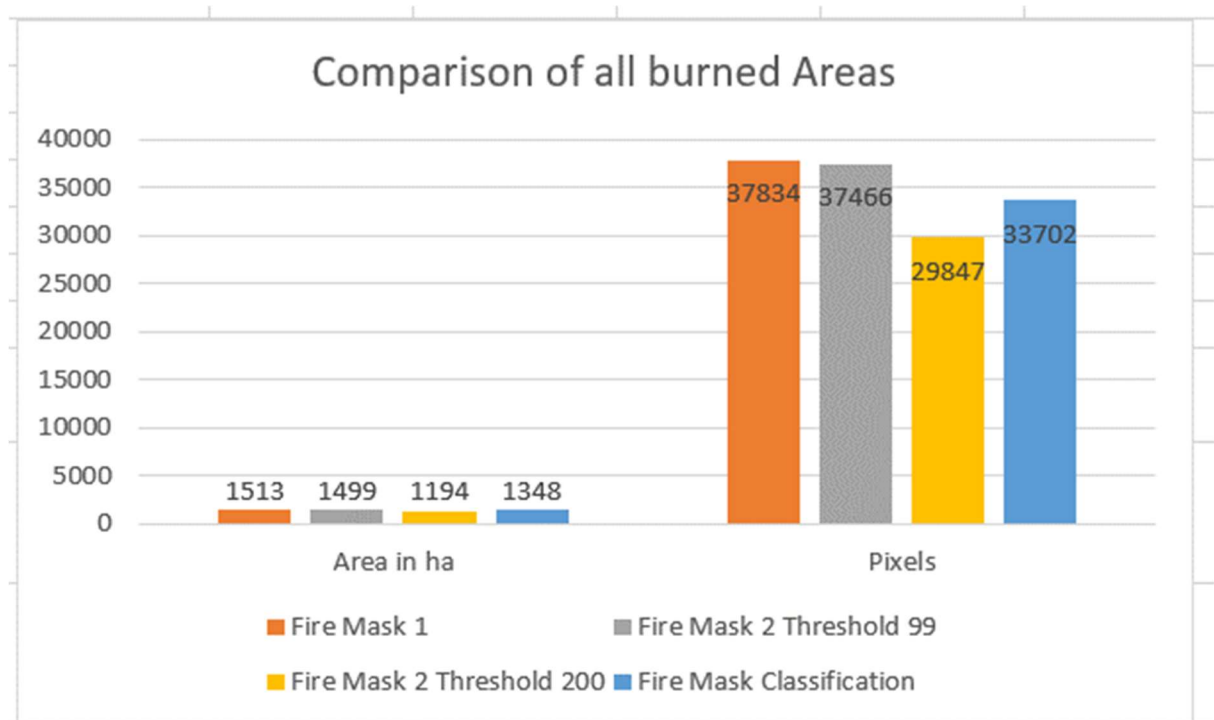


Figure 65: Comparison of all burned areas

Looking at all statistics and results I come to the conclusion that both workflows are suitable to detect burn areas in Sentinel-2 data, but overall the first method gives better results and is more user-friendly and automated. Both methods have their advantages and disadvantages. In the first workflow, which is much more automated, the biggest problems and therefore also the wrongly classified areas are in shadow areas of clouds. Even NDWI / MNDWI cannot localize these areas completely, so that in these areas fundamentally erroneous results are to be expected. All in all, it is user-friendly, since only a few settings need to be made to adapt to the existing scene. The second workflow is more user-defined, especially with thresholds for the delimitation of areas. In addition, more work steps are necessary to find the appropriate pre- and post-images. It therefore does not run automatically. In addition, it leads to erroneous areas distributed over the entire image, especially where the spectral signature is very similar to the burnt area. In the end, however, the second workflow also delivers very good results, taking into account the incorrect individual pixels.

A final comparison with the provided data of the EMS should verify both workflows in comparison to each other.

4.2.5 Accuracy Assessment with the EMS Delineation Map



Figure 66: Delineation Map from the EMS, mapped burnt areas are shown in orange

Another way to perform an accuracy analysis is to compare the results from the workflow with the published result of the EMS (EMSR300 2018). This data, which are freely available, were loaded into the project. An Area of Interest and the result of the classification or evaluation of the burnt areas are available.



```
Sum Pix for ObservedAreaMask is:
▼ Object (1 property)
  sum: 44203
```

```
total Area in ha for ObservedAreaMask
1768.12
```

Figure 67: Observed Event from the EMS (Lila) on the left side; Statistic for the Area (right side)

The Delineation Map of the EMS (EMSR300 2018) shows that 1768 ha were concerned due to the event. The map also shows that 1275,9 ha were classified as burnt. A classification into different severities of the event is not given here. Similarly, the mask does not indicate the type of area involved, i.e. no subdivision into urban or vegetation is made.

- Comparison of the mapped Event to the Fire mask from the first workflow

```
//-----Using the data from the EMS-----//

// Observed Area
// Conversion of the Observed area vector into a Raster format and creating a Mask
var ObservedAreaImage = ObservedArea
  .reduceToImage({
    properties: ['dmg_src_id'],
    reducer: ee.Reducer.first()});
// Create a binary Observed area mask
var ObservedAreaMask = ObservedAreaImage.eq(1).toInt().reduce('sum');
// get the statistic (pixel count and area in ha) for the burned Area from EMS
var statObservedAreaMask = ObservedAreaMask.reduceRegion({
  reducer: ee.Reducer.count(),
  geometry: bounds,
  scale: 20,
  maxPixels: 1e9});
print ('Sum Pix for ObservedAreaMask is: ', statObservedAreaMask);
var pixelArea = ObservedAreaMask.multiply(ee.Image.pixelArea());
var totalArea = pixelArea.reduceRegion('sum', bounds, 20);
var pix = ee.Number(statObservedAreaMask.get('sum'));
var hectObserved = pix.multiply(400).divide(10000);
print ('total Area in ha for ObservedAreaMask', hectObserved);
// Comparison between the first Fire mask and the observed Area
var CompObsFire = ObservedAreaMask.eq(1).or(Firemask.eq(1)).reduce('sum').toInt();
var statCompObsFire = CompObsFire.reduceRegion({
  reducer: ee.Reducer.sum(),
  geometry: bounds,
  scale: 20,
  maxPixels: 1e9});
print ('Sum Pix from CompObsFire is: ', CompObsFire);
var pixelAreas = CompObsFire.multiply(ee.Image.pixelArea());
var totalAreas = pixelAreas.reduceRegion('sum', bounds, 20);
var pixCompObsFire = ee.Number(statCompObsFire.get('sum'));
var hectCompObsFire = pixCompObsFire.multiply(400).divide(10000);
print('total Area in ha for CompObsFire is:', hectCompObsFire);

Sum Pix from Comparison Firemasks is:
▼Object (1 property)
  sum: 32884

total Area in ha for Comparison Firemasks is:
1315.36
```

Figure 68: Statistic for the burned Area in Comparison of the two Masks and statistic for the overlapping area

The statistics now show that within the Area concerned of the EMS 1315 ha burnt area was detected by the mask generated from the first workflow.

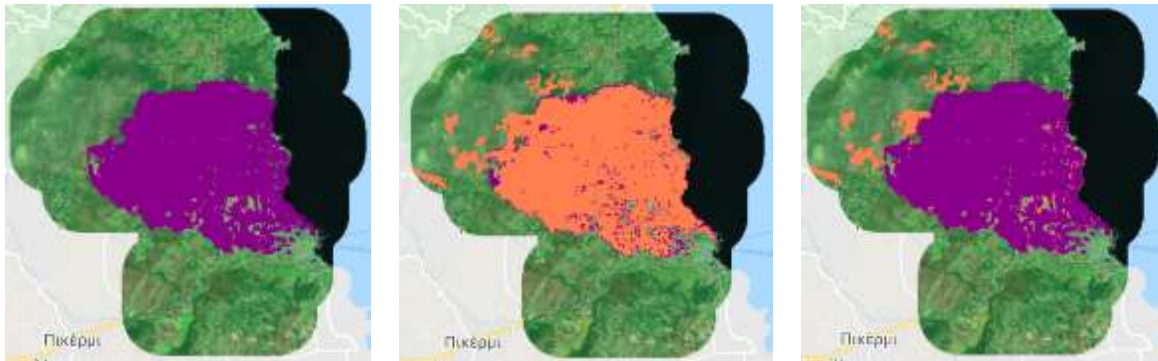


Figure 69: Left: Observed Area (purple); Center: Observed Area (purple), overlaid by Fire mask (orange); Right: Fire mask, overlaid by Observed Area

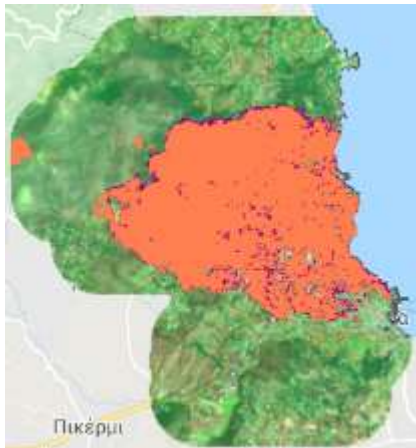
The Comparison already shows at first glance that the result from the dNBR from the first method to the Area concerned from EMS shows a large contract. Apart from the faulty areas in the northwest and west, which have already been mentioned, there is an almost complete optical agreement. The difference of 453 ha shows on the one hand, that the generated fire mask shows areas as burnt, which are not burnt (especially in the north-western part). On the other hand, it cannot be deduced whether burned areas within the Area concerned of the EMS were not classified or whether areas are shown as burned but not burned at all. According to the delineation map published by EMS (EMSR300 2018), 1.275,9 ha of bushes, forest areas and housing estates were destroyed by fire. If one takes the result from the overlap area between the monitored area of the EMS and the generated fire mask, one comes to the conclusion that very good results can be derived using the workflow. The faulty areas outside of the Area concerned need closer examination and possibly corrections, for example in the cloud mask.

Another source of error or reason for the deviation is the fact that the burned areas were visually created using Pleiades data. Pleiades data have a spatial resolution of 50 cm. Therefore, the smallest burnt areas that cannot be detected with Sentinel-2 data were also detected. It is therefore plausible that more areas are detected which cannot be detected with Sentinel-2 data with the lower spatial resolution.

Therefore, the published result of the EMS is only used as an aid and not as absolute accuracy.

- Comparison of the mapped Event to the Fire masks from the second workflow

The statistics from the overlap area of the second mask by Using the Threshold 99 with the Area concerned shows that 1332 ha were detected overlapping.



```
Sum Pix from CompObsFire is:
▶ Object (1 property)
```

```
total Area in ha for CompObsFire is:
1332.2
```

Figure 70: Left: Observed Area EMS (purple), overlaid by Fire mask (orange); Right: statistic for the overlapping area between Observed Area and the Fire mask from the second workflow (threshold 99)

The statistics from the overlap area of the second mask by Using a higher Threshold with the Area concerned shows that 1.162 ha were detected overlapping.



```
Sum Pix from Comparison Firemasks2 is:
▼ Object (1 property)
  sum: 29061
```

```
total Area in ha for Comparison Firemasks2 is
1162.44
```

Figure 71: left side: Fire Event from EMS, overlaid by Fire mask using Threshold 200; right side: statistic for the overlapping area

With a higher threshold value, the single wrong pixels are omitted, but the burned area is also reduced and not completely covered anymore. The optical comparison to the area of the EMS shows that in the first case.

- Comparison in ha between the Observed Area, the burned Area by EMS and the three masks

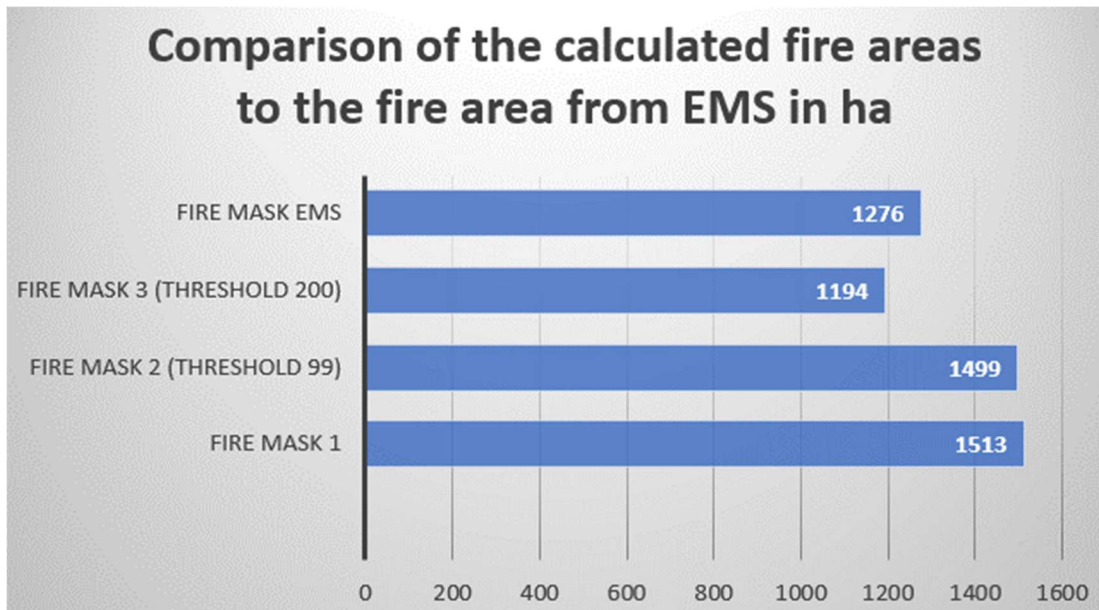


Figure 72: Comparison of the fire masks to the burned area from EMS

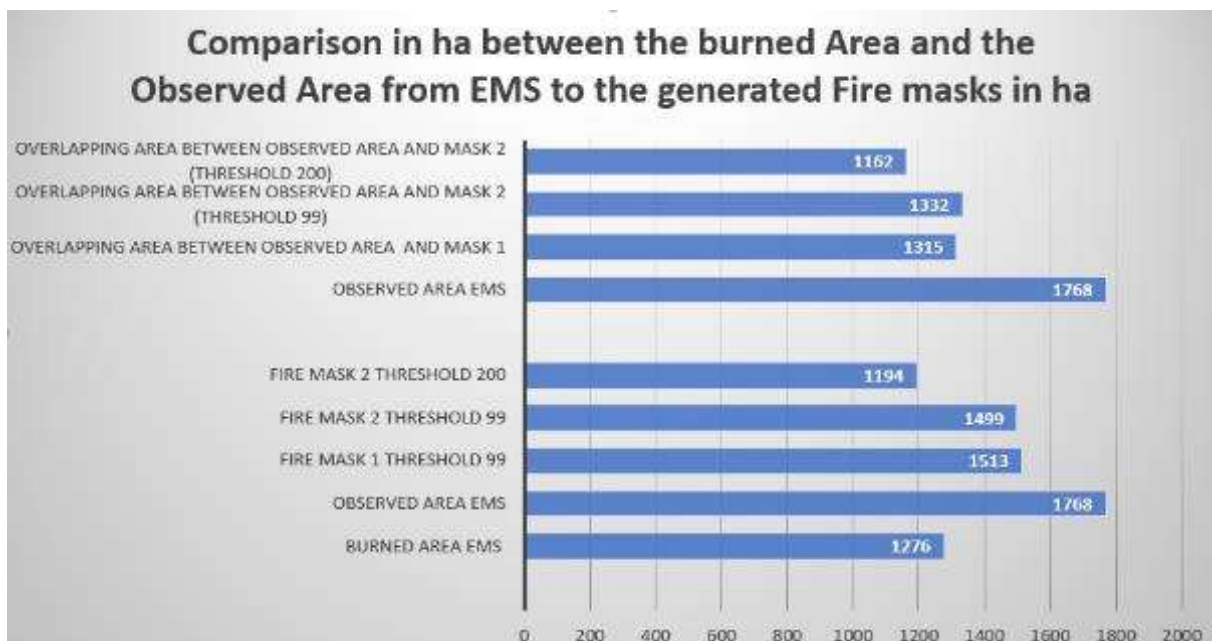


Figure 73: Comparison in ha between the burned area and the area concerned to the three different Fire masks generated from the two approaches

It is now shown that compared to the Area concerned, both workflows produce good results, provided the same threshold value is applied.

The differences in the area size of the actual burnt area can be explained by the fact that the EMS uses different images as a data basis and certainly also uses a different approach for the detection of burnt areas, which is not documented.

4.2.6 Destroyed Settlement Monitoring

Finally, on the basis of freely available settlement data, a statement should be made as to whether and how many settlement areas were affected by a registered fire.

- *Settlement Data from the EMS*

After activation, the EMS makes its data and results freely accessible. These can be downloaded from the EMS website (EMSR300 2018) and uploaded to the GEE as external data. In the present case, the available settlement dataset was used to make a statement about how many settlement structures were affected by the fire.

In the first step, the data, which are available as vector data, are converted into raster data and generated into a mask for easier calculation.

```
// Conversion of the Settlement vector into a Raster format and creating a Mask

var SettlementImage = Settlement
  .reduceToImage({
    properties: ['dmg_src_id'],
    reducer: ee.Reducer.first()
  });
print("SettlementImage is: ", SettlementImage);

// Specify a projection
var proj = ee.Projection('EPSG:32634');

var SettlementImage_reproject = SettlementImage.reproject(proj, null, 20);

// Create a binary Settlement mask
var Settlementmask = SettlementImage_reproject.eq(1);
```

In the second step, the settlement mask is compared with the three different fire masks. The result is the settlement areas affected by the fire.

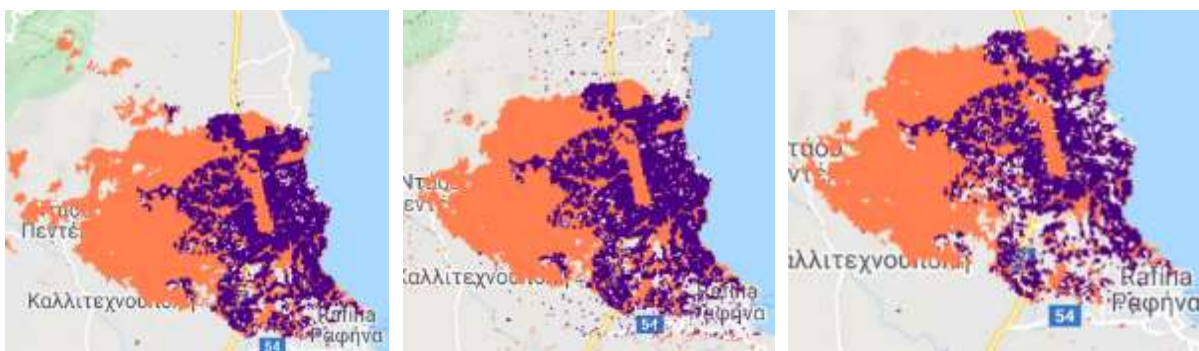


Figure 74: Fire Mask 1 (orange) and the affected Settlement structures (blue) (left); Fire Mask 2 and the affected Settlement structures (blue) (center); Fire Mask 3 and the affected Settlement structures (blue) (right side)

- *Statistic for the burned Settlement structures*

```

var statBurntSettlement = burntSettlementArea.reduceRegion({
  reducer: ee.Reducer.sum(),
  geometry: bounds,
  scale: 20,
  maxPixels: 1e9
});
print ('Sum Pix for Burnt Settlement is: ', statBurntSettlement);

var pixelArea = burntSettlementArea.multiply(ee.Image.pixelArea());
var totalArea = pixelAreas.reduceRegion('sum', bounds, 20);
print('total Area for burnt Settlement is: ', totalAreas);

var pixBurntSettlement = ee.Number(statBurntSettlement.get('sum'));
var hectBurntSettlement = pixBurntSettlement.multiply(400).divide(10000);
print('total Area in ha for Burnt Settlement is:', hectBurntSettlement);

```

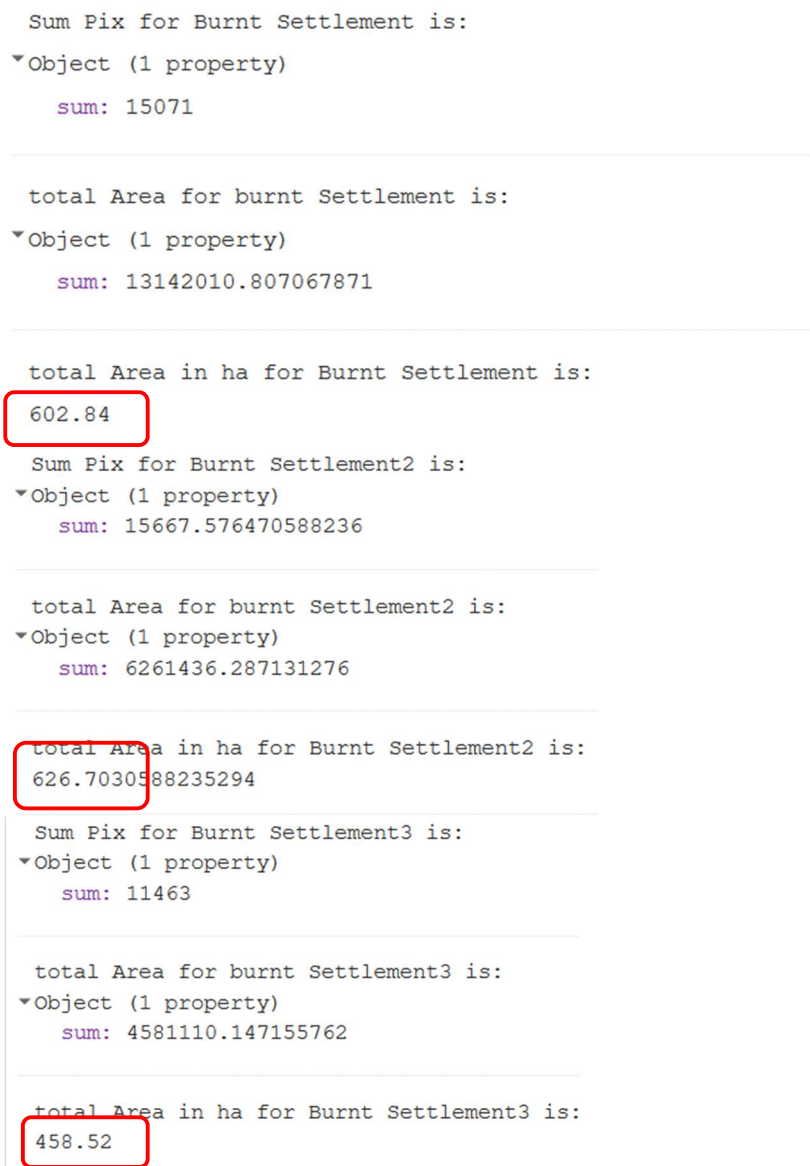


Figure 75: Statistics for the burned Settlement

According to the map, 690 ha of settlement structures are affected. Under the condition that the settlement data provided is current and correct, 600 ha of settlement area are affected by the fire in the first workflow. In the second workflow, 626 ha are affected at a lower threshold value and 459 ha settlement areas at a higher threshold value.

It should also be noted that the EMS uses an undocumented approach to the detection of burnt areas. Furthermore, the settlement data provided do not indicate the data basis on which the data were collected. The only indication that high-resolution Pleiades data were used for the optical interpretation can be found. Therefore, the comparison should also only be seen as an indication and not as an absolute result.

From the available statistics and comparisons, it can be deduced that burn area generated from the first workflow and burn area from the second workflow, which was calculated with a lower threshold value, lead to very similar results and also have the greatest agreement with the specified result of the EMS. This can also be seen in the graphic below.

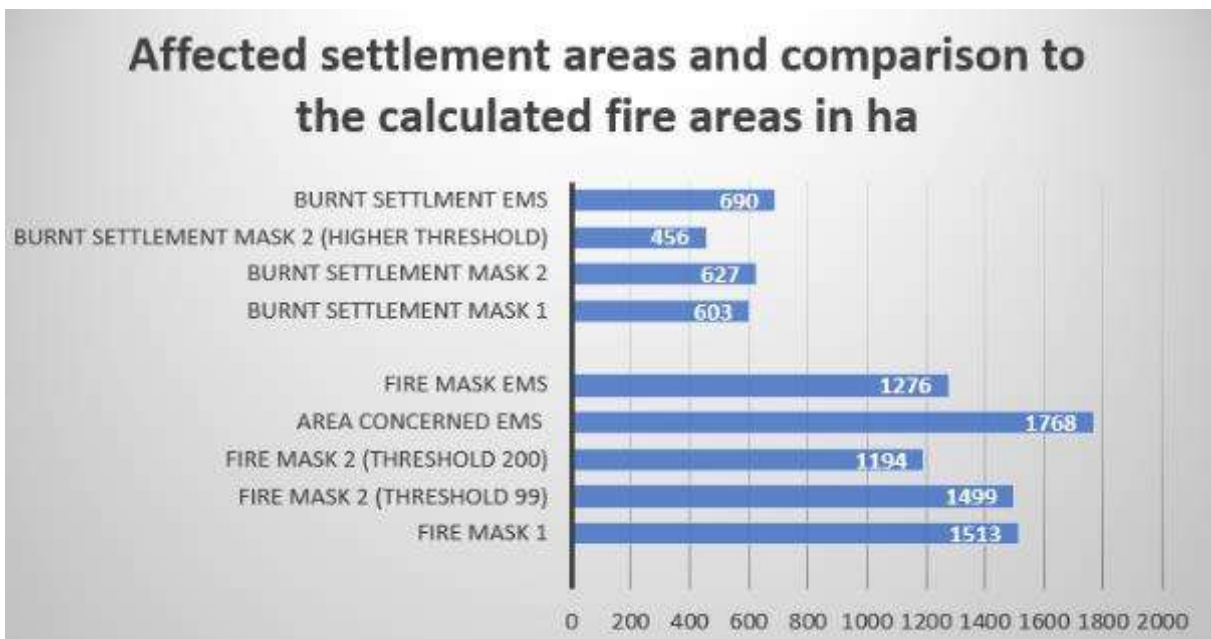


Figure 76: Affected settlement structures

- Comparison with settlement data provided by the GEE

Only in rare cases is it possible to access ready-made and evaluated settlement data, which are freely available. In most cases, data from an open source is used, but it is usually neither up-to-date, complete nor evaluated. For comparison, however, these data were also used.

```
var dataset: Image "GHSL: Global Human Settlement Layers, Built-Up Grid 1975-...
  type: Image
  id: JRC/GHSL/P2016/BUILT_LDSMT_GLOBE_V1
  version: 1571719398982399
```

Figure 77: Import of the Global Human Settlement Layer

```
// Loading Settlement data

var builtUp = dataset.select('built').clip(bounds);
var visParams = {
  min: 1.0,
  max: 6.0,
  palette: ['0c1d60', '000000', '448564', '70daa4', '83ffbf', 'ffffff'],
};
print('builtUp is: ', builtUp);
//Map.addLayer(builtUp, visParams, 'Built-Up');

// Specify a projection
var proj = ee.Projection('EPSG:4326');

var builtUp_reproject = builtUp.reproject(proj, null, 20);

var builtUpmask = builtUp_reproject.gt(3);

Map.addLayer(builtUpmask.updateMask(builtUpmask), {palette: ['DC143C']}, 'builtUpmask');

// Comparison between Settlement and the different firemasks
// 1. Comparison between the Firemask and the builtUp mask

var burntBuiltUpArea = Firemask.eq(1).and(builtUpmask.eq(1));
print('burntBuiltUpArea is: ', burntBuiltUpArea);
Map.addLayer(burntBuiltUpArea.updateMask(burntBuiltUpArea), {palette: ['4B0082']}, 'burntBuiltUpArea');
```

Figure 78: Loading Settlement data and comparison with the first Fire mask

Only the derived burn area from the first workflow was used for evaluation and comparison.

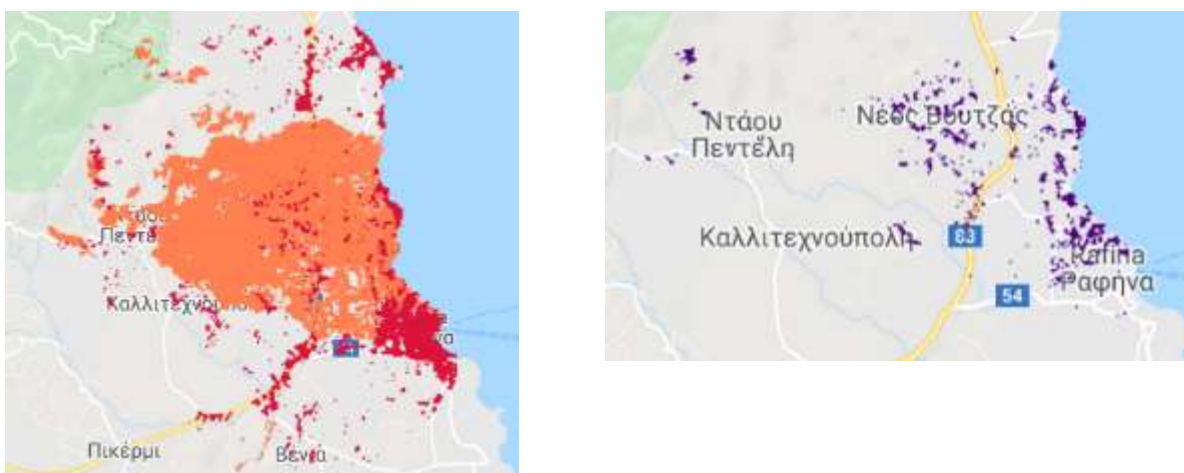


Figure 79: Fire Mask (orange) and Open Source Settlement Layer (red) as Overlay on the left side; affected Settlement structures (blue) on the right side

- *Statistic for the burned BuiltUpArea*

```

var statsBurntBuiltUpArea = burntBuiltUpArea.reduceRegion({
  reducer: ee.Reducer.sum(),
  scale: 20,
  geometry: bounds,
  maxPixels: 1e12
});
print('Sum Pix from burntBuiltUpArea is: ', statsBurntBuiltUpArea);

var pixelAreas_burnt = burntBuiltUpArea.multiply(ee.Image.pixelArea());
var totalAreas_burnt = pixelAreas_burnt.reduceRegion('sum', bounds, 20);
print('totalAreas from burntBuiltUpArea is: ', totalAreas_burnt);

var pixel = ee.Number(statsBurntBuiltUpArea.get('sum'));
var hectar = pixel.multiply(400).divide(10000);

print('total Area in ha for BurntBuiltUpArea', hectar)

```

```

Sum Pix from burntBuiltUpArea is:
▼ Object (1 property)
  sum: 2287

totalAreas from burntBuiltUpArea is:
▼ Object (1 property)
  sum: 913983.3096923828

total Area in ha for BurntBuiltUpArea
91.48

```

Figure 80: *Statistic for the burned BuiltUpArea*

Calculation of the detected fire area with the GHSL shows that approx. 92 ha of settlement area were affected by the fire. Compared to the information provided by the EMS (approx. 700 ha), it is clear that no statement can be made about the affected settlement structures on the basis of the available population data because the data show considerable gaps, have a lower resolution and are not up to date.

It must therefore be concluded that a precise statement is only necessary about the independent collection of the data, i.e. the digitization or delineation of the settlement structures from high resolution Satellite data.

The complete code for both workflows can be viewed in GEE with the following link:

<https://code.earthengine.google.com/44db301c8497842f3a6d5163eda26a8d>

<https://code.earthengine.google.com/c9d2343abf7c838770b53e669b0942c2>

4.2.7 Results

On the basis of the statistics and comparisons collected, I come to the following assessment.

A sub goal of this work is to find burnt areas in Sentinel-2 data based on FIRMS alarms. Experience has now shown that not every alarm indicates a burned area large enough to be detected by Sentinel-2 data. The difficulty is also that each alarm can be viewed separately, as only the highest-ranking alarm is displayed, even though several events have occurred in the same geographic area. Therefore, this part of the workflow cannot be automated. Each visually displayed alarm must be recorded and broken down into the underlying time periods. Only from this point on, the workflow can be adopted for every area of the earth.

The use of the cloud mask shows considerable differences and problems in the individual results of the workflow. Clouds and aerosols are present in the Sentinel-2 Level 1C images and must be blanked out before further processing (Verhegghen et al. 2016). No robust cloud masking was available for S2 at the time of processing. Together with the Level 1C product, ESA provides a quality band that masks clouds and cirrus clouds. Verhegghen et al. (2016) also confirm that this quality band did not provide sufficiently reliable results for the study area. The visual inspection and the results showed this also. The example below shows a post-fire cloud, which has not been masked completely and was then falsely classified.



Figure 81: Clouds (left), not detected by the masking algorithm (center) and falsely classified (right).

With Sentinel-2 optical data, cloud cover limits the data available and Fires, no matter how big they are, inevitably lead to clouds. The longer an event lasts, the longer there is no cloud-free data available for setting up an Image Collection. However, it is precisely this cloud-free data that is needed to capture fire data in Sentinel-2. Snow, clouds and shadows are masked in one of the pre-processing steps. Nevertheless,

masking algorithms sometimes fail to cover e.g. shadows entirely or cirrus clouds (already mentioned) which can later lead to false detections. Especially cirrus clouds are not always completely captured with the cloud mask and therefore the underlying information may be incorrectly included in the calculations. An adjustment of the approved Cloudy Pixel Percentage is therefore always necessary for each individual test area. Therefore, the algorithm cannot run fully automated. For the first test area, however, very good results could be achieved using the first workflow, after choosing a sufficiently large time period despite the cloud mask. Caution is required, however, when it comes to the choice of the period. If the time period is selected too short, not enough data is available for the calculation. Because the workflow is a change detection process, where data from before and after an event are deducted from each other, also non-fire-related changes in the environment can be detected as wildfire damage. Examples include changes in natural vegetation, deforestation and other land cover changes. Slight changes in vegetation (following the natural vegetation period) or high cirrus cloud cover not covered by the cloud mask may also be detected as low severity burn in the final result, which is why this class should be treated with special care. These problems are particularly acute when the time frame is too long. A deliberate trade-off between the amount of available data and irrelevant environmental changes needs to be made.

Therefore, the workflow should be adapted as soon as surface reflectance data from the Sentinel-2 satellites are available.

The advantage of the first workflow is certainly its high user-friendliness. Only a few entries have to be made to classify burnt areas in the end. The final result shows a clearly defined burnt area. Apart from a few exceptions, which probably result from the shadow of the Cirrus clouds, the area could be detected and classified very well. This is contrasted with the observation of the second workflow. The attempt was made to dispense with the cloud mask and to include only the data with the lowest Cloud Cover in the calculation. The classification of the burned areas stands and falls here strongly with the choice of the appropriate threshold value. When choosing the same threshold value as in the first workflow, no satisfactory results were achieved using the second workflow. Although the actual burnt area was also detected, numerous misclassified pixels can be seen spread over the entire study area, which result from the omission of the cloud mask. An increase of the threshold value could reduce the incorrectly

classified pixels, but the actual burnt area was also detected reduced. In Figure 82 the comparison is clearly visible. The left picture shows a part of the burnt area from the first workflow. The burnt area was well detected, but faulty areas are present due to the Cirrus clouds. In the middle is the burn mask, generated with a lower threshold value. The numerous areas classified as faulty can be seen immediately. An increase of the threshold value reduces these, but the mask no longer covers the actual burnt area (right picture).



Figure 82: Comparison between the burned areas

Accuracy analysis using a supervised classification gives the same picture. As shown under point 4.2.3 the first method achieves a higher overall accuracy than the second method. The comparison with the data provided by the EMS also confirms this. Here, the difference in the second method due to the choice of the threshold value becomes even more apparent. The lower threshold value thus provides the significantly better results, but is significantly more error-prone in the second method than in the first method.

A possible source of error in the comparison of the two workflows is the fact that the study area is covered by two so-called tiles, which are considered separately from each other in the second workflow in contrast to the first approach. In the first approach, the Image Collection is used to view the study area in its entirety and the workflow also uses all available data. In the second approach a selection of the tiles is performed by querying the lowest Cloud Cover. Since the two overlap the study area, the query does not lead to any further restrictions. This will certainly lead to a change in the workflow in the second study area, which is covered by several tiles lying next to each other due to its size.

Finally, it can be deduced that the first workflow leads to significantly better results overall, even if the settings regarding the permissible cloud cover and the threshold value allow deviations in the result.

4.3 Evaluation and Adaptation of the workflow

4.3.1 *Second Study Area - Paradise, California*

The second event (Paradise – CALIFORNIA; (Disastercharter 591 2018)) was located near the town of Paradise in Butte County, about 250 km northeast of San Francisco and involved the detection of recurring fire sources over a very large area and over a long period of time (International Charter Space and Disaster Management 2019). The fire, known as "Campfire", spread to an area of more than 30,000 hectares in one day, reaching 44,000 hectares on November 12. According to the authorities, the small town of Paradise was almost completely destroyed. Until 17 November 2018, 50 people had died, more than 1000 people were missing. In addition, nearly 20,000 houses were damaged or destroyed (Camp Fire (2018) 2019)) in the whole region.

The fires are a result of warm temperatures in a region which has experienced no rain for a month. Wind caused the fire outbreaks to spread. Several hundred thousand people had to be evacuated and dozens died. Butte County in northern California was particularly hard hit (Munich Re 2018). California often experiences wildfires in the summer and early autumn, but fires such as these leave some experts concerned that a changing climate may make the fires more common throughout the year (International Charter Space and Disaster Management 2019). According to the Munich Re (Munich Re 2018), forest fires in California in 2018 were the heaviest fires of all time for the insurance industry. The world's largest reinsurer, put the total economic loss at 24bn US dollars (21bn euros), a multiple of the usual amount for fires. Munich Re's climate researchers see this also as an indication of climate change. The reinsurer clearly emphasizes that the losses are so high, because the settlement of the Californian mountain region is increasing more and more. California is also one of the regions that have warmed at an above-average rate in recent decades. It must therefore be mentioned that the number of fires has not increased, but that the affected areas are larger and burn faster (Munich Re 2018).

The second study Area (Figure 82) was selected from a registered event of the International Charter Space and Disaster Management (Disastercharter 591 2018) which allowed me to use the final maps also as a reference for the accuracy assessment. The study area is located near the town of Paradise in Butte County, about 250 km northeast of San Francisco.

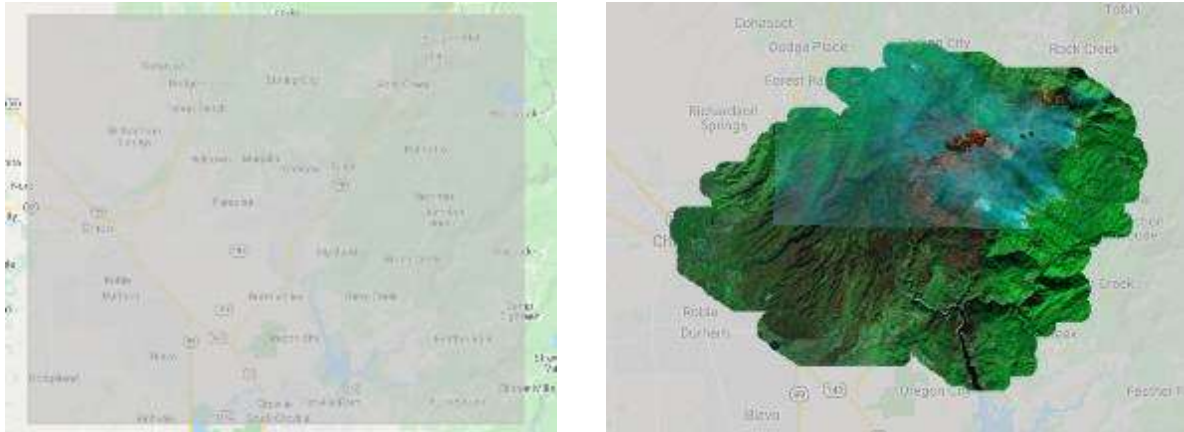


Figure 83: second study Area (left side) and the new study area in False Color

The following workflow, which has already been displayed, is used:

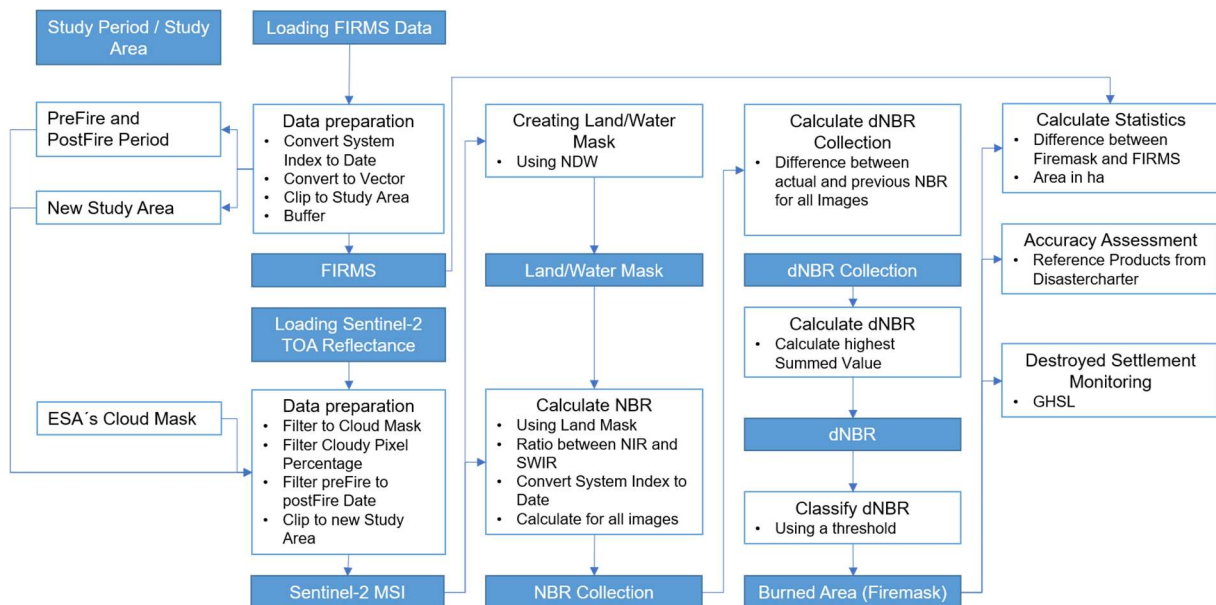
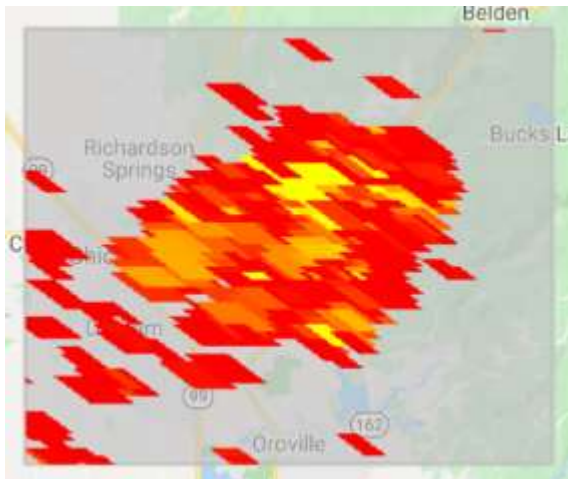


Figure 84: Workflow for the second study area

4.3.2 FIRMS Alarms in AOI



- List of Fires in AOI is:
- ▼List (28 elements)
 - ▶0: Date (2018-01-06 00:00:00)
 - ▶1: Date (2018-01-31 00:00:00)
 - ▶2: Date (2018-02-05 00:00:00)
 - ▶3: Date (2018-02-10 00:00:00)
 - ▶4: Date (2018-02-15 00:00:00)
 - ▶5: Date (2018-04-21 00:00:00)
 - ▶6: Date (2018-05-11 00:00:00)
 - ▶7: Date (2018-06-05 00:00:00)
 - ▶8: Date (2018-06-25 00:00:00)
 - ▶9: Date (2018-06-30 00:00:00)
 - ▶10: Date (2018-07-05 00:00:00)
 - ▶11: Date (2018-07-10 00:00:00)
 - ▶12: Date (2018-07-15 00:00:00)
 - ▶13: Date (2018-08-14 00:00:00)
 - ▶14: Date (2018-09-08 00:00:00)
 - ▶15: Date (2018-09-18 00:00:00)
 - ▶16: Date (2018-09-28 00:00:00)
 - ▶17: Date (2018-10-08 00:00:00)
 - ▶18: Date (2018-10-13 00:00:00)
 - ▶19: Date (2018-10-18 00:00:00)
 - ▶20: Date (2018-10-23 00:00:00)
 - ▶21: Date (2018-10-28 00:00:00)
 - ▶22: Date (2018-11-02 00:00:00)
 - ▶23: Date (2018-11-07 00:00:00)
 - ▶24: Date (2018-11-12 00:00:00)
 - ▶25: Date (2018-11-17 00:00:00)
 - ▶26: Date (2018-12-07 00:00:00)
 - ▶27: Date (2018-12-12 00:00:00)

Figure 85: FIRMS Alarms in AOI for 2018

In 2018, 28 alarms were registered for the present AOI, which are displayed in 13 alarms. To evaluate the workflow, the largest centrally located area was selected, buffered and recorded as a single AOI. Eight time periods were then identified for this sub-area. For a better overview and comparison to the results of the registered event of the International Charter Space and Disaster Management (Disastercharter 591 2018) only the events in November were selected.



- List Fire in newAOI:
- ▼List (8 elements)
 - ▶0: Date (2018-02-15 00:00:00)
 - ▶1: Date (2018-06-30 00:00:00)
 - ▶2: Date (2018-07-10 00:00:00)
 - ▶3: Date (2018-09-18 00:00:00)
 - ▶4: Date (2018-10-23 00:00:00)
 - ▶5: Date (2018-11-07 00:00:00)
 - ▶6: Date (2018-11-12 00:00:00)
 - ▶7: Date (2018-11-17 00:00:00)

Figure 86: new Study Area and registered Fires

4.3.3 Burned Area mapping using Sentinel-2 TOA reflectance data with the Cloud mask

In the second test area, the workflow generated from the first test area is transferred. First, the pre- and post-fire period is selected based on the presented alarms. This is relatively difficult in the second test area, because here a chronologically close accumulation of events occurs, which leads to the fact that several events are recorded in the data during the test period. Furthermore, the filtering of the cloud coverage must be taken into account when making a selection. If you filter less than 5% Cloudy Pixel Percentage, too little data is found for the collection because the events are close together in time. Therefore, a filtering with less than 20% is used. After selecting the Sentinel-2 TOA Reflectance data, the NBR is calculated for the entire Image Collection and added as a band. Fig. 87 now shows the first problem that arises for the present study area.

```

*23: Image (14 bands)
  type: Image
  bands: List (14 elements)
  properties: Object (6 properties)
    ID: 20181116T185639_20181116T190144_T10TFK
    date: Date (2018-11-16 00:00:00)
    date time: Date (2018-11-16 19:03:19)
    system:footprint: Polygon, 1130 vertices
    system:index: 20181116T185639_20181116T190144_T10TFK
    system:time_start: 1542394998840
*24: Image (14 bands)
  type: Image
  bands: List (14 elements)
  properties: Object (6 properties)
    ID: 20181201T185731_20181201T185930_T10SEJ
    date: Date (2018-12-01 00:00:00)
    date time: Date (2018-12-01 19:03:31)
    system:footprint: Polygon, 246 vertices
    system:index: 20181201T185731_20181201T185930_T10SEJ
    system:time_start: 1543691011940
*25: Image (14 bands)
  type: Image
  bands: List (14 elements)
  properties: Object (6 properties)
    ID: 20181206T185749_20181206T185746_T10SEJ
    date: Date (2018-12-06 00:00:00)
    date time: Date (2018-12-06 19:03:35)
    system:footprint: Polygon, 246 vertices
    system:index: 20181206T185749_20181206T185746_T10SEJ
    system:time_start: 1544123075040
*26: Image (14 bands)
*27: Image (14 bands)
  properties: Object (20 properties)
  
```

The resulting Image Collection is shown opposite. As already mentioned, the study area is covered by four so-called tiles. When filtering the Image Collection, each tile is considered individually, so that data is not available for each tile due to the settings. Thus, on 2018-12-01 a data set is only available for the tiles with the ID SEJ. On 2018-12-06 only data for the SEJ, SFJ and TEK tile are available.

Figure 87: Image Collection with the missing Tiles

Numerous experiments have shown that increasing the allowed Cloud Coverage does not show any improvement, because the missing data show a cloud coverage of almost 100% and the resulting Image Collection has too many holes in the data.

Following the workflow, in the next step the NBR is calculated for the entire collection.

Figure 88 shows the NBR listed by date and shown in the GEE. The list also shows that it was not possible to create an NBR for each date.

```

NBRlist
*List (28 elements)
 0: Date (2018-10-12 00:00:00)
 1: Date (2018-10-12 00:00:00)
 2: Date (2018-10-12 00:00:00)
 3: Date (2018-10-12 00:00:00)
 4: Date (2018-10-17 00:00:00)
 5: Date (2018-10-17 00:00:00)
 6: Date (2018-10-17 00:00:00)
 7: Date (2018-10-17 00:00:00)
 8: Date (2018-10-22 00:00:00)
 9: Date (2018-10-22 00:00:00)
10: Date (2018-10-22 00:00:00)
11: Date (2018-10-22 00:00:00)
12: Date (2018-11-06 00:00:00)
13: Date (2018-11-06 00:00:00)
14: Date (2018-11-06 00:00:00)
15: Date (2018-11-06 00:00:00)
16: Date (2018-11-11 00:00:00)
17: Date (2018-11-11 00:00:00)
18: Date (2018-11-11 00:00:00)
19: Date (2018-11-11 00:00:00)
20: Date (2018-11-16 00:00:00)
21: Date (2018-11-16 00:00:00)
22: Date (2018-11-16 00:00:00)
23: Date (2018-11-16 00:00:00)
24: Date (2018-12-01 00:00:00)
25: Date (2018-12-06 00:00:00)
26: Date (2018-12-06 00:00:00)
27: Date (2018-12-06 00:00:00)
    
```

The problems arising from the permitted cloud cover cannot be avoided without restrictions. An increase in the time period during which sentinel data is selected leads to the problem that, for example, phenological changes come into play which have nothing to do with the actual fire event. Furthermore, especially in the second study area, an accumulation of fire events that are close together in time can be seen, which, if the time period is increased, leads to an even greater mixture of the burnt areas and thus no longer leads to the desired goal.

Figure 88: List of all calculated NBR (left side)

- Calculation of the NBR

The NBR is calculated according to the same scheme as for the first test area. First, a land mask is created to exclude water and shadow areas as much as possible from the calculation. Then the NBR for the entire Image Collection, reduced to the land mask, is calculated and displayed as median NBR.

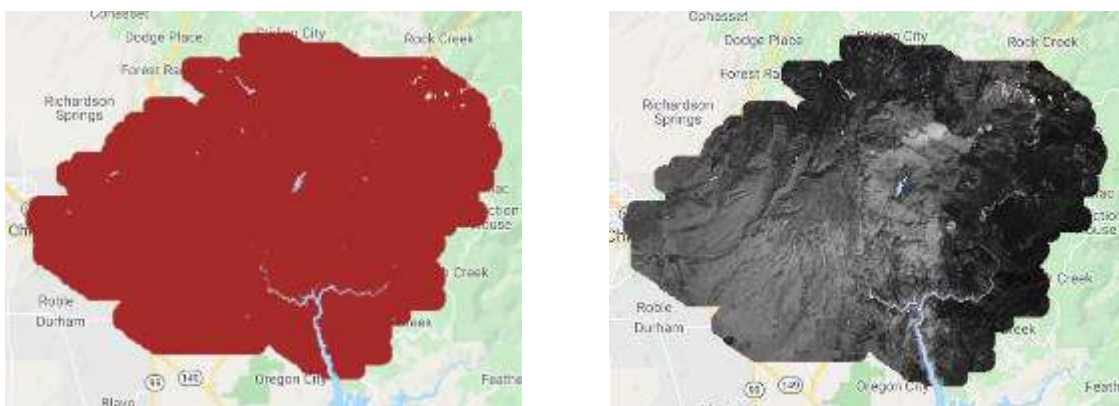


Figure 89: Land Mask in red (left side) and median NBR in greyscale (right side)

- *Calculation of the dNBR for the whole Collection*

At this point, the problems in the workflow arise. The dNBR results from the offsetting of two successive scenes. Of course, it is important to make sure that this is done for the whole Image Collection and therefore for all tiles per date. But since not all four scenes are available for each date, the dNBR Image Collection has holes in the data. The biggest problem still is that the algorithm uses the date or the index to find the matching data (see code below) and thus different tiles are offset against each other. An example can be seen on 2018-12-06: For this date the data set from the tile TFK is missing, i.e. for a part in the southern part of the study area no data sets and therefore no NBR's are available. The algorithm works incorrectly here, because it tries to find the matching data via the date or the index and now works across scenes or tile.

```
*properties: Object (7 properties)
  ID: 20181116T185639_20181116T190144_T10SEJ
  date: Date (2018-11-16 00:00:00)
  date_time: Date (2018-11-16 19:03:37)
  system:footprint: Polygon, 248 vertices
  system:index: 23
  system:index_previous: 20181116T185639_20181116T190144_T10SEJ
  system:time_start: 1542395017680

*24: Image (2 bands)
  type: Image
  bands: List (2 elements)
  *properties: Object (7 properties)
    ID: 20181201T185031_20181201T185980_T10SEJ
    date: Date (2018-12-01 00:00:00)
    date_time: Date (2018-12-01 19:03:31)
    system:footprint: Polygon, 248 vertices
    system:index: 24
    system:index_previous: 20181116T185639_20181116T190144_T10SEJ
    system:time_start: 1543691011940

*25: Image (2 bands)
  type: Image
  bands: List (2 elements)
  *properties: Object (7 properties)
    ID: 20181206T185749_20181206T185746_T10TEK
    date: Date (2018-12-06 00:00:00)
    date_time: Date (2018-12-06 19:03:20)
    system:footprint: Polygon, 402 vertices
    system:index: 25
    system:index_previous: 20181201T185031_20181201T185980_T10SEJ
    system:time_start: 1544723000060

*26: Image (2 bands)
*27: Image (2 bands)
```

This is illustrated by the example of image 25. The actual (current image) is a scene from Tile TEK. As previous image the scene from the tile SEJ is used.

This problem is then also apparent when calculating the summed highest values of the dNBR. The highest dNBR (calculated as the sum of all values per scene) is reached on 2018-12-01, since the calculation of the sum is also carried out for each tile individually. The pictorial representation now shows that in the southern area the burnt area is shown. The use of the cloud mask in the form of the holes, which the data set shows, can also be seen very clearly.

Fig. 92 shows the fire mask generated from the modified result and the corresponding statistics. The threshold value to derive the burned areas was chosen purely empirically.

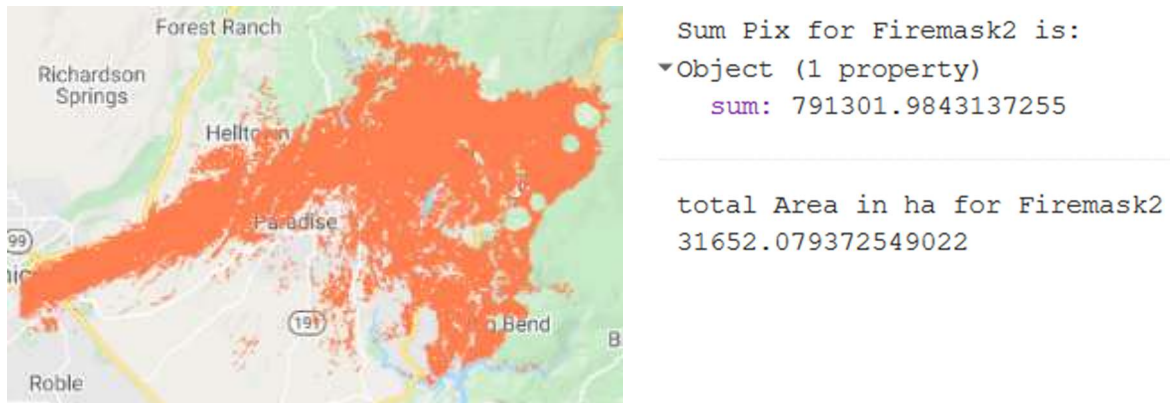


Figure 92: generated Fire mask and burned area in ha

According to the present result 31.652 ha of land have been detected as burnt area. However, the problems and errors already mentioned lead to the conclusion that this result is more a rough estimate than a reliable result. A modification of the workflow is necessary at this point.

The complete code can be viewed in the Google Earth Engine with the following link:

<https://code.earthengine.google.com/47ec569e7a2dd076f84a62edc82c9569>

4.3.4 Options for modifying the workflow

- Mosaic all scenes with the same date

The workflow is modified according to the following scheme:

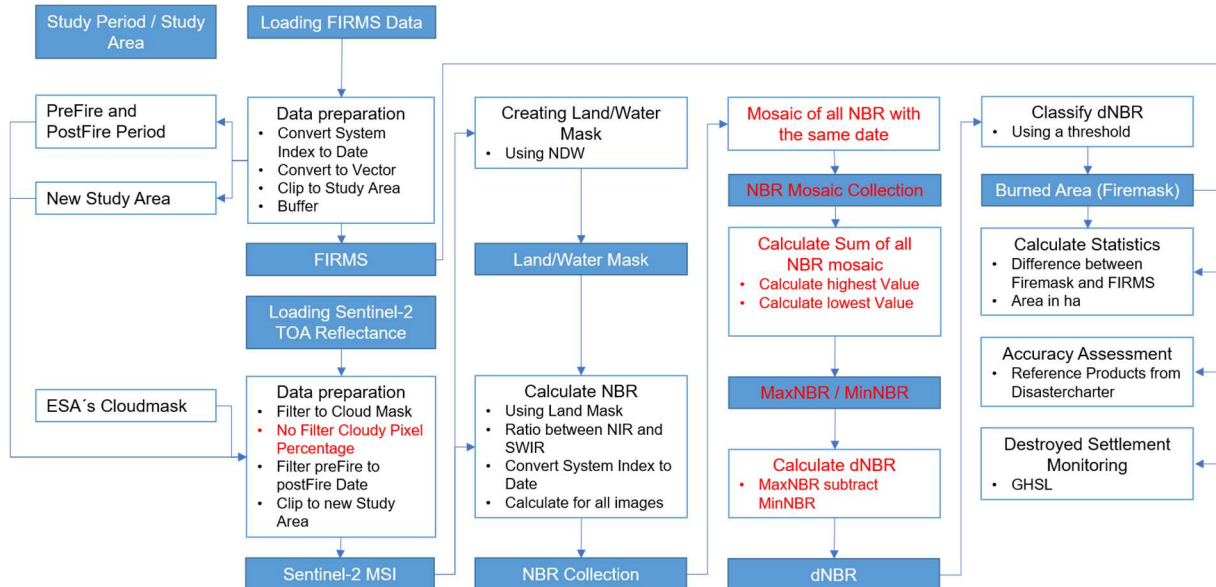


Figure 93: modified workflow, Changes are shown in red

The idea now is to include all data in the collection regardless of the Cloud Cover, to calculate the NBR for each data set and finally to mosaic all NBR's with the same date. The result is an Image Collection, consisting of, in this case, twelve individual mosaics, each with the same date.

```

// mosaic all NBR images with the same date
// Difference in days between start and finish
var diff = postFire.difference(preFire, 'day');

// Make a list of all dates
var range = ee.List.sequence(0, diff.subtract(1))
.map(function(day){return preFire.advance(day, 'day')});

// Functon for iteraton over the range of dates
var day_mosaics = function(date, newlist) {
  // Cast
  date = ee.Date(date);
  newlist = ee.List(newlist);

  // get date as YEARMONTHDAY.
  var date_formatted = ee.Number.parse(date.format('YYYYMMdd'));
  // make date band as an 32 bit unsigned integer and rename it as 'date'
  var dateband = ee.Image.constant(date_formatted).toUint32()
  .rename('date');

  // Filter collection between date and the next day
  var filtered = S2NBR.filterDate(date, date.advance(1, 'day'));

  // Make the mosaic
  var image = ee.Image(filtered.mosaic().clip(newAOI)).addBands(dateband);

  // Add the mosaic to a list only if the collection has images
  return ee.List(ee.Algorithms.If(filtered.size(), newlist.add(image), newlis
});

// Iterate over the range to make a new list, and then cast the list to an im
var NBR_newcol = ee.ImageCollection(ee.List(range.iterate(day_mosaics, ee.Lis
print('NBR_newcol', NBR_newcol);
    
```

```

NBR_newcol
▼ ImageCollection (12 elements)
  type: ImageCollection
  bands: []
  ▼ features: List (12 elements)
    ▼ 0: Image (2 bands)
      type: Image
      ▼ bands: List (2 elements)
        ► 0: "NBR", float, EPSG:4326, 1x1 px
        ► 1: "date", int ∈ [20181012, 20181012],
      ► properties: Object (2 properties)
    
```

Then all NBR values per mosaic are summed and the mosaic scene with the highest NBR values and the scene with the lowest NBR values is selected. The principle is that the highest NBR values are recorded before a fire event and the lowest values after a fire event. Below you can see that on 2018-10-22, i.e. before the fire event, the highest summed NBR values are recorded. After the event, i.e. according to the calculation on 2018-11-21, the lowest NBR values can be seen. However, this result leads to misinterpretations. The value 0, which was found as the lowest value, does not stand for the minimum, but for the fact that at this time the NBR could not be calculated, because due to the high Cloud Cover (almost 100%) no reflection values are recorded and therefore the NBR could not be calculated.

```

NBRmaxsum is:
  Image (2 bands)
    type: Image
    bands: List (2 elements)
      0: "NBR", float, EPSG:4326, 1x1 px
      1: "date", int ∈ [20181022, 20181022], EI
    properties: Object (3 properties)
      sum: 1870393.260087389
      system:footprint: Polygon, 1509 vertices
      system:index: 2

NBRminsum is:
  Image (2 bands)
    type: Image
    bands: List (2 elements)
      0: "NBR", float, EPSG:4326, 1x1 px
      1: "date", int ∈ [20181121, 20181121], I
    properties: Object (3 properties)
      sum: 0
      system:footprint: Polygon, 1509 vertices
      system:index: 8
    
```

Figure 94: Maximum NBR image, minim

Fig. 94 shows the scenes from 2018-11-21 which already clearly show that due to the complete cloud coverage no information can be derived.



Figure 95: Complete Cloud Coverage after a fire event

Thus, the first change to the workflow is not followed up.

The complete code with the first Modification can be viewed in the Google Earth Engine with the following link:

<https://code.earthengine.google.com/6908c0ab4172f5d1fbb8ae57453a52bd>

- Limiting the data to one scene before and one scene after the event

Last results show that very close fire events lead to misinterpretations or the high cloud cover caused by the fire leads to insufficient data for the calculation of the dNBR. Therefore, a further attempt is shown in which only the last recorded data before and after the event are used as pre- and post-fire data. In order to obtain the information for the entire study area, the scenes are combined into a mosaic. The NBR is thus calculated once from the PreFire mosaic and once from the PostFire mosaic. Finally, the dNBR is derived and classified.

The following workflow shall illustrate this. Changes are shown in red again.

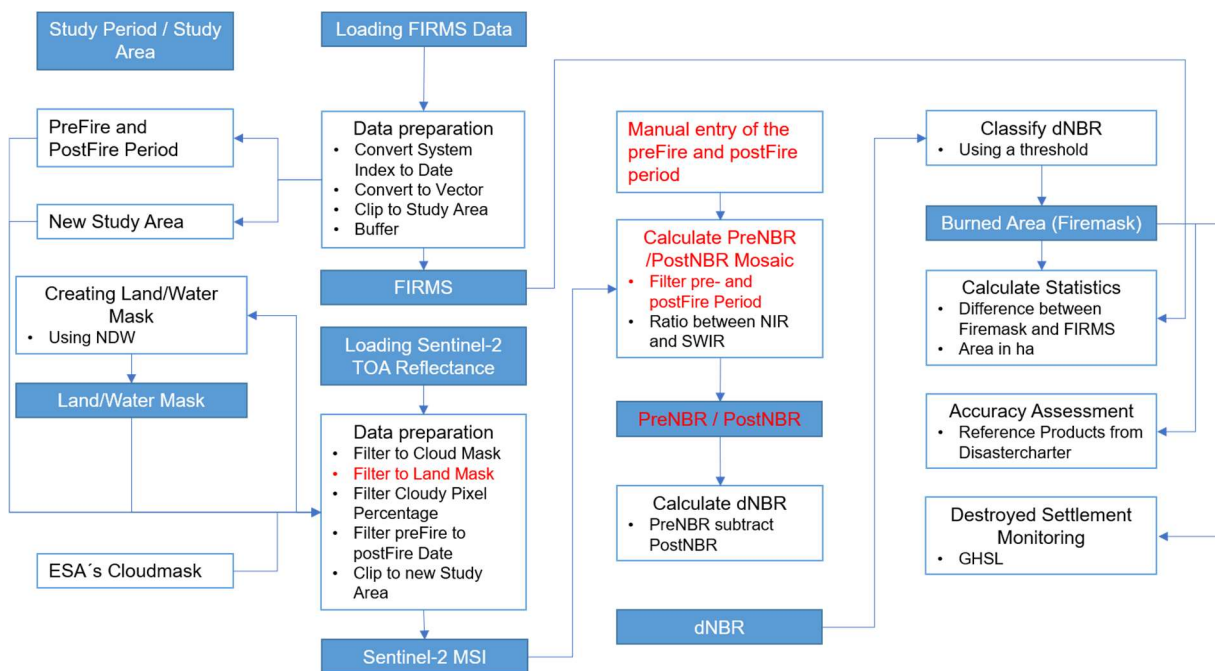


Figure 96: modified workflow for second study Area

```

var Sentinel2 = S2.map(function(image){return image.updateMask(landmask)})
print('Sentinel2: ', Sentinel2);

//-----//
//-----Create a small prefire and postfire timeseries-----//

var prefire_start = '2018-11-01';
var prefire_end = '2018-11-07';

var postfire_start = '2018-11-08';
var postfire_end = '2018-11-12';

var preFireData = Sentinel2.filterDate(prefire_start,prefire_end);
var postFireData = Sentinel2.filterDate(postfire_start, postfire_end);

//-----//
//-----Mosaic and clip images to study area-----//

var prefire_mos = preFireData.mosaic();
var postfire_mos = postFireData.mosaic();

//-----//
//-----Calculate preNBR and PostNBR-----//

var preNBR = prefire_mos.normalizedDifference(['B8A', 'B12']);
var postNBR = postfire_mos.normalizedDifference(['B8A', 'B12']);

//-----//
//-----Calculate difference between pre- and post NBR-----//
// The result is called delta NBR or dNBR

var dNBR_unscaled = preNBR.subtract(postNBR);

// Scale product to USGS standards
var dNBR = dNBR_unscaled.multiply(1000);

```

Figure 97: Earth Engine Code getting dNBR from a single pre- and postFire Mosaic



Figure 98: dNBR in greyscale (left) and classified dNBR (right)

Figure 98 shows the result after changing the workflow. The cloud mask still leads to holes in the data, but due to the mosaicking there is enough data to cover the whole study area and to get a result.



```
Sum Pix for Firemask is:
▼Object (1 property)
  sum: 1034185.4196078433
```

```
total Area in ha for Firemask
41367.41678431373
```

Figure 99: Fire Mask on the left side (in orange) and the statistic

According to the present calculation, the first fire registered in November (2018-11-07) affected an area of 41.367 ha (Fig. 99). In contrast to the regular workflow, the entire area has been recorded, as the images were mosaicked at the beginning of the calculation. Therefore, more burned area is given than in the regular calculation. However, the cloud mask again leads to holes in the data, so no calculation of the dNBR can take place.

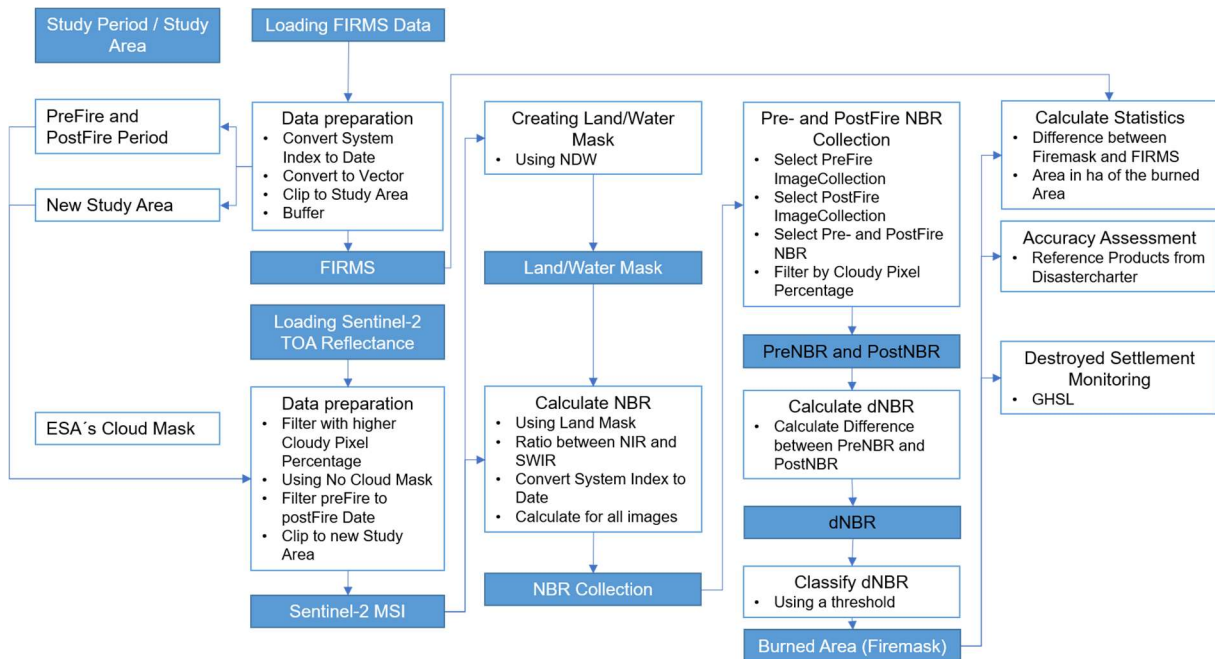
Furthermore, it is easy to see that the still predominant active fire triggers a cloud of smoke, which could not be detected and thus filtered by the cloud mask. This "veil", which covers the whole collection, does not allow a clear assignment of burnt and unburnt areas everywhere. Especially in the southwestern part, following the direction of the smoke cloud, an unambiguous classification of the pixels into burned or unburned is not possible.

The complete code with the first Modification can be viewed in the GEE with the following link:

<https://code.earthengine.google.com/5551003c489f1c292aa62026ed8773a4>

4.3.5 Burned Area Mapping using Sentinel-2 TOA reflectance data without the Cloud mask

Similar to the first test area, all available data with less than 20% Cloudy Pixel Percentage will be used. A cloud mask is not applied. The following workflow is used.



- Loading the data

After loading the data with the desired criteria, an Image Collection consisting of 28 data sets results for the study area.

As already shown in the first method, the study area consists of several tiles. For each selected date four data sets would have to be available even without using the cloud mask. Due to the settings, however, it is also apparent in the second workflow that, for example, three data sets are available for the period 2018-12-06 and only one data set is available on 2018-12-01 (see list below). An increase in the permitted Cloud Cover does not lead to better results here and gaps in the coverage with data remain.

- ▶ 23: Image COPENICUS/S2/20181116T185639_20181116T190144_T10SEJ (1 band)
- ▶ 24: Image COPENICUS/S2/20181201T185731_20181201T185930_T10SEJ (1 band)
- ▶ 25: Image COPENICUS/S2/20181206T185749_20181206T185746_T10TEK (1 band)
- ▶ 26: Image COPENICUS/S2/20181206T185749_20181206T185746_T10SFJ (1 band)
- ▶ 27: Image COPENICUS/S2/20181206T185749_20181206T185746_T10SEJ (1 band)

- Calculate the NBR

The NBR is then calculated for the entire *Image Collection*, reduced to the land mask.

```
//-----Create a function to calculate NBR per image-----//

function addNBR(image) {
  // Compute the NBR
  var nir = image.select('B8A');
  var swir = image.select('B12');
  var nbr = nir.subtract(swir).divide(nir.add(swir)).rename('NBR');
  return image.addBands(nbr);
}
var S2_collection = S2Data.map(addNBR)
  .map(function(image) {
    var date = ee.Date(image.get('system:time_start')).format("YYYY-MM-dd");
    return image.set('date', ee.Date(date));
  })
  .map(function(image) {
    var ID = ee.String(image.get('system:index'));
    return image.set('ID', ID);
  })
  .map(function(image) {
    var date = ee.Date(image.get('system:time_start'));
    return image.set('date_time', date);
  })
  // clip image to the landmask
  .map(function(image){
    return image.updateMask(landmask);
  });
print ('S2_collection: ', S2_collection);
var NBR = S2_collection.select('NBR').sort('system:time_start');
```

According to the already evaluated workflow from the first test area, successful calculation of the NBR is followed by filtering of the NBR via the Cloudy Pixel Percentage.


```

//      modifying the workflow      //
// mosaic all images with the same date
// Difference in days between start and finish
var diff = postFire.difference(preFire, 'day')

// Make a List of all dates
var range = ee.List.sequence(0, diff.subtract(1)).map(function(day){return preFire.advance(day, 'day')});
//print('range', range)
// Function for iteration over the range of dates
var day_mosaics = function(date, newList) {
  // Cast
  date = ee.Date(date);
  newList = ee.List(newList);

  // get data as YEARMONTHDAY. For example, for January 8th 2016
  // would be: 20160108
  var date_formatted = ee.Number.parse(date.format('YYYYMMd'));
  // new0 date band as an 32 bit unsigned integer and rename it as 'date'
  var dateband = ee.Image.constant(date_formatted).toInt32()
  //print('date', date);

  // Filter collection between date and the next day
  var filtered = NBR.filterDate(date, date.advance(1, 'day'));

  // Make the mosaic
  var image = ee.Image(filtered.mosaic().clipToMask(0.1).addBands(dateband));

  // Add the mosaic to a list only if the collection has images
  return ee.List(ee.Algorithms.If(filtered.size(), newList.add(image), newList));
};

// Iterate over the range to make a new list, and then cast the list to an imagecollection
var NBR_newcol = ee.ImageCollection(ee.List(range).iterate(day_mosaics, ee.List([])));
print('NBR_newcol', NBR_newcol);

```

```

*ImageCollection COPERNICUS/S2 (28 elements)
S2_m01_preFire
*ImageCollection COPERNICUS/S2 (16 elements)
S2_m01_postFire
*ImageCollection COPERNICUS/S2 (12 elements)
NBR_newcol
*ImageCollection (8 elements)
type: ImageCollection
newcol: []
*features: List (8 elements)
#0: Image (2 bands)
  type: image
  *number: List (2 elements)
  #0: "NBR", float, BRQA:4326, 1st pr
  #1: "date", int, 0 [20160108, 201610]
  *properties: Object (2 properties)
  *system:index: 0
#1: Image (2 bands)
#2: Image (2 bands)
#3: Image (2 bands)
#4: Image (2 bands)
#5: Image (2 bands)
#6: Image (2 bands)
#7: Image (2 bands)

```

Figure 101: NBR mosaic Image Collection

The result is an *Image Collection* consisting of eight data sets for the selected period. Unfortunately, when creating the mosaics in the Google Earth Engine, necessary information is lost. A query about Cloudy Pixel Percentage is no longer possible, since this property is no longer provided as metadata for the individual mosaics (an averaging over all existing data would be nice here). Furthermore, the date is no longer provided as an index, but is attached to the data as an extra band. It is also no longer possible to calculate the NBR's in time and thus to create the dNBR. Therefore, this method will not be pursued further.

It now becomes apparent that the already evaluated second workflow for the second test area cannot be applied without restrictions either. Various adjustments have not led to the desired result. Therefore, the workflow will be modified in the further course of the evaluation.

The complete code with the first Modification can be viewed in the GEE with the following link:

<https://code.earthengine.google.com/6e5a585e767e45aaf780a630cc189567>

4.3.6 Modifying the second workflow

In the first step, the pre- and postFire data including NBR will be created separately as an Image Collection and each will be calculated into a mosaic without specifying the cloud coverage. With the preFire and postFire NBR data thus obtained, the dNBR can be calculated and classified.

The process is shown in Fig. 102. Significant changes to the workflow of the first test area are marked in red.

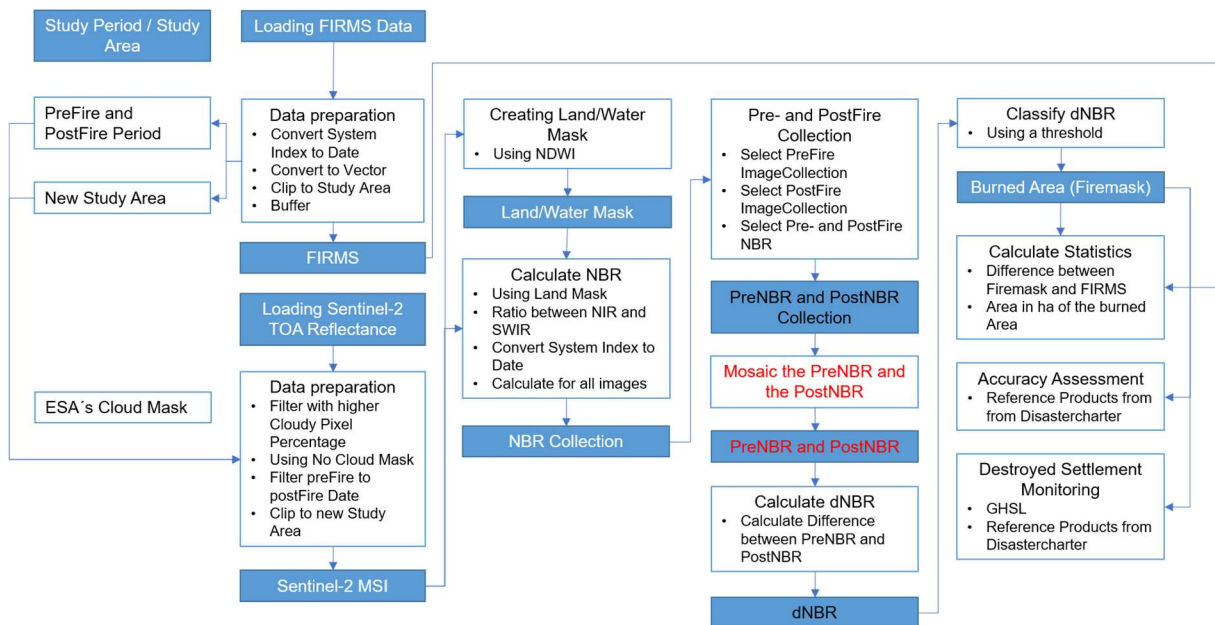


Figure 102: Changed workflow for the second study area

- Calculating the pre- and postFire NBR Mosaic

In contrast to the previous method, a mosaic of all calculated NBR's is now created before the fire event and after the fire event.

```
//-----Make a mosaic of all Pre- and PostFire NBR-----//
// Mosaic and clip images to study area
var prefire_mos_NBR = S2_collection_preFire_NBR.mosaic().clip(newAOI);
var postfire_mos_NBR = S2_collection_postFire_NBR.mosaic().clip(newAOI);

print("Pre-fire NBR Mosaic: ", prefire_mos_NBR);
print("Post-fire NBR Mosaic: ", postfire_mos_NBR);
```

The fire event in the Figures below can be seen very well in the PostFire data. Here the still active fires can even be seen in the false colour image at the end of the smoke clouds. Also, the already burned areas in the image can be localized well.

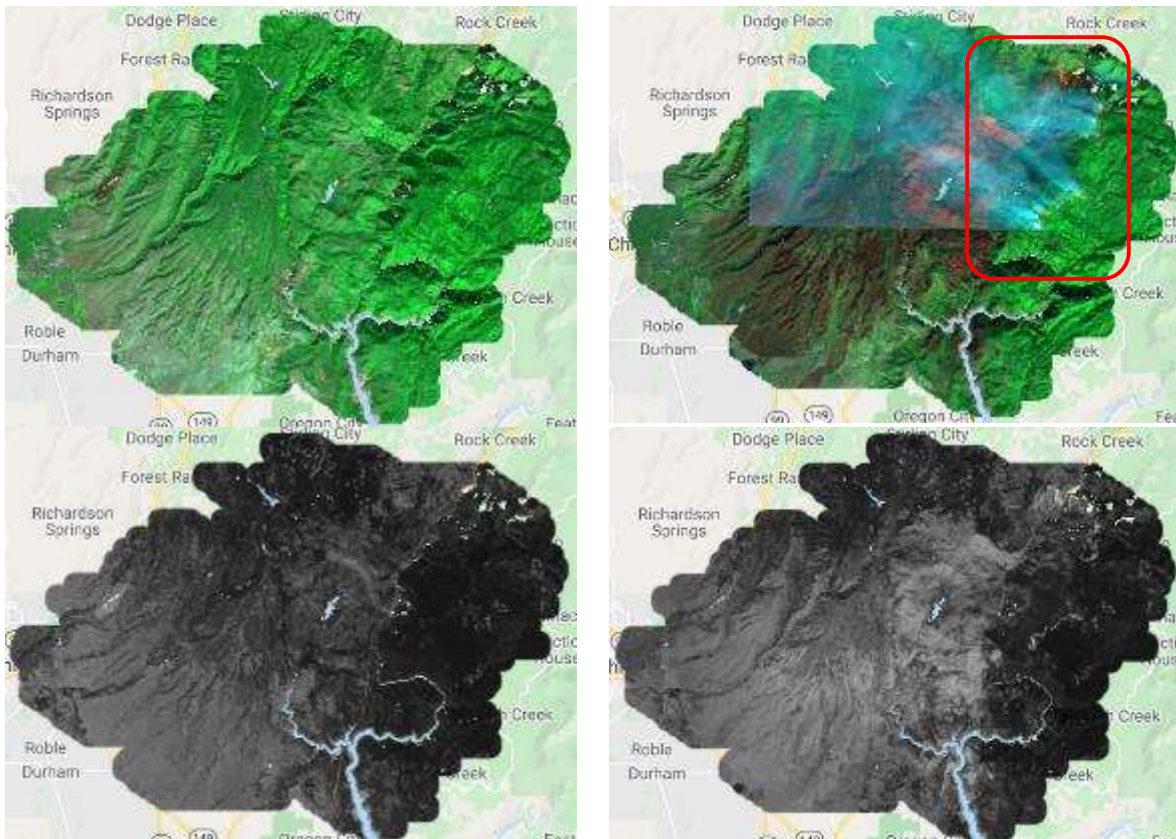


Figure 103: preFire Image Collection in False Color (upper left); postFire Image Collection in False Color (upper right); preNBR mosaic (lower left) and postNBR mosaic (lower right)

With the now calculated pre- and postFire NBR mosaic the dNBR can be calculated according the formula and displayed.

```
// difference between pre- and post-fire mosaic
// The result is called delta NBR or dNBR

var dNBR_unscaled = prefire_mos_NBR.subtract(postfire_mos_NBR);

// Scale product to USGS standards
var dNBR = dNBR_unscaled.multiply(1000);

print("Difference Normalized Burn Ratio: ", dNBR);
```

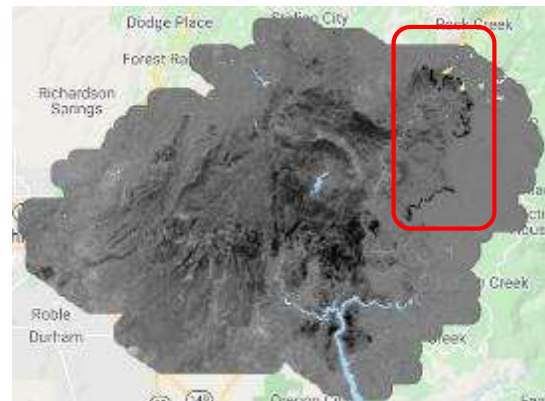


Figure 104: Earth Engine Code calculating dNBR and result on the right side

The result of the dNBR shows a clear and unambiguous representation of the burnt or still burning areas in the study area. Especially noticeable are the still active fires in the eastern part of the area, which are particularly dark and clearly demarcated from the surrounding area (see marking).

Finally, the workflow can be used as in the first study area (Rafina), i.e. a fire mask is created over a purely empirically found threshold, a comparison is made to the FIRMS alarm and a classification of the entire dNBR is performed.

- *Creating the Fire Mask and Comparison of burned areas to FIRMS alarm*

With the result as dNBR it is now also possible to create a thematic layer using a threshold value, which is used as a comparison to the FIRMS alarm.

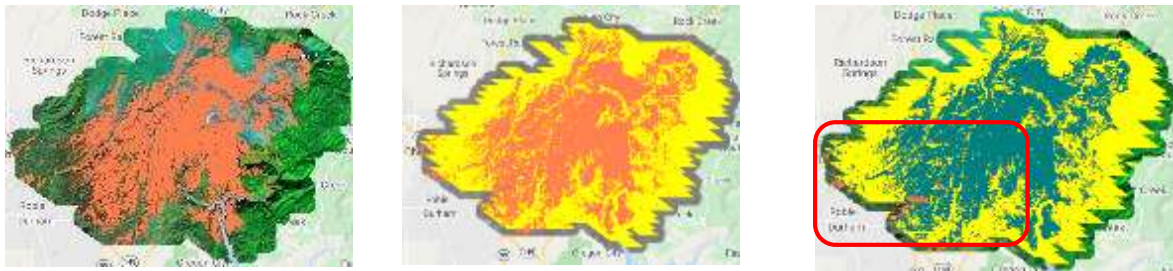


Figure 105: Fire Mask in orange (left side), T21 Mask in yellow (center), overlaid from the Fire Mask and the Comparison between the two masks in green (right side)

Large parts of the created fire mask are covered by the FIRMS Alarm. Only in the south-western and western part of the area there are areas which are only generated from the workflow as burned areas (see marking).



Figure 106: Statistic of the Fire Mask and the Comparison to the T21 Mask

The statistics show this just as clearly. As a result of the workflow, just under 58,000 ha of land are shown as burnt areas. In a comparison with the FIRMS alarm, almost 56,000 ha are shown as burnt areas. This shows at first glance that the modified workflow can be used to detect very well burned areas from Sentinel-2 data, despite the incomplete data.

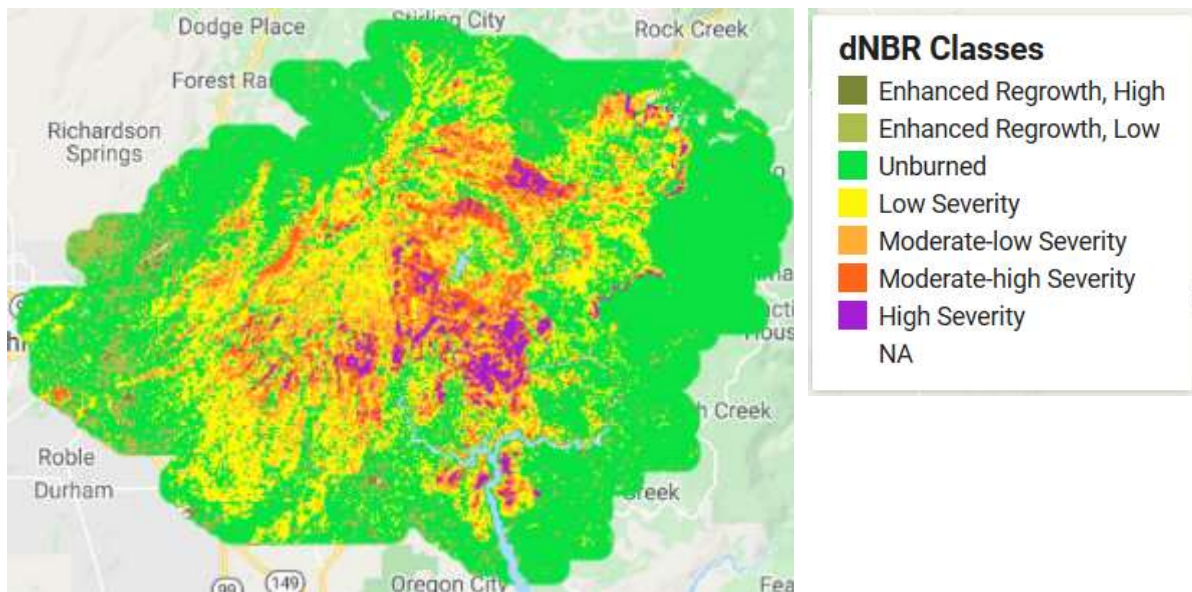


Figure 107: classified burned area as final result

The classification of the dNBR into different classes of severity proves to be useful, since the still active fires in the eastern part are particularly well exposed in the High Severity class.

The complete modified code can be viewed in the Google Earth Engine with the following link:

<https://code.earthengine.google.com/407f7a29d9f085eec61ac4df432f5df0>

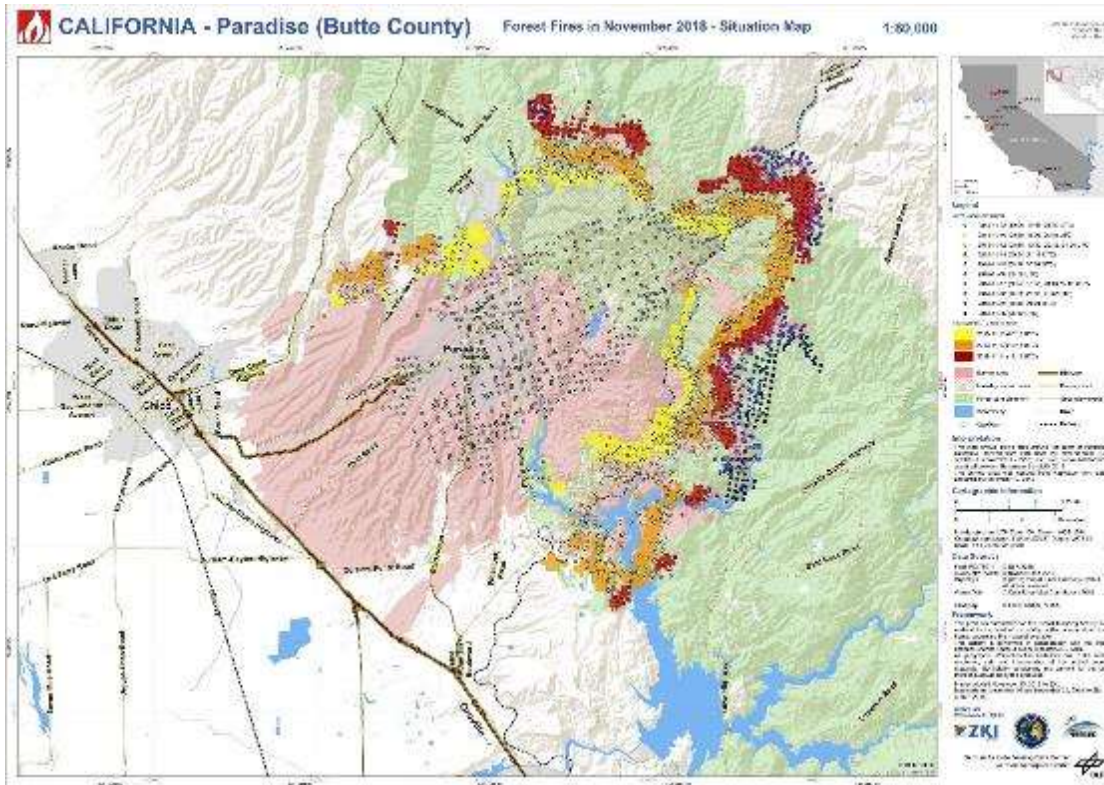


Figure 109: Forest Fires in November 2018 – Situation Map; burned area in pink (Disastercharter 591 2018)

The map shows active fires around the town of Paradise, California, derived from data from the experimental DLR satellite FireBird/TET-1 (150m) and from Suomi-NPP/VIIRS, acquired between November 8 and 20, 2018. The active fires are shown in yellow, orange and red (depending on the date). The burned area was derived from RapidEye (5m) data, acquired on November 16, 2018 and is shown in pink.

Optical Comparison to the Fire Situation Map:



Figure 110: optical Comparison between the three different Masks. Left: first Fire Mask from the first Workflow, center: second Fire mask from the first Workflow, right: Fire Mask from the second Workflow

The optical comparison shows that a similar burned area is only achieved with the second, adapted approach. Deviations are to be expected, since the RapidEye satellites have a significantly higher temporal resolution due to their constellation (5 satellites in one orbit) and therefore more data is available in a short time and the

satellites have a higher geometric resolution, which means that smaller areas can also be identified.

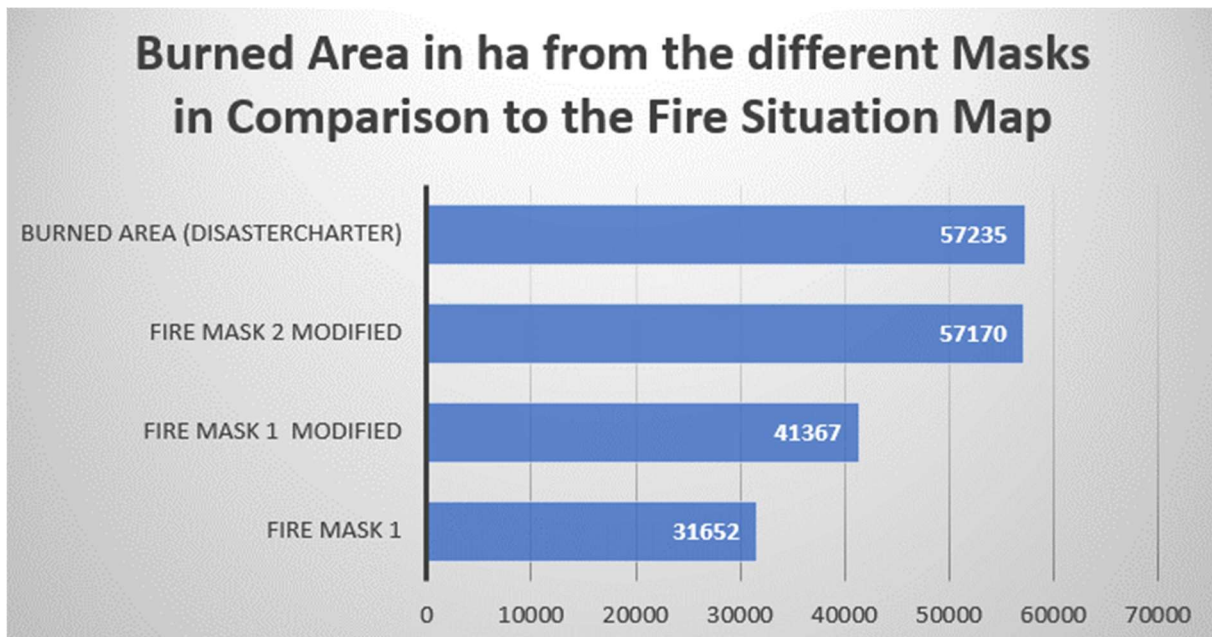


Figure 111: Comparison of the different burned areas in ha

The statistics and the optical result of the generated fire masks allow the conclusion that the second workflow leads to very good results in the interpretation of burned areas. According to the Disastercharter Organisation (Disastercharter 591 2018) estimated 57.235 ha burned by the fires in November 2018. With the help of the second workflow, 57,417 ha of burnt area can be specified. In contrast, the result from the first workflow is in no way comparable to this.

4.3.8 Destroyed Settlement Monitoring

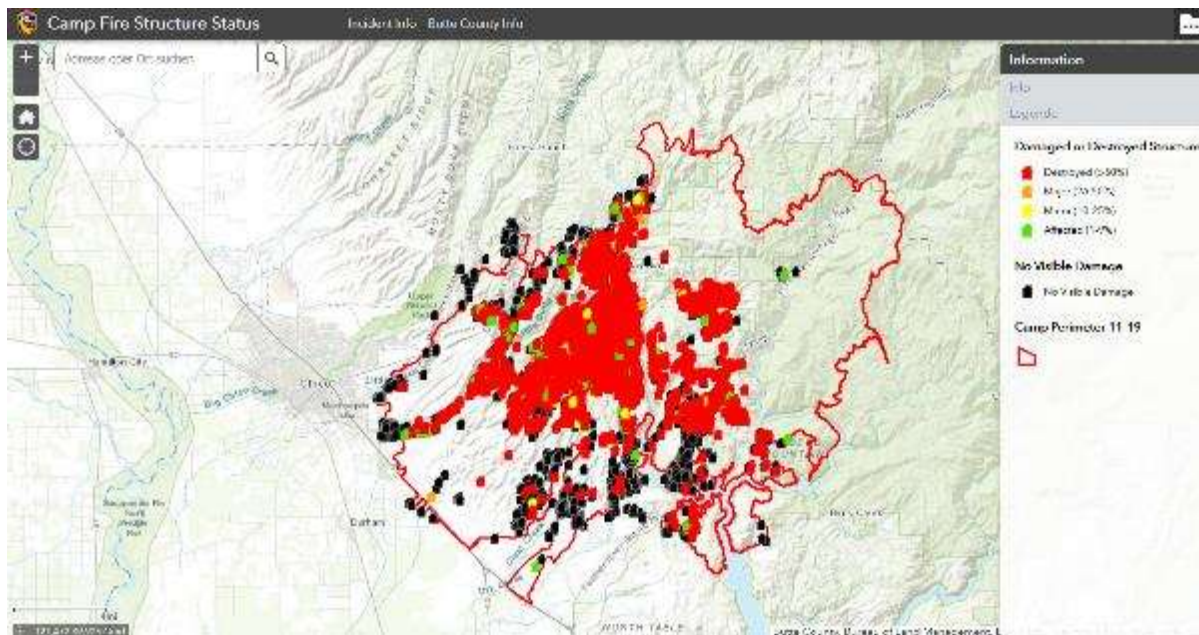


Figure 112: Damaged or Destroyed Structures in Butte County

(<https://calfire-forestry.maps.arcgis.com>)

The map (Fig. 112) is intended to give a visual impression of which settlement structures were damaged or destroyed in the fires in November 2018 in the study area. For the master thesis, the GHSL (DG/JRC/E1 2016) were loaded into the GEE and merged with the detected burned area from the second workflow. Figure 113 shows the loaded data. In the background the generated fire mask. Already at first sight it is obvious that the existing data stock on settlement structures shows considerable gaps. This is also shown by the optical comparison to Fig. 112. In figure 114, only the affected settlement structures (shown in red) are still visible. A comparison with the map also permits the conclusion that the GHSL is not complete and quality-controlled, as the proportion of settlement structures is too small compared with the map.

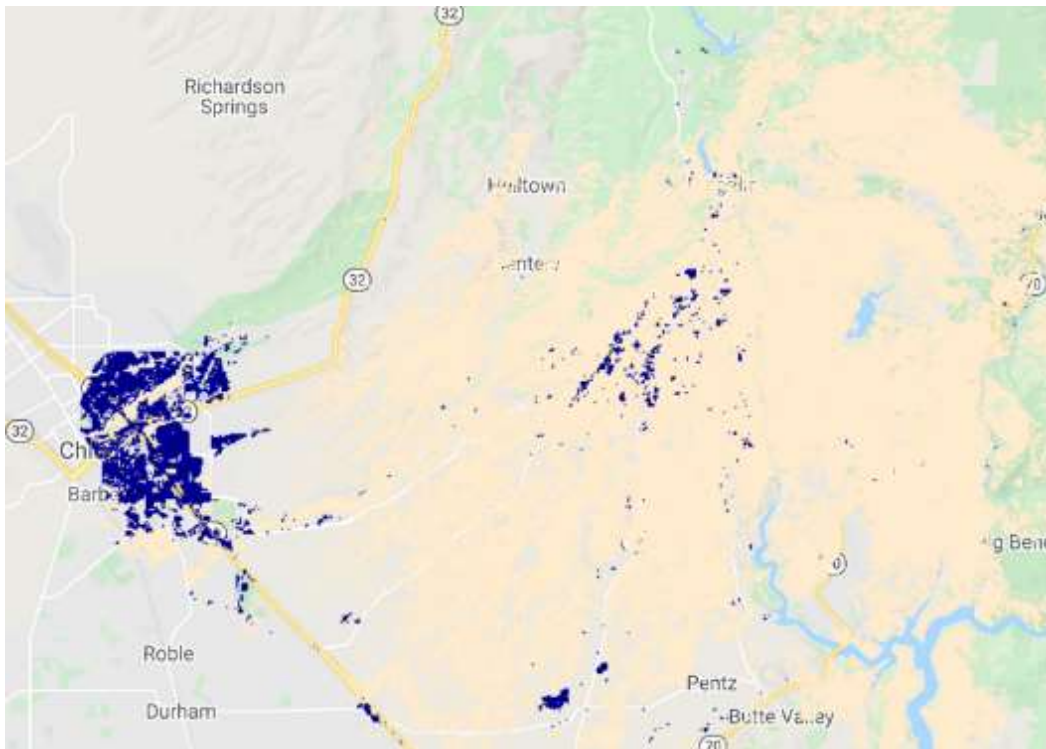


Figure 113: Fire mask (light orange); overlaid from GHSL

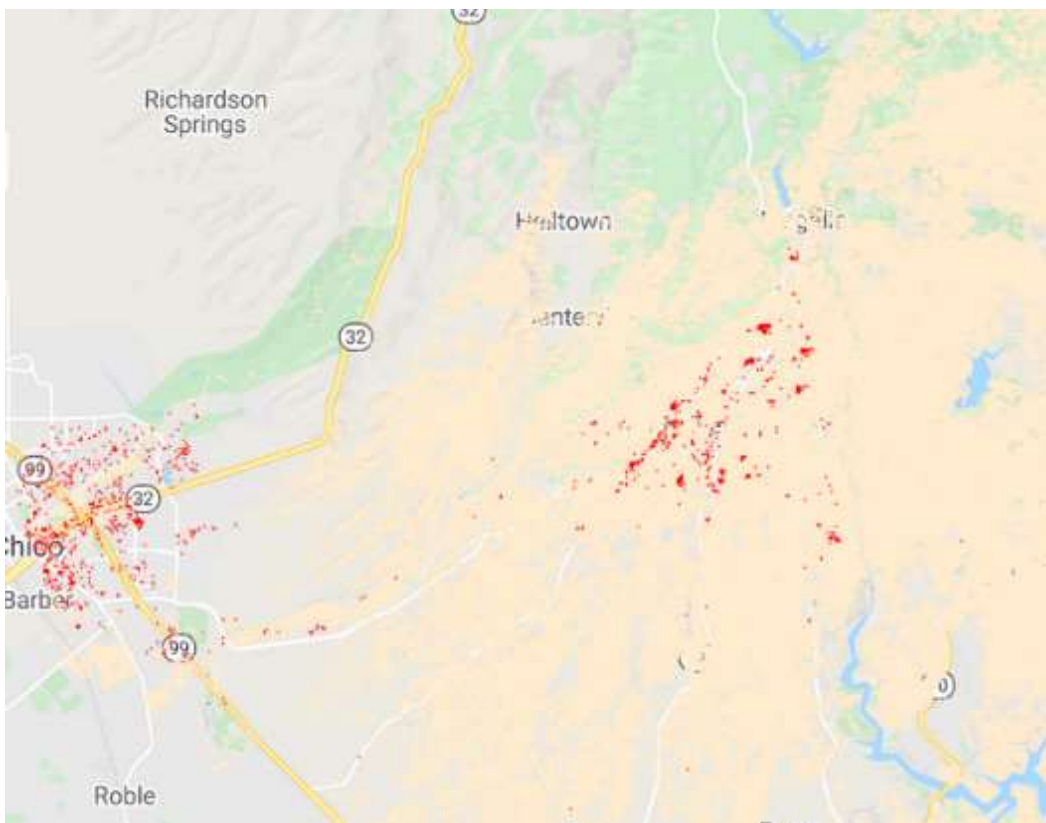


Figure 114: affected Human Settlement Structures

```
Sum Pix from burntBuiltUpArea is:  
▼Object (1 property)  
  sum: 11077.611764705884  


---

totalAreas from burntBuiltUpArea is:  
▼Object (1 property)  
  sum: 3402819.5226021563  


---

total Area in ha for BurntBuiltUpArea  
443.10447058823536
```

The Statistic shows that 443 ha of settlement structures were affected by the fire. A statement about whether these structures are damaged or destroyed cannot be derived. In comparison to the map 'damaged or destroyed Structures' it can be seen very quickly that the GHSL provided is not sufficient to make a statement about how many structures were affected.

4.3.9 Results

The workflow evaluated from the first study area cannot be transferred to the second test area without restrictions. This is mainly due to the fact that the test area is covered by four so-called tiles. Without mosaicking the scenes, a complete run-through of the workflow is only possible to a limited extent.

A selection of the cloud coverage in the test area was set to 20%. The result was an Image Collection, in which not enough data could be found for the investigation period. However, an increase of the allowed cloud coverage did not lead to better results either, because especially during or after a fire event only data with more than 90% cloud coverage is available. An attempt was made to record all available data without selection for cloud cover. The result was an Image Collection with almost 50 data sets. Unfortunately, the computer reached its computing power for calculating the dNBR for the entire collection with this amount of data, so this approach could not be pursued further. The following mosaicking of all scenes per the same date could not yield satisfactory results either, because too much data in the collection showed too much cloud coverage and therefore either did not yield any values for the NBR or was not included in the collection at all. The last attempt, in which only the data closest in time to the respective fire event were selected, led to a relatively exact localization of the burnt areas, but the cloud mask also caused holes in the data, so that here, too, only a limited result can be seen.

The second workflow, i.e. no cloud mask is used, also had to be adapted. Since the area is not covered by one tile but by four tiles, filtering according to the lowest cloud coverage in the image cannot take place, since without prior mosaicking of the data, each tile is considered individually and therefore different scenes can be considered. Therefore, the second workflow was modified. First the NBR is calculated for all existing scenes, then all NBR before the fire event and all NBR after the fire event are mosaiced. From the resulting PreNBR and PostNBR data the dNBR could be derived. Although all data are included in the calculation and no cloud mask is used, this approach yielded the best results. The statistics and the optical comparison to the reference maps confirm this.

The statement as to whether human settlement structures are affected and if so, to what extent, can only be answered to a limited extent. As long as freely available and also evaluated and quality-checked data are available, the results of the workflow can

certainly be used to make a statement about this. The freely available data used, by means of a visual comparison with the reference maps, quickly shows that only very limited information can be provided. In this case, it would make sense to derive settlement structures from high-resolution, commercially distributed data.

5. Conclusion

The introductory research question “is it possible, based on existing FIRMS alarms, to automatically or semi-automatically extract fire areas from Sentinel-2 MSI data and to derive affected human settlement structures?” can be answered with limitations after this work. The existing FIRMS alarms can be used to derive a pre- and post-fire period and a location for the detection of burned areas. However, it is often the case that not every registered alarm is displayed, as the alarms are graded according to the importance or severity of the fire and only the highest rated alarm is finally displayed. The alarms must be separated manually for the respective investigation area. Therefore, a completely automated workflow must be avoided. Additionally, not every registered fire in FIRMS creates a burned area that can be detected using Sentinel-2 data and not every registered fire is a forest fire because it could also be a volcanic eruption or the flare from a gas well (FIRMS FAQ | Earthdata). There is no way of knowing which type of thermal anomaly is detected based on the MODIS alone (FIRMS FAQ | Earthdata). Therefore, each alarm must be checked individually.

Sentinel-2 Level 1C data in two different approaches were selected for the detection of burnt areas. Level 1C products are provided as TOA reflectance. Huang et al. (2016) point out in their study, that Atmospheric correction from TOA to surface reflectance is usually considered as a requirement for change detection applications like the dNBR. The spatial and temporal influence of the atmosphere depends not only on the atmospheric components but also on the surface reflection, since the multiple scattering of the reflected radiation at the surface and in the atmosphere creates a dependence between the surface reflection and the contribution of the atmosphere to the reflection of the TOA (Huang et al. 2016). Huang et al. (2016) therefore recommend that an atmospheric correction of the data should be performed. His study shows that there are several ways to correct atmospheric influence (Huang et al. 2016). But for his studies these are inappropriate as smoke aerosols and pyrogenic emissions may be quite dynamic and spatially heterogeneous (Huang et al. 2016). Consequently, the data were atmospherically corrected to surface reflectance using the recent radiative transfer based SEN2COR atmospheric correction software (Huang et al. 2016). In the Google Earth Engine™, it is possible to choose between Sentinel-2 TOA reflectance data and already processed Sentinel-2 surface reflectance data. However, the surface reflectance data are only made available for download for a limited part of the earth's

surface. According to the Sentinel-2 user manual the software SEN2COR is also used for correction. Unfortunately, a worldwide coverage of the data is not yet provided in the GEE. The independent implementation of the SEN2COR software in the GEE is also not supported, so that at this time a calculation of the burned areas on atmospherically corrected data in the GEE is not possible.

In the first approach, therefore, the cloud mask provided by ESA was used in addition to the TOA reflectance data to obtain cloud-free images over a selected time period. But many optical comparisons allow the conclusion that not all clouds are recorded in the cloud mask. Therefore, the calculation of the dNBR leads to misclassifications, especially in those areas where existing cirrus clouds were not captured by the mask. Furthermore, the use of the cloud mask resulted in "gaps" in the data, because due to the tight time frame not enough cloud-free images were available to "fill up" the holes.

In the second approach, the cloud mask was not used. This has the advantage that filtering is possible according to a cloudy pixel percentage. If only images with a very low percentage were loaded into the collection, good results could be derived, at least in the first study area. Thus, for the Rafina area it can be concluded that both approaches lead to good results. A PostFire period of 30 days was chosen. This means that the "final" evaluation can only be done one month after the event. This period could be shortened by using PlanetScope imagery with daily coverage.

The comparison with a supervised classification and the reference data of the EMS confirm this. However, the two selected study areas show a difference in the selection of data, which makes it impossible to apply the workflow unchanged for each area of the earth.

The Sentinel-2 Level 1C tiles have a very complex structure. Huang et al. (2016) mention in their study the problems that arise from the classification of the images and points out that therefore only data of the same tiles are used in his study. The Paradise study area is significantly greater and is covered by four of these tiles. The results of the Master Thesis now show that as soon as an area is no longer covered by one tile alone, the dNBR within an Image Collection can no longer be calculated, because either satellite images are not available for each tile in the entire time period or the tiles are incorrectly calculated to each other due to the date and time of recording (the combination forms the system index in the image). A query about the lowest Cloudy

Pixel Percentage also makes no sense anymore, because the tiles are viewed separately from each other and therefore different image sections are calculated together. Therefore, the scenes have to be mosaiced in this case. So, it is almost impossible to detect the entire burn area with only one workflow. Although mosaicking the data creates the complete coverage of the area, it was then no longer possible within the GEE to apply further queries and filters to the resulting data set.

In the case of the first study area, FIRMS registered an alarm over a relatively long period of time. The fire area derived from the workflow, whether from the first or second approach, can be easily derived and classified by severity. In the case of the second study area, FIRMS registered a high number of alarms within a very short period of time. This makes it almost impossible to find a suitable time period for selecting the Sentinel-2 data, firstly because few cloud-free images are available over a long period of time and secondly because the burnt areas found overlap. This problem is reflected in the results of both approaches. When using the cloud mask, many "gaps" in the data occur, because most of the available images have a high cloud coverage and not enough cloud-free images are available within the time period. The derived fire mask is therefore very patchy and, due to the frequency of events, also shows older burnt areas. If, on the other hand, you select only the most recent before and after scenes of an event, mosaic them into an overall image, under the condition no cloud mask is used, you obtain relatively exactly the burned area at the current time.

The question whether affected settlement structures could be derived can only be answered as long as the registered alarm is not a false alarm, the fire can be detected as a burnt area in Sentinel-2 data, the burnt area is geographically definable and settlement data are available, which are up-to-date, quality-controlled and available for use in GEE. In order to be able to make a more precise statement on settlement structures affected, the digitization or delineation of settlement structures from very-high resolution satellite data or the use of Open Street Map would be a possibility.

Bibliography

2018 Attica wildfires. Online verfügbar unter https://en.wikipedia.org/wiki/2018_Attica_wildfires, zuletzt geprüft am 21.01.2020.

Akar, Özlem; Güngör, Oğuz (2012): Classification of multispectral images using Random Forest algorithm. In: *J Geod Geoinf* 1 (2), S. 105–112. DOI: 10.9733/jgg.241212.1.

Camp Fire (2018) (2019). Online verfügbar unter [https://en.wikipedia.org/wiki/Camp_Fire_\(2018\)](https://en.wikipedia.org/wiki/Camp_Fire_(2018)), zuletzt aktualisiert am 25.06.2019, zuletzt geprüft am 30.01.2020.

Chuvieco, Emilio (Hg.) (2009): Earth observation of wildland fires in mediterranean ecosystems. Heidelberg: Springer.

DG/JRC/E1 (2016): Global Human Settlement - Datasets - European Commission. Online verfügbar unter <https://ghsl.jrc.ec.europa.eu/datasets.php#2016public>, zuletzt aktualisiert am 06.07.2016, zuletzt geprüft am 31.01.2020.

Disastercharter 591 (2018): fire in united states. activation 591. Online verfügbar unter <https://disasterscharter.org/web/guest/activations/-/article/fire-in-united-states-activation-591->, zuletzt geprüft am 18.07.2019.

Du, Yun; Zhang, Yihang; Ling, Feng; Wang, Qunming; Li, Wenbo; Li, Xiaodong (2016): Water Bodies' Mapping from Sentinel-2 Imagery with Modified Normalized Difference Water Index at 10-m Spatial Resolution Produced by Sharpening the SWIR Band. In: *Remote Sensing* 8 (4), S. 354. DOI: 10.3390/rs8040354.

Earth Engine Data Catalog: GHSL: Global Human Settlement Layers, Built-Up Grid 1975-1990-2000-2015 (P2016). Online verfügbar unter https://developers.google.com/earth-engine/datasets/catalog/JRC_GHSL_P2016_BUILT_LDSMT_GLOBE_V1, zuletzt geprüft am 31.01.2020.

Earthdata.nasa.gov (2019): FIRMS_c6-mcd14dl. Online verfügbar unter <https://earthdata.nasa.gov/earth-observation-data/near-real-time/firms/c6-mcd14dl>, zuletzt aktualisiert am 18.04.2019, zuletzt geprüft am 12.07.2019.

EMSR300 (2018): Forest Fires in Attica, Greece. Online verfügbar unter <https://emergency.copernicus.eu/mapping/ems/copernicus-ems-monitors-forest-fires-attika-greece>, zuletzt geprüft am 30.06.2019.

European Space Agency (2015): Sentinel-2 User Handbook. Online verfügbar unter https://earth.esa.int/documents/247904/685211/Sentinel-2_User_Handbook, zuletzt geprüft am 22.12.2019.

European Space Agency (2019): User Guides Sentinel 2 MSI. Online verfügbar unter <https://earth.esa.int/web/sentinel/user-guides/sentinel-2-msi>, zuletzt geprüft am 08.07.2019.

Filipponi, Federico (2018): BAIS2: Burned Area Index for Sentinel-2. In: *Proceedings 2 (7)*, S. 364. DOI: 10.3390/ecrs-2-05177.

FIRMS FAQ | Earthdata. Online verfügbar unter <https://earthdata.nasa.gov/faq/firms-faq>, zuletzt geprüft am 30.01.2020.

Giglio, Louis (2016): MODIS Aqua & Terra 1 km Thermal Anomalies and Fire Locations V006 NRT. Land Atmosphere Near real-time Capability for EOS Fire Information for Resource Management System. Online verfügbar unter <https://earthdata.nasa.gov/earth-observation-data/near-real-time/firms>, zuletzt geprüft am 27.12.2018.

Giglio, Louis; Descloitres, Jacques; Justice, Christopher O.; Kaufman, Yoram J. (2003): An Enhanced Contextual Fire Detection Algorithm for MODIS. In: *Remote Sensing of Environment* 87 (2-3), S. 273–282. DOI: 10.1016/S0034-4257(03)00184-6.

Google Earth Engine (2019): FIRMS: Fire Information for Resource Management System. Online verfügbar unter <https://developers.google.com/earth-engine/datasets/catalog/FIRMS>, zuletzt aktualisiert am 06.03.2019, zuletzt geprüft am 12.07.2019.

Gorelick, Noel; Hancher, Matt; Dixon, Mike; Ilyushchenko, Simon; Thau, David; Moore, Rebecca (2017): Google Earth Engine: Planetary-scale geospatial analysis for everyone. In: *Remote Sensing of Environment* 202, S. 18–27. DOI: 10.1016/j.rse.2017.06.031.

Gutjahr, Walter J.; Nolz, Pamela C. (2016): Multicriteria optimization in humanitarian aid. In: *European Journal of Operational Research* 252 (2), S. 351–366. DOI: 10.1016/j.ejor.2015.12.035.

Hu, Yunfeng; Hu, Yang (2019): Land Cover Changes and Their Driving Mechanisms in Central Asia from 2001 to 2017 Supported by Google Earth Engine. In: *Remote Sensing* 11 (5), S. 554. DOI: 10.3390/rs11050554.

Huang, Haiyan; Roy, David; Boschetti, Luigi; Zhang, Hankui; Yan, Lin; Kumar, Sanath et al. (2016): Separability Analysis of Sentinel-2A Multi-Spectral Instrument (MSI) Data for Burned Area Discrimination. In: *Remote Sensing* 8 (10), S. 873. DOI: 10.3390/rs8100873.

International Charter Space and Disaster Management (2019). Online verfügbar unter <https://disasterscharter.org/web/guest/about-the-charter>, zuletzt geprüft am 18.07.2019.

Joint Research Centre (2016): Operating procedure for the production of the Global Human Settlement Layer from Landsat data of the epochs 1975, 1990, 2000, and 2014. Hg. v. Publications Office of the European Union. Online verfügbar unter <http://publications.jrc.ec.europa.eu/repository/handle/JRC97705>.

Kumar, S. S.; Roy, D. P. (2017): Multi-year MODIS active fire type classification over the Brazilian Tropical Moist Forest Biome. In: *International Journal of Digital Earth* (Vol. 10), S. 54–84. Online verfügbar unter <https://doi.org/10.1080/17538947.2016.1208686>.

Lang, Stefan; Füreder, Petra; Wendt, Lorenz; Rogenhofer, Edith (2016): Fernerkundungsbasierte Informationsdienste für humanitäre Einsätze in Flüchtlingslagern. In: *AGIT Journal für Angewandte Geoinformatik* 2-2016, S. 86–92. DOI: 10.14627/537622013.

Lentile, Leigh B.; Holden, Zachary A.; Smith, Alistair M. S.; Falkowski, Michael J.; Hudak, Andrew T.; Morgan, Penelope et al. (2006): Remote sensing techniques to assess active fire characteristics and post-fire effects. In: *Int. J. Wildland Fire* 15 (3), S. 319. DOI: 10.1071/WF05097.

Li, Jian; Roy, David P. (2017): A Global Analysis of Sentinel-2A, Sentinel-2B and Landsat-8 Data Revisit Intervals and Implications for Terrestrial Monitoring. In: *Remote Sensing* 9 (9), 902, 1 - 17. DOI: 10.3390/rs9090902.

Martino, PESARESI; Daniele, EHRLICH; STEFANO, FERRI; ANETA, FLORCZYK; MANUEL, CARNEIRO FREIRE SERGIO; Stamatia, HALKIA et al. (2015): Operating procedure for the production of the Global Human Settlement Layer from Landsat data of the epochs 1975, 1990, 2000, and 2014. Publications Office of the European Union. Online verfügbar unter <https://publications.jrc.ec.europa.eu/repository/handle/JRC97705>, zuletzt aktualisiert am 03.03.2016, zuletzt geprüft am 30.01.2020.

McFEETERS, S. K. (1996): The use of the Normalized Difference Water Index (NDWI) in the delineation of open water features. In: *International Journal of Remote Sensing* 17 (7), S. 1425–1432. DOI: 10.1080/01431169608948714.

Munich Re (2018). Online verfügbar unter <https://www.munichre.com/touch/naturalhazards/en/naturalhazards/climatological-hazards/wildfire/index.html?QUERYSTRING=Wildfire>.

Mutanga, Onesimo; Kumar, Lalit (2019): Google Earth Engine Applications. In: *Remote Sensing* 11 (5), S. 591. DOI: 10.3390/rs11050591.

Petropoulos, George P.; Griffiths, Hywel M.; Kalivas, Dionissios P. (2014): Quantifying spatial and temporal vegetation recovery dynamics following a wildfire event in a Mediterranean landscape using EO data and GIS. In: *Applied Geography* 50, S. 120–131. DOI: 10.1016/j.apgeog.2014.02.006.

Poursanidis, Dimitris; Chrysoulakis, Nektarios (2017): Remote Sensing, natural hazards and the contribution of ESA Sentinels missions. In: *Remote Sensing Applications: Society and Environment* 6, S. 25–38. DOI: 10.1016/j.rsase.2017.02.001.

Roteta, E.; Bastarrika, A.; Padilla, M.; Storm, T.; Chuvieco, E. (2019): Development of a Sentinel-2 burned area algorithm: Generation of a small fire database for sub-Saharan Africa. In: *Remote Sensing of Environment* 222, S. 1–17. DOI: 10.1016/j.rse.2018.12.011.

Schroeder, Wilfrid; Oliva, Patricia; Giglio, Louis; Quayle, Brad; Lorenz, Eckehard; Morelli, Fabiano (2016): Active fire detection using Landsat-8/OLI data. In: *Remote Sensing of Environment* 185, S. 210–220. DOI: 10.1016/j.rse.2015.08.032.

Teodoro, Ana; Amaral, Ana (2019): A Statistical and Spatial Analysis of Portuguese Forest Fires in Summer 2016 Considering Landsat 8 and Sentinel 2A Data. In: *Environments* 6 (3), S. 36. DOI: 10.3390/environments6030036.

Verhegghen, Astrid; Eva, Hugh; Ceccherini, Guido; Achard, Frederic; Gond, Valery; Gourlet-Fleury, Sylvie; Cerutti, Paolo (2016): The Potential of Sentinel Satellites for Burnt Area Mapping and Monitoring in the Congo Basin Forests. In: *Remote Sensing* 8 (12), S. 986. DOI: 10.3390/rs8120986.

Weirather, Mira; Zeug, Gunter; Schneider, Thomas (2018): Automated Delineation Of Wildfire Areas Using Sentinel-2 Satellite Imagery. In: *gforum* 1, S. 251–262. DOI: 10.1553/giscience2018_01_s251.

Wooster, M. J.; Xu, W.; Nightingale, T. (2012): Sentinel-3 SLSTR active fire detection and FRP product: Pre-launch algorithm development and performance evaluation using MODIS and ASTER datasets. In: *Remote Sensing of Environment* 120, S. 236–254. DOI: 10.1016/j.rse.2011.09.033.